This is to certify that the

dissertation entitled

FREQUENCY DEPENDENT RESPONSE OF
DIAMOND SCHOTTKY BARRIER DIODE TO
LARGE AND SMALL ELECTRICAL SIGNALS
presented by

Boonchoat Paosawatyanyong

has been accepted towards fulfillment
of the requirements for

Ph.D. degree in Electrical Eng

Donnie K Reinhard
Major professor

Date 11/13/98

Frequency Dependent Response of Diamond Schottky Barrier diode to Large and Small Electrical Signals

By

Boonchoat Paosawatyanyong

A DISSERTATION

Submitted to
Michigan State University
In partial fulfillment of the requirements
For the degree of

DOCTOR OF PHILOSOPHY

Department of Electrical Engineering

1998

Abstract

Frequency Dependent Response of Diamond Schottky Barrier diode to Large and Small Electrical Signals

By
Boonchoat Paosawatyanyong

The response of diamond Schottky barrier diodes to time varying signals has been studied as a function of frequency and bias voltage. Both small signal waveforms superimposed upon a dc bias, as well as large signal sinusoidal waveforms which drive the diode between reverse and forward bias have been studied. The diodes are formed on thin polycrystalline diamond films deposited by a microwave plasma assisted deposition process. The Schottky metal is typically aluminum. The ohmic contact is generally a back-contact p-type silicon wafer on which the diamond is deposited, although tungsten contact overlaid with protective a layer of gold has also been successfully used. Coaxial microprobes contact the test wafers which are placed on a temperature controlled substrate holder. Measurements are performed over a temperature range of 27 °C to 127 °C. Films synthesized under various growth conditions have been tested in this study.

The experimental results of small signal test are compared to three computer models, which are: (I) a simple model that includes as input parameters the bulk series resistance, the capacitance associated with the bulk material between the space-charge layer and the ohmic contact, the space-charge layer capacitance, and the diode dynamic resistance; (II) a model with additional of a contact resistance; and (III) a model which

includes the effect of trap states represented by frequency-dependent capacitance and resistance.

The experimental results of the large switching signal test are compared to computer (SPICE) simulations which include as input parameters the bulk series resistance, the ideality factor, and diode saturation current, obtained from dc measurements. Also included are the space-charge layer capacitance, and the capacitance associated with bulk material between the space-charge layer and the ohmic contact obtained from curve-fitting. Good agreement is obtained between experimental switching observations and model predictions. For the diodes in this study, the best large signal switching frequency between forward and reverse bias is approximately 10 KHz, and the highest small signal varistors frequency performance is approximately 200 KHz.

For many operating conditions, the speed response of the diode is limited by the high bulk resistivity of the undoped diamond films. The simulation study indicates that doping the diamond film and constructing diodes with a lower bulk resistance while maintaining the space-charge layer properties would significantly improve the diode switching speed performance.

Acknowledgements

I would like to express my sincere gratitude to my advisor Dr. Donnie K. Reinhard for his guidance, support, encouragement, and patience. He has been an excellent mentor throughout the years. Great appreciation goes to Dr. Brage Golding who always gives the best suggestion throughout my academic career and life at Michigan State University. I also would like to thank my committee members, Dr. Timothy Grotjohn and Dr. Jes Asmussen for their valuable discussions and comments.

Many thanks go to Dr. Michael Ulzynski, Dr. Saeid Khatami, and Dr. Mohannad Bataineh, who were always willing to help and give suggestions in the laboratory, Dr. Michale Jaeger, Dr. Lowell McCann and Dr. Amy Engebretson who spent many hours helping me with sample preparation. Dr. Ulczynski and Dr. Khathami are particularly thanked for providing some of the samples used in this study.

My greatest appreciation goes out to my parents in Thailand. Their patience, unconditional support, and love gave me strength to finish this work. A special thanks to Sudawan for her love and patience over the last ten years. She was always there for me and helped in more ways than she knows.

I thank the MSU Center for Fundamental Materials Research, the Department of Electrical Engineering, the Physics and Astronomy Department, and The Graduate School for support throughout this research. The research also was supported in part through equipment received from NSF grant no. 9413727.

Table of contents

List of tables

List of figures

CHAPTER 1

Introduction

1.1 Research motivation

The utilization of semiconducting diamond for high performance electronic devices has been of interest to researchers for many years. For example, the electronic properties of diamond have been investigated since the 1930's and attempts to fabricate diamond semiconductor devices started in the 1950's [1]. Some of the initial interest in semiconducting diamond was mainly for high temperature and corrosion resistant semiconductor application, based on diamond's high energy gap and chemical stability. However, as the material parameters became better known, it became evident that diamond possesses a combination of material properties that, in many respects, make it ideal for various electronic applications. To date diamond has been proposed for use as power and microwave devices (bipolar and field-effect [2] [3] transistors), thermistors [4], switching devices, display array (field-emission diodes [5]) and various types of detectors (radiation [6], X-ray [7], and ultraviolet photo-detectors [8]).

The early attempts to utilize diamond were delayed by technological problems related to crystal growth, purity and doping, and also to the development of suitable ohmic and rectifying contacts [9]. Moreover, the high cost of even small diamond

samples has been an inhibiting factor in diamond device progress. Lately, a less expensive, low-pressure diamond synthesis technique, which uses chemical vapor deposition (CVD), has been developed. The economical deposition of diamond over relatively large substrates (≥10 cm in diameter) is now possible. The resulting CVD diamond is polycrystalline, unless the underlying substrate is single crystal diamond. Although the properties of CVD diamond rival those of natural diamond [10] [11], device physics of CVD diamond is still primitive compared to Si and GaAs.

Most, if not all, devices rely on rectifying contacts or rectifying junctions for their operation. Because of fabrication simplicity, diamond Schottky barrier diodes have been studied by many researchers. However, most previous reports are based on dc characteristics and have investigated the current transport mechanism through the metal/diamond contact by means of thermionic emission theory [12][13][14][15][16] while ac properties of metal/diamond contact have received much less attention.

There are several questions regarding frequency dependent electrical properties of the diamond Schottky diode which need to be answered if diamond-based technology is to be developed to the point where high performance devices can be realized. For example, it is not currently clear whether the observed frequency dependencies of diamond Schottky diodes are primary due to barrier dynamic or bulk resistivity effects. Identification of the appropriate equivalent circuit to represent the electrical properties of diamond Schottky diodes is also another question to be resolved.

1.2 Research objective

The main objective of this study is to add to the current understanding of the frequency-related performance under both large signal switching and small signal responses of diamond Schottky barrier diodes. To the investigator's knowledge, information on the experimental switching large-signal responses of diamond Schottky barriers were not been previously published prior to the investigator's paper at the Diamond 1997 Conference, 3-8 August 1997, Edinburgh, Scotland.

The small signal responses of diamond Schottky barrier diodes have been previously studied [15][17][18][19], however, these studies only emphasized the capacitance versus reverse bias voltage characteristics. As a result, the more general issue of complex admittance versus frequency still remains to be studied. There are currently two interpretations on capacitance-voltage-frequency relation on diamond Schottky barrier diode. One includes the effect of deep state traps in diamond [15] [18] [19] [20], the other explains the relation only by the combination of junction, bulk, and contact properties of the diode without a trap role in diamond [17] [21]. This research explores further the possibility of both interpretations by investigating the entire small signal admittance, not only the capacitance, at both reverse and forward bias.

1.3 Dissertation organization

This dissertation is divided into seven chapters. After an introduction in this current first chapter, the dissertation is organized and covered in the following order.

Chapter 2 provides background and previous studies of electrical characteristics of Schottky barrier diode, particularly in diamond. Also included is the review of electrical models of diamond Schottky diode proposed by other researchers.

Chapter 3 described the sample preparation process, the experiment setup and equipment used in this research.

Chapter 4 presents the experimental results and discussion on dc characteristics of diamond Schottky barrier diodes. The dc model simulations are created based on the experimental data.

Chapter 5 presents the results of the small signal responses of the diamond Schottky diodes. The results are compared with three types of circuit simulations; basic model, basic model with contact resistance effects, and model which include trap state effects.

Chapter 6 presents the results of the large switching signal responses of the diamond Schottky diodes. The model simulations are generated to match the experimental results. Methods for possible improvement in diode speed are also discussed.

Chapter 7 concludes this study with an analysis of the presented results and a discussion of the open research issues and suggestions for future work.

CHAPTER 2

Background

2.1 Chapter overview

This chapter reviews the background necessary for discussing the electrical characteristics and responses of diamond Schottky barrier diodes under dc and time varying signals. It begins with a discussion of Schottky barrier diodes in general followed by a description of the basic equations used to describe the dc voltage-current characteristic of the diode. Next, the response of a general Schottky diode to ac signals is considered. Models, equations and possible expectations are given for small and large signal excitation. The electrical properties of diamond as a semiconductor are then briefly discussed. Finally, the focus falls on diamond Schottky barrier diodes in particular, in terms of both dc and ac responses reported by others.

2.2 Schottky barrier diodes

Metal contacts to semiconductor can be ohmic, rectifying or in between. When a metal is placed in contact with a semiconductor, charge transfer occurs until the Fermi levels align at equilibrium. This process alters the potential level in both materials. In a metal the Fermi level is essentially at the highest occupied state in the conduction band.

Actually the Fermi level corresponds to 50% occupancy probability for a given state, however the Fermi-Dirac distribution falls off rapidly above the Fermi energy. An energy required to remove an electron at Fermi level of the metal to the vacuum level is defined as the metal's work function ϕ_m. Also, the work function for the semiconductor ϕ_s is defined as the distance from the semiconductor Fermi level to the vacuum level [22].

Let us first consider a metal contact with p-type semiconductor. For a p-type material, the Fermi level lies closer to the valence band than to the conduction band at equilibrium. In the case $\phi_s > \phi_m$ as in Figure 2.1(a), the metal' s Fermi level is initially higher than that of semiconductor. When a metal is placed in contact with such a p-type semiconductor under zero applied voltage, holes; majority carriers vacate from the semiconductor to the metal and create a negative charge region of width W in the semiconductor near the junction interface. This interface region which is vacated by holes is called a "depletion region" or "space charge region". The change in potential caused by uncompensated ionized acceptors bend the bands in semiconductor as shown in Figure 2.1(b), creating a contact or built-in potential V_{bi}, which prevents further net hole diffusion from the semiconductor into the metal. This contact potential V_{bi} retarding hole diffusion at equilibrium is given by $\phi_s - \phi_m$. The potential barrier height ϕ_{Bp} for hole injection from metal into the semiconductor valence band is $E_g - (\phi_s - \chi)$, where χ (called electron affinity) is measured from the vacuum level to the semiconductor conduction band edge, and E_g is the band gap energy of the semiconductor [23] [24]. The equilibrium potential difference V_{bi} can be decreased or increased by the application of either forward or reverse bias voltage. Note that band bending in metal is negligible because of its much higher carrier density.

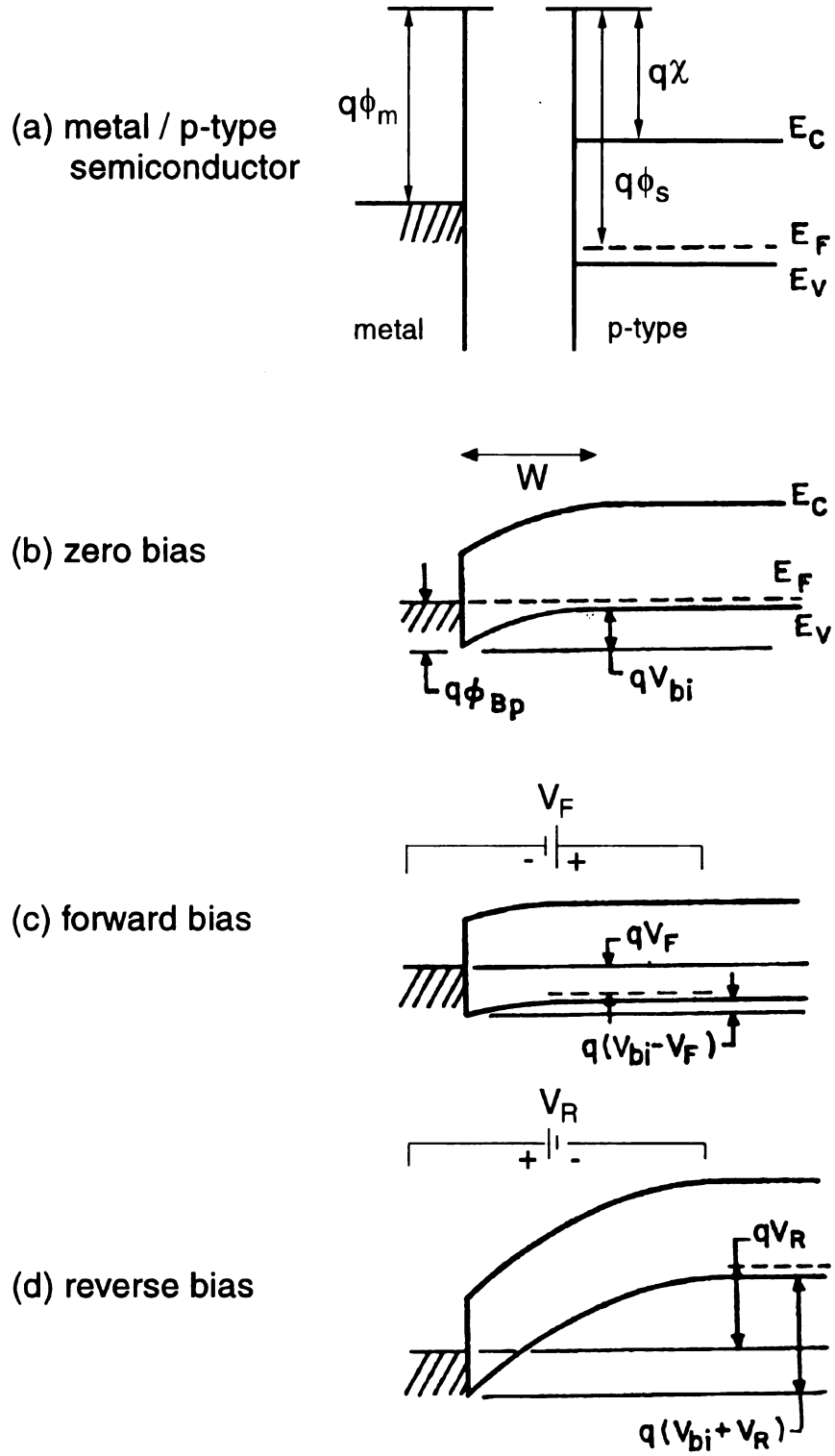

Figure 2.1 Schematic band diagram for metal to p-type semiconductor contact when $\phi_s > \phi_m$ showing band bending in the semiconductor [22] [23]

A similar description can be given for a metal and n-type semiconductor contact. However, in n-type material, the Fermi level is lying closer to the conduction band at equilibrium. Figure 2.2(a) illustrates a metal contact on a n-type semiconductor, with $\phi_m > \phi_s$. In this case aligning the Fermi levels at equilibrium requires a negative charge on the metal side and a positive charge on the semiconductor side of the junction. The positive charge is accommodated by a depletion region W in which ionized donors are left uncompensated by electrons. The potential barrier V_{bi} retarding electron diffusion from the semiconductor to the metal is $\phi_m - \phi_s$, and as before this barrier can be raised or lowered by the application of voltage across the junction. The limiting value of the barrier height ϕ_{Bn}, is given by $\phi_m - \chi$.

At zero applied voltage, the system is at equilibrium. The negative charges (p-type) or positive charges (n-type) due to uncompensated carriers within W match the opposite charges on the metal and the net current will be zero across the junction. If a forward (V_F) or reverse (V_R) bias is applied across the junction, the semiconductor bands will shift down or up in energy relative to the metal as shown in Figure 2.1(c) and Figure 2.1(d) in p-type and Figure 2.2(c) and Figure 2.2(d) in n-type semiconductor, respectively.

In equilibrium the net current flow across the Schottky junction is zero since the carrier flow from metal to semiconductor and from semiconductor to metal are equal, but in opposite directions, hence they cancel. A metal-to-p-type junction is forward biased when the semiconductor is positively biased relative to the metal. When forward biased as in Figure 2.1(c), the barrier for p-region holes is decreased by the value of bias voltage, and the semiconductor to metal current flow across the junction increase sharply.

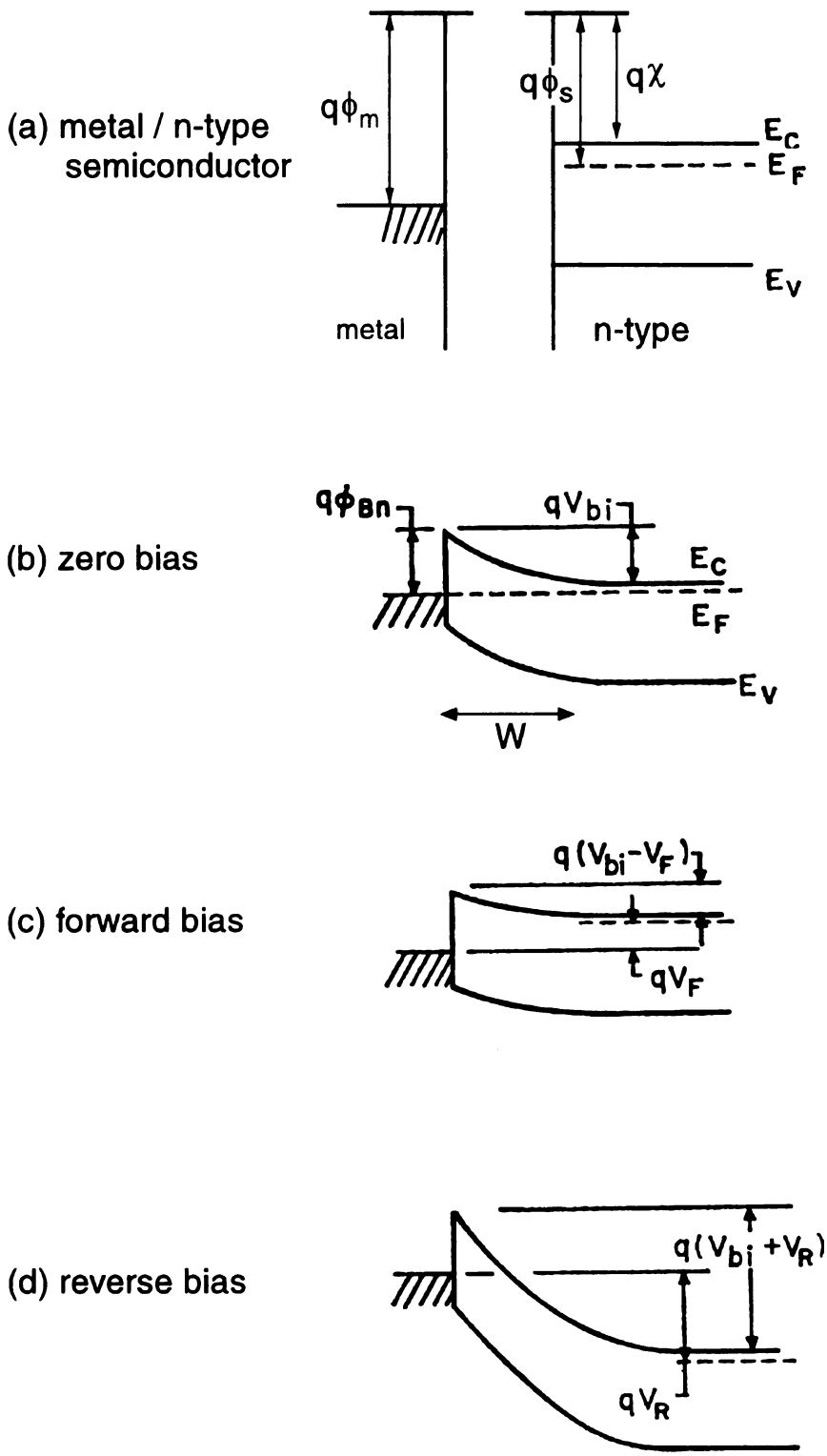

Figure 2.2 Schematic band diagram for metal to n-type semiconductor contact when $\phi_m > \phi_s$ showing band bending in the semiconductor [22] [23]

Hence the net current in the diode increases. When reverse biased as in Figure 2.1(d), the barrier for semiconductor holes is increased, reducing the semiconductor to metal current flow to essentially zero. However, the metal to semiconductor carrier flow remains the same since the metal to semiconductor barrier height is unchanged by bias. Under this condition, a small reverse current flows.

Contacts that behave as described above are called Schottky barrier diodes and exhibit non-linear I-V characteristics as shown in Figure 2.3 for an ideal diode, where positive voltage represents forward bias.

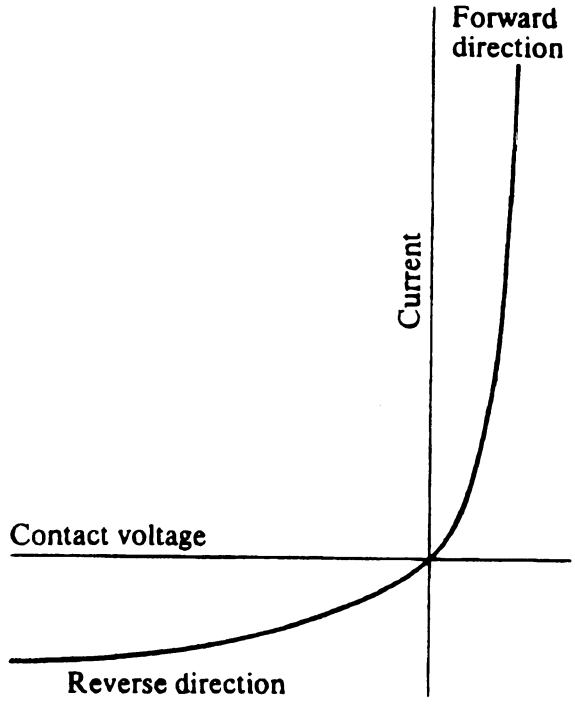

Figure 2.3 Current-voltage characteristics for an ideal Schottky barrier diode [25]

2.3 Schottky barrier diodes current-voltage equation

One difference between Schottky barrier diodes and p-n junction diodes is that Schottky barrier diodes operate as a majority-carrier device under low-level injection conditions [26]. As a consequence, storage delay time (due to storage of minority carriers) on switching from forward to reverse bias is eliminated and fast response is obtained.

The forward current-voltage (I-V) characteristics of a Schottky barrier diode obeying the thermionic emission theory is given by the following Shockley equation [22] [23] [27] [28]

$$I = I_O[\exp(qV_J / kT) - 1] \qquad (2.1)$$

where q is the electronic charge, V_J the voltage applied across the diode, k is the Boltzmann constant, and T is the absolute temperature. The value I_O can be determined from the equation

$$I_O = A_e A^{**} \cdot T^2 \exp(-q\phi_B / kT) \qquad (2.2)$$

where A_e is the effective area of the diode, A** is the effective Richardson's constant and ϕ_B is the Schottky barrier height of the diode.

A complication of the current-voltage relationship in practical diodes is that, for large forward currents, the voltage drop across the diode series resistance R_B associated

with the neutral region of the semiconductor (between the depletion region and the ohmic contact) causes the actual voltage developed across the barrier region (V_J) to be less than the voltage applied to the terminals of the diode (V). The voltage V_J across the diode can then be expressed in terms of the total voltage drop V across the series combination of the diode and the resistor. Thus, $V_J = V - IR_B$, and for $V_J \geq 3kT/q$, I becomes

$$I \cong I_O[\exp(q(V - IR_B) / kT)]$$

where I is the current through the diode. Figure 2.4 shows the diversion from the straight line of I-V plot of a diode, which indicates the effect of series resistance at high forward voltages.

Furthermore, most Schottky diodes show deviations from ideal behavior. It is a common practice to approximately account for many of the effects by which the diode characteristics deviate from the above equation (i.e. non-ideal effects) by a empirically determined dimensionless parameter called the ideality factor η such that.

$$I \cong I_O[\exp(q(V - IR_B) / \eta kT)] \qquad (2.3)$$

Low forward bias non-ideal effects include barrier height lowering, quantum mechanical tunneling of carriers through the junction, and recombination of the carriers in the depletion region. On the other hand, the effects of drift and diffusion of carriers in the space charge layer and minority carrier injection are significant at very high bias corresponding to high field and large current density [27]

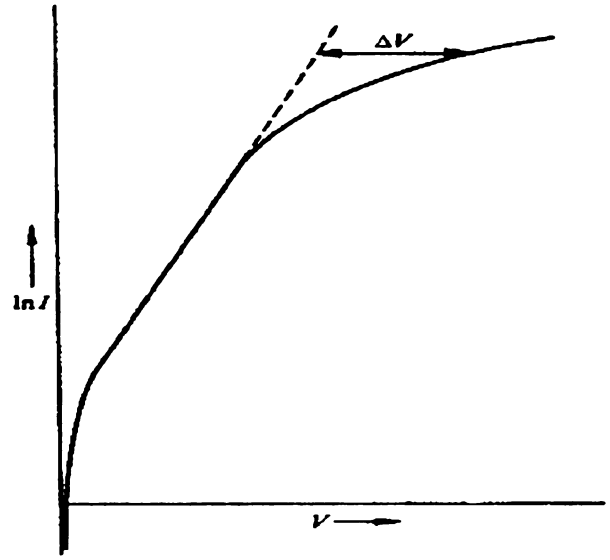

Figure 2.4 Deviation from ideal diode characteristic straight line when series resistance R_B is presented [29]. ΔV is the bulk voltage IR_B.

With the proper choice of I_O, η, and R_B, Equation 2.3 can be generally used to approximately describe the behavior of a given diode. However, when using current-voltage data to provide diagnostic information about the barrier, it is necessary to treat this equation with caution because different barrier structures can result in the same value of η over a given range of current [30].

A method to extract the series resistance R_B of ideal Schottky diodes (i.e., $\eta = 1$) was proposed by Norde [31]. For the $\eta > 1$ cases, Sato and Yasumura [32] modified Norde' s approach to extract the values of η, ϕ_B, and R_B from the forward I-V data of a Schottky diode. For a given Schottky diode, their approach requires two or more experimental I-V measurements conducted at different temperatures and the determination of the corresponding minima of the modified Norde's function. This

research, however, did not use their method since most I-V measurements were conducted at room temperature.

The barrier height of a Schottky diode is also an important parameter in the simulation of the device. From Equation 2.2, if the value of the effective Richardson's constant A** is known then the barrier height ϕ_B can be obtained from

$$\phi_B = \frac{kT}{q}\ln(\frac{A_e A^{**} T^2}{I_O}) \qquad (2.4)$$

Generally, A** is not known. However, the value of ϕ_B is not very sensitive to the choice of A**, since at room temperature, a 100% rise in A** will only cause the increase of 0.018 Volt in ϕ_B.

Another traditional method for evaluating the barrier height from the I-V data is the activation energy method. Equation 2.2 may be rewritten as

$$\ln\left(\frac{I_O}{T^2}\right) = \ln(A_e A^{**}) - \frac{q\phi_B}{k}\left(\frac{1}{T}\right) \qquad (2.5)$$

One can experimentally obtain the saturation current I_O at several temperatures, consequently, the slope of a semi-log plot of (I_O/T^2) versus (1/T) yields the value of effective barrier height and the intercept on the axis gives the logarithm value of effective Richardson's constant. The advantage offered by this method is that prior knowledge of either the Richardson's constant A** or the diode's effective area A_e is not necessary.

Analysis of the I-V characteristic at different temperatures could also yield the value of another parameter, the activation energy E_A. The temperature dependence of the

bulk resistance R_B of the semiconductor is inversely related to bulk conductivity σ, which can often be described by the equation [15][18][23]

$$\frac{1}{R_B} \propto \sigma = \text{const} \cdot \exp\left(\frac{-E_A}{kT}\right) \tag{2.6}$$

Thus, a semi-log plot of R_B versus (1/T) should be linear and the slope would correspond to the activation energy of the semiconductor.

As mentioned above, Schottky barrier diodes operate with majority carriers, however at sufficiently high current densities, minority-carrier effects can become significant. Injection of minority carriers leads to excess carrier storage in the bulk of the devices. The stored excess carriers, in turn, change Schottky barrier diodes I-V characteristics as shown in Figure 2.5. Under forward bias, minority carriers are injected into the bulk of the semiconductor and travel for an average distance of the diffusion length before they recombine with majority carriers. For semiconductors with large diffusion lengths compared to the semiconductor thickness, such as Si [33], most of the minority carriers reach the contact before being recombined. Hence, minority carrier injection leads to the presence of excess minority carriers throughout the bulk part of the devices. The excess minority carrier concentration can be considerably higher than the material's equilibrium concentration. These excess minority carriers, in addition to the excess majority carriers stored in the bulk to maintain quasi charge neutrality, give rise to an increase in the bulk conductivity, σ. The increase in conductivity, or conductivity modulation, $\Delta\sigma$, is given by [29]

$$\Delta\sigma = q(\mu_n \Delta n + \mu_p \Delta p)$$

Where Δn and Δp are excess electron and hole concentration and μ_n and μ_p are electron and hole mobilities. Conductivity modulation results in a decrease of the resistance of the epitaxial layer, consequently, the diode conducts a larger value of current for a given voltage compared to without modulation.

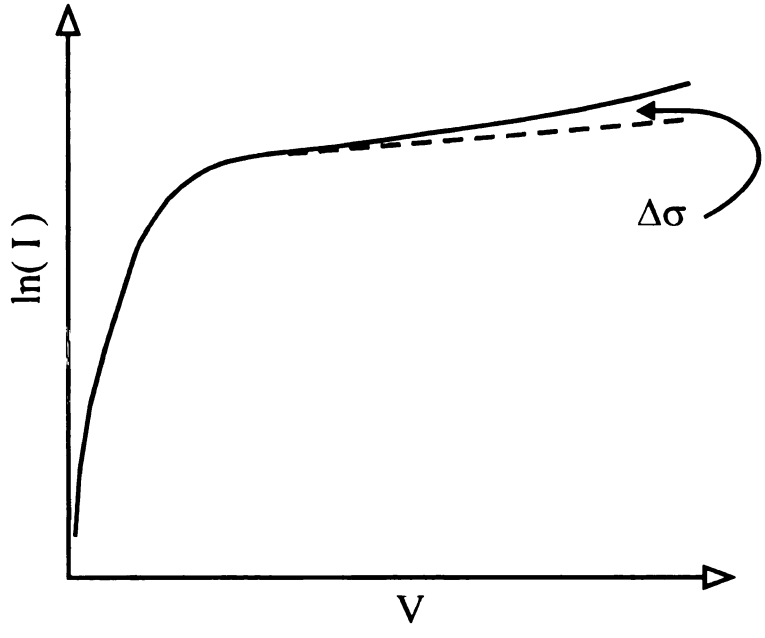

Figure 2.5 Minority carrier injection results in bulk conductivity modulation

2.4 Small signal response of Schottky barrier diodes

In the last section, the response of Schottky barriers to a dc voltage has been described. However, most of the important applications of the Schottky barrier diode involve time varying signals, either small signal or large signal. The responses of the diode to a small signal (sine wave) voltage superimposed upon the dc voltage is therefore one issue we wish to study. The term "small signal" implies that the peak value of the ac signal current and voltage are much smaller than the dc values.

Usually the signal responses are studied in term of small signal admittance (Y), of which the real part is related to resistance and the imaginary part is primarily related to capacitance in the equivalent circuit models. A simple approach to model the Schottky barrier diode for small signal purposes is by parameters R_j, C_j, R_B, and C_B as illustrated in Figure 2.6(a) [34][35][36][37]. The device admittance can be represented either by a parallel or series equivalent circuit as shown in Figure 2.6(b).

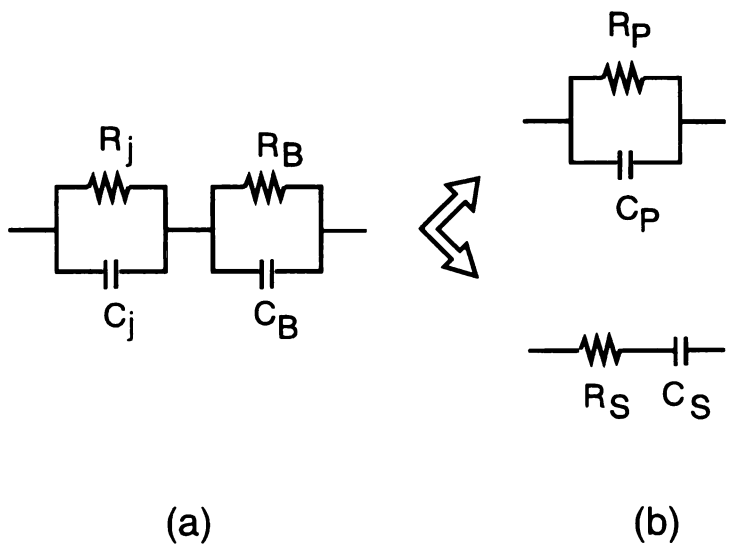

Figure 2.6 (a) Schottky barrier diode is modeled by a combination of C_j, R_j, C_B and R_B. (b) The measurement circuit can then be represented by parallel or series equivalent models.

As in the last section, the bulk resistance of the diode is labeled as R_B. However, under time varying signals, we also need to consider the capacitive effect from the geometry of the bulk part. R_B is then modeled in parallel with capacitance C_B. This combination is in series with the depletion region, which modeled by the parallel combination of a small-signal resistance Rj, and capacitance C_j.

The capacitance C_j of a Schottky barrier is associated with its depletion region, which in some respects resembles a parallel-plate capacitor with a separation between the plates that increases when reverse bias is applied and decreases with forward bias [27]. Such phenomenon is caused by a change in the depletion layer width. Consider the depletion region at some fixed value of reverse bias voltage V_J. For a Schottky barrier diode, the depletion width is given by [32]

$$W = \left[\frac{2\varepsilon}{qN} \left(V_{bi} - V_J - \frac{kT}{q} \right) \right]^{1/2} \tag{2.7}$$

Where V_{bi} is the difference between the work function of metal and semiconductor and N is the semiconductor dopant concentration, assumed to be uniform. With a small signal superimposed, V_J is replaced by (V_J+v_j) and W changes by an increment ΔW. The depletion-region capacitance C_j is obtained from the parallel plate capacitance formula as

$$C_j = \frac{\varepsilon A_e}{W} \tag{2.8}$$

where ε is the dielectric constant of material and A_e is area of the diode. The above equation, however, is valid provided W is essentially fixed; that is, ΔW must be small compared to W [83]. For a small signal $|v_j| << |V_J|$, then $\Delta W << W$ gives

$$C_j = \left[\frac{q\varepsilon A_e N}{2(V_{bi} - V_J - kT/q)} \right]^{1/2}$$

The above equation is often generalized and written in term of the zero-biased junction capacitance C_{jo}. At $V_J = 0$; then the definition of C_{jo} is as follows

$$C_{jo} = C_j|_{V_J=0} = \left[\frac{q\varepsilon A_e N}{2(V_{bi} - kT/q)} \right]^{1/2} \qquad (2.9)$$

This gives

$$C_j = \frac{C_{jo}}{\left[1 - \frac{V_J}{V_{bi}}\right]^{1/2}} \qquad (2.10)$$

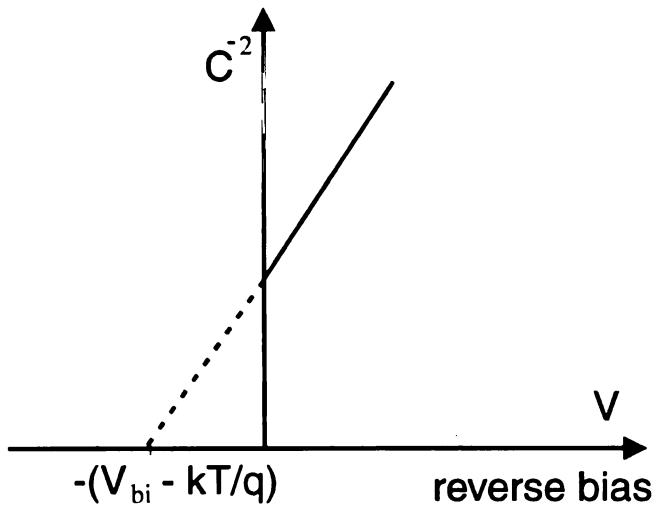

Figure 2.7 Variation of $(1/C_j)^2$ with reverse bias V_J for Schottky barrier diode [27]

If N is constant throughout the depletion region, a plot of $(1/C_j)^2$ versus V_J should give a straight line with an intercept of $-(V_{bi}-kT/q)$ on the voltage axis as shown in Figure 2.7.

The depletion region resistance R_j of Schottky barrier diode is derived under the assumption that the carriers are able to response to the signal quasi-statically; that is the carriers return to near steady state in much less time than the period of the signal. Thus, the diode reacts instantaneously to a small signal (v_j) superimposed on the dc value (V_J) and the time-dependent response can be treated as a series of dc solutions at incremental step [24][38]. The diode Equation 2.1 with the perturbed small signal is then becomes

$$I(V_J + v_j) = I_O[\exp(q\,(V_J + v_j) / kT) - 1]$$

And the small signal current i is defined as $i = I(V_J+v_j) - I(V_J)$. By Taylor series expansion, keeping only first two terms, i can be written as

$$i = v_j\left[\frac{dI}{dV_J}\right]$$

The small signal conductance of the junction is defined from above equation as

$$G = \frac{i}{v_j} = \frac{dI}{dV_J}$$

By differentiating the ideal diode equation, $I(V_J) = I_O[\exp(q\,V_J/kT) - 1]$, we obtain the small signal conductance as

$$G = \frac{dI}{dV_A} = I_O \frac{q}{kT} \exp\left(\frac{qV_J}{kT}\right) = \frac{q}{kT}(I + I_O)$$

Then the junction or "dynamic resistance" R_j can be obtained from the reciprocal of G

$$R_j = \frac{1}{G} = \frac{kT}{q(I + I_0)} \approx \frac{kT}{qI} \tag{2.11}$$

As can be derived, according to circuit in Figure 2.6, the Schottky barrier diode can be represented in either parallel or series equivalent circuit model with the following parameters

$$\begin{aligned} C_P &= \frac{C_j R_j^2 + C_B R_B^2 + \omega^2 R_j^2 R_B^2 C_j C_B (C_j + C_B)}{(R_j + R_B)^2 + \omega^2 R_j^2 R_B^2 (C_j + C_B)^2} \\ R_P &= \frac{(R_j + R_B)^2 + \omega^2 R_j^2 R_B^2 (C_j + C_B)^2}{(R_j + R_B) + \omega^2 R_j R_B (C_j^2 R_j + C_B^2 R_B)} \end{aligned} \tag{2.12}$$

and

$$\begin{aligned} C_S &= \left(\frac{\omega^2 R_j^2 C_j}{1 + \omega^2 R_j^2 C_j^2} + \frac{\omega^2 R_B^2 C_B}{1 + \omega^2 R_B^2 C_B^2} \right)^{-1} \\ R_S &= \left(\frac{R_j}{1 + \omega^2 R_j^2 C_j^2} + \frac{R_B}{1 + \omega^2 R_B^2 C_B^2} \right) \end{aligned} \tag{2.13}$$

Here ω is the frequency of the small signal, C_j and R_j are the depletion region capacitance and dynamic resistance respectively, R_B is the bulk series resistance associated with the

neutral region of the semiconductor as described in section 2.3, and C_B represents the capacitance of this bulk part of the diode (between the depletion region and the ohmic contact). If L is the total length of the diode, C_B can be calculated from

$$C_B = \frac{\varepsilon A}{L - W} \tag{2.14}$$

Let us examine the two limiting cases.

(I) At low frequency ($\omega \rightarrow 0$), C_P in Equation 2.12 becomes

$$C_P(0) = \frac{C_j R_j^2 + C_B R_B^2}{(R_j + R_B)^2}$$

The value of $C_P(0)$ depends whether the diode is under forward or reverse bias. Under reverse bias, R_j is very large due to small reverse bias current; $R_j >> R_B$. As a result, $C_P(0) \rightarrow C_j$. However, if the diode is under forward bias, R_j is small ($R_j << R_B$). Then $C_P(0) \rightarrow C_B$.

(II) At high frequency ($\omega \rightarrow \infty$), C_P in Equation 2.12 instead becomes

$$C_P(\infty) = \frac{C_j C_B}{C_j + C_B} = \frac{(\varepsilon A)^2 \left(\frac{1}{W}\right)\left(\frac{1}{L-W}\right)}{\varepsilon A \left(\frac{1}{W} + \frac{1}{L-W}\right)} = \frac{\varepsilon A}{L}$$

This means $C_P(\infty)$ approaches the geometrical capacity of the whole diode regardless of the bias condition. Figure 2.8 shows the typical C_P responses one would expect from the model of Figure 2.6(a) and the above limiting cases [39].

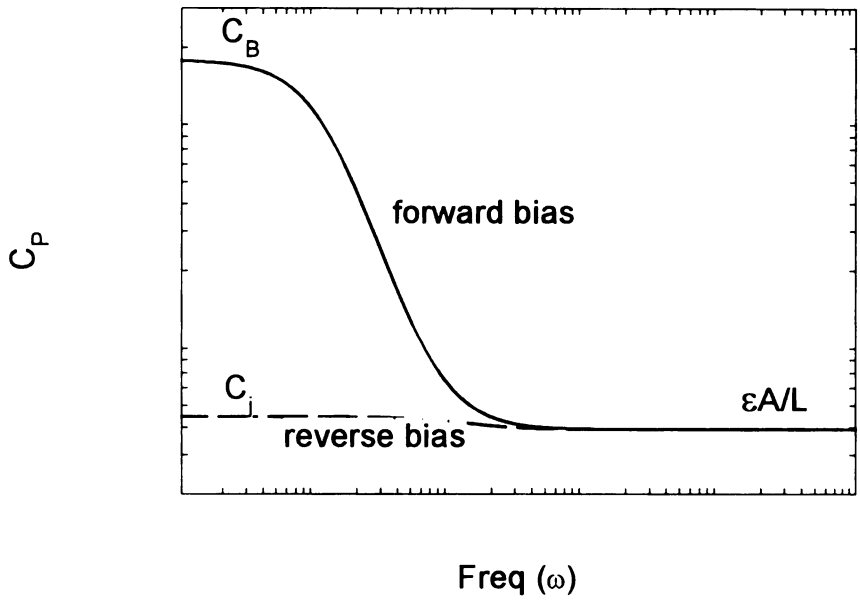

Figure 2.8 Anticipated log-log plots of C_P versus frequency from Equation 2.12 under forward and reverse bias

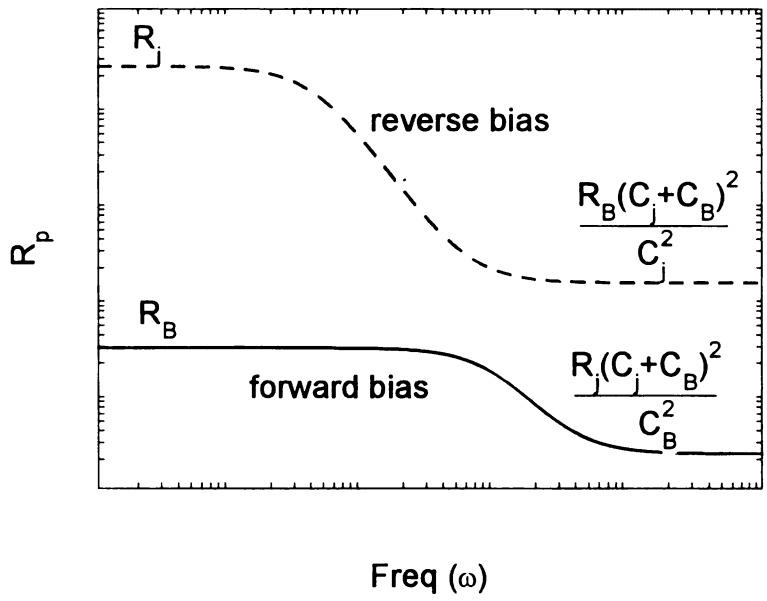

Figure 2.9 Anticipated log-log plots of R_P versus frequency from equation 2.12 under forward and reverse bias

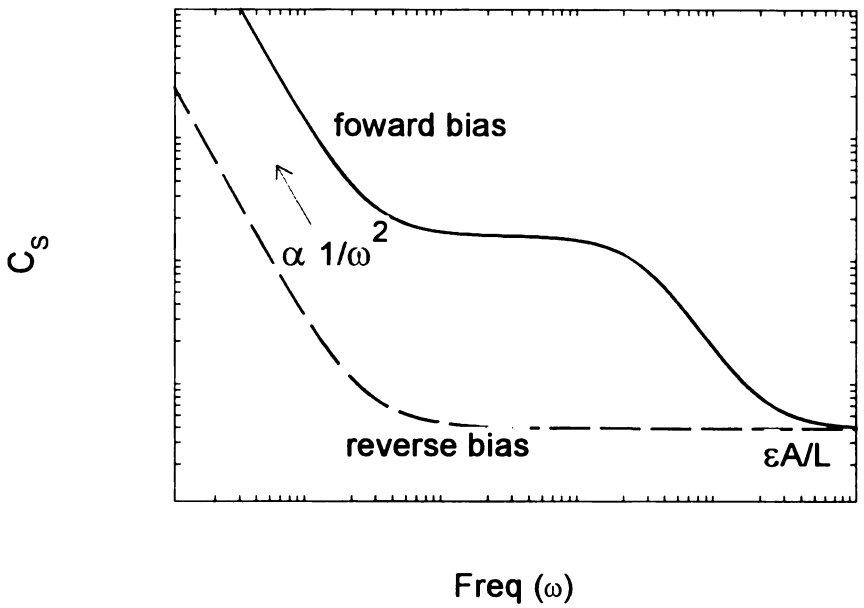

Figure 2.10 Anticipated log-log plots of C_S versus frequency from equation 2.13 under forward and reverse bias

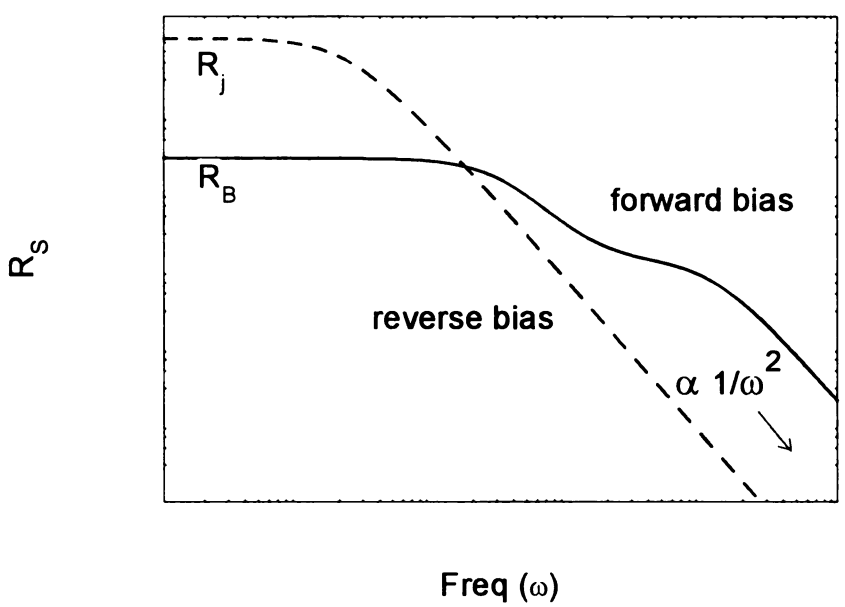

Figure 2.11 Anticipated log-log plots of R_S versus frequency from equation 2.13 under forward and reverse bias

We can also explore the two limiting cases of R_P.

(I) At low frequency ($\omega \rightarrow 0$), R_P in Equation 2.12 becomes just (R_j+R_B). The value of $R_P(0)$ again depends on the bias condition of diode. Under reverse bias, $R_j >> R_B$. Thus, $R_P(0) \rightarrow R_j$. Under forward bias, $R_j << R_B$ then $R_P(0) \rightarrow R_B$.

(II) At high frequency ($\omega \rightarrow \infty$), R_P in Equation 2.12 now becomes

$$R_P(\infty) = \frac{R_j R_B (C_j + C_B)^2}{(C_j^2 R_j + C_B^2 R_B)}$$

$$\rightarrow \frac{R_B (C_j + C_B)^2}{C_j^2} \quad ; \text{ reverse bias } R_j >> R_B$$

$$\rightarrow \frac{R_j (C_j + C_B)^2}{C_B^2} \quad ; \text{ forward bias } R_j << R_B$$

Typical R_P responses one would expect from the model of Figure 2.6(a) and above limiting cases are illustrated in Figure 2.9. By same consideration, we can reach the limiting cases result for C_S and R_S shown in Figure 2.10 and 2.11 respectively.

2.5 Large signal response of Schottky barrier diodes

In circuit applications, Schottky barrier diodes are also often used as a switch which is "ON" when the diode is conducting in forward direction and "OFF" or non-conducting when a reverse potential is applied to the devices. Consider a forward bias voltage V_f applied to the circuit so that the Schottky barrier diode is the ON state carrying a current $I_f \approx V_f/R_L$, where the current is limited by a circuit load resistance R_L much greater than the diode junction and series resistance. Now consider that the potential is

suddenly reversed in an attempt to place the diode into the non-conducting OFF state. At low forward bias, the minority carrier injection level in a Schottky barrier diode is negligible [33] and the entire switching current is due to discharge of the junction and parasitic capacitance. Figure 2.12 gives an idealized plot of the reverse-recovery current through the load resistor R_L as a function of time [24].

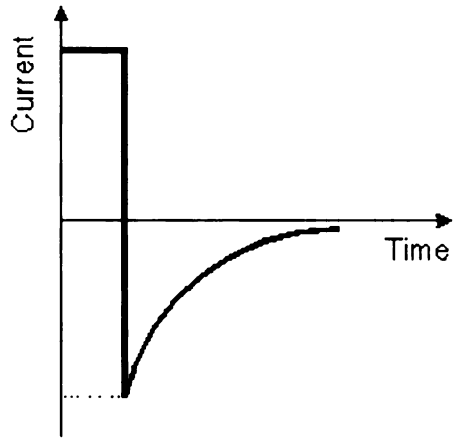

Figure 2.12 Idealized Schottky barrier diode switching waveform [33]

Again at high forward bias voltage, minority-carrier effects have been reported to become significant in Si Schottky diodes. Injection of minority carriers leads to excess carrier storage in the bulk of the diodes. Consequently, upon rapid switching from forward to reverse bias, a reverse current flows while the excess carriers stored in the quasi-neutral regions are being swept out [38]. This removal process of the excess minority carriers induces a switching delay time. Integration of the reverse-recovery current yields the total charge associated with excess minority carriers stored in the diode

prior to switching. Figure 2.13 shows the switching current of a high-injection recovery involving minority carrier discharge.

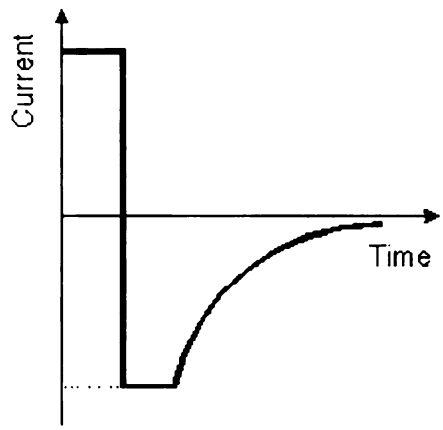

Figure 2.13 Reverse-recovery waveform involving minority-carrier discharge [33]

Krakauer [65] developed a measurement method to observe the response of the diode to large-signal sinusoidal inputs. Figures 2.14 and 2.15 show SPICE [26] simulation results of the response of a diode to sinusoidal excitation. Figure 2.14 shows the response of a device with purely capacitive charge storage corresponding to a linear reverse-recovery current. Figure 2.15 shows the response of a device in which some minority carrier storage is present. As shown in this figure, the reverse-recovery current due to excess minority carriers can easily be distinguished from the linear capacitive current. Krakauer developed an expression for a figure of merit concerning the excess minority carrier storage in the device, which is related to the exciting frequency, the source voltage, the impedance involved in the test circuit and the ratio of I_f to I_r as shown in Figure 2.15.

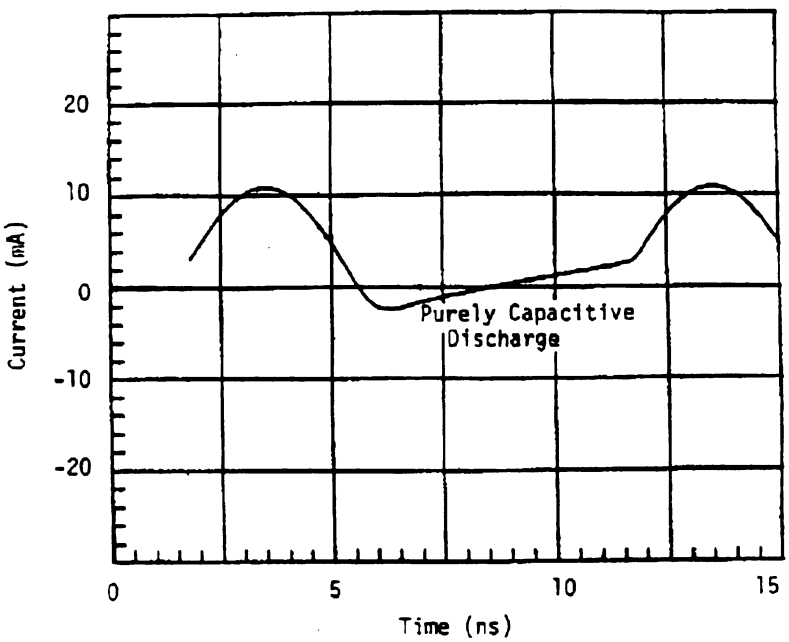

Figure 2.14 SPICE simulation results for the current through a diode excited by a sinusoidal signal when minority carrier storage is not present [29].

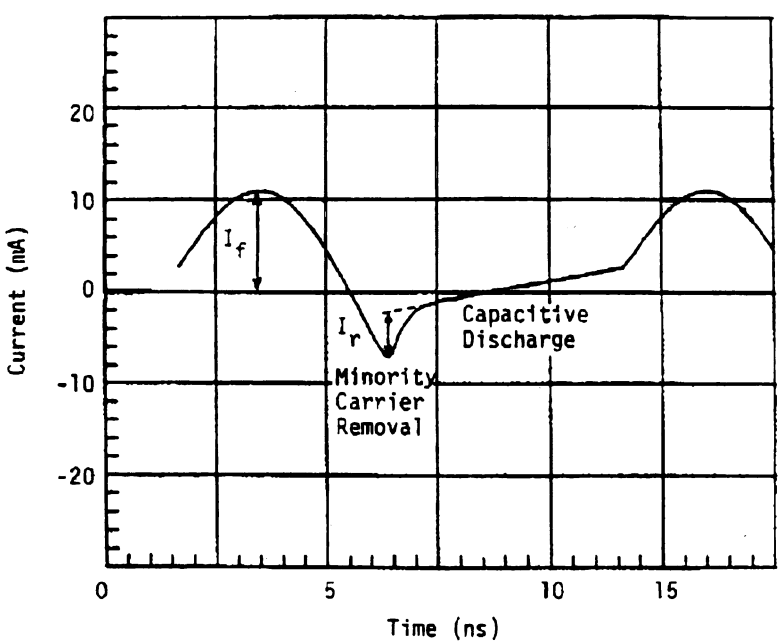

Figure 2.15 SPICE simulation results for the current through a diode excited by a sinusoidal signal when minority carrier storage in diode is significant [29].

2.6 Electrical properties of diamond

For years diamond has been known as a promising material for several types of semiconductor devices. In the past decade, a renewed interest in electronic applications of semiconducting diamond has stemmed from the development of the chemical vapor deposition (CVD) processes for the growth of thin diamond film.

Diamond, when considered as a semiconductor material, possesses a unique combination of desirable electrical and physical properties (see Table 2.1). Two distinct advantages of diamond over other semiconductors are its high thermal conductivity and high electric field breakdown. The higher the thermal conductivity, the more power a device can dissipate for the same temperature rise. The wide energy gap of diamond (E_g = 5.45eV at 300K) is responsible for the high breakdown field [20]. This combined with the surface stability of diamond at high temperatures (500-600 °C in air) [40] makes it an ideal candidate for high temperature device applications. In this respect, it is notable that diamond also has higher carrier mobilities than other wide band gap semiconductors (i.e. SiC, GaP, AlAs) at both room and higher temperature [20]. Other advantages of diamond include a high saturation velocity, i.e. the velocity at which electrons move in a high electric field, which is nearly 3 times of Si and GaAs,

The intrinsic material limits to electronic performance are usually compared in term of figures of merit. Two commonly used figures of merit are Johnson's figure of merit and Keyes's figure of merit. Johnson's figure of merit (JFM) is defined as [40]

$$JFM = \frac{E_c v_s}{2\pi} \qquad (2.15)$$

where E_c is the breakdown field and v_s is the charge carriers saturation velocity. The JFM for diamond is roughly about 90 times higher than the corresponding value for Si. Note that in some publications JFM is defined as $(E_c v_s/2\pi)^2$ so that a ratio of $(JFM)_{diamond}$ to $(JFM)_{Si}$ of 8206 is often quoted. The JFM is useful for predicting the suitability of a semiconductor for operating with large internal electric fields, such as in power devices [41]. JFM comparisons for other semiconductors are listed in Table 2.1.

Keyes's figure of merit (KFM) is used to estimate a material's potential for digital or high-speed circuits. As defined by Keyes,

$$KFM = \lambda\left(\frac{cv_s}{4\pi\varepsilon_r}\right)^{1/2} \qquad (2.16)$$

Where λ is the thermal conductivity, c is the velocity of light in vacuum, and ε_r is the dielectric constant of the material. The ratio of $(KFM)_{diamond}$ to $(KFM)_{Si}$ comes out to be 32.2 [40]. Compared to other materials, as shown in Table 2.1, the KFM indicates that diamond has the potential of being one of the best materials for digital or high-speed devices.

Intrinsic diamond, that is, diamond in its pure form with no impurities, is electrically insulating at room temperature. This is because the energy gap is sufficiently large that hole and electron concentrations are negligible. Resistivities of highly pure diamond have been measured in the 10^{12} Ω-cm range and above. However, band conduction can occur if impurities or defects act in such a way so as to introduce either holes in the valence band or electrons in the conduction band.

Properties	Si	GaAs	SiC	Natural diamond	Polycrystalline diamond
Band gap, E_g (eV)	1.11	1.43	2.3	5.45	
Intrinsic resistivity, ρ (Ω.cm)	$2.5x10^5$	$4x10^8$	10^{10}	10^{16}	
Dielectric constant, ε_r	11.8	13.2	10.2	5.5	6.7 [42]
Electron mobility, μ_n ($cm^2/V.s$)	1350	8500	1000	2200	
Hole mobility, μ_p ($cm^2/V.s$)	480	400	50	1600	2.8-10 [21]
Break down field, E_B (10^5 V/cm)	3	60	40	100	1 - 10 [43]
Saturated electron velocity (10^7 cm/s)	1.0	2.0 (peak)	2.5	2.7	
Thermal conductivity, λ (w/cm.K)	1.45	0.5	5	20	4 - 21.8 [44]
Thermal expansion coefficient, κ (10^{-6}/°c)	2.6	5.9	4.7	1.1	
Lattice constant, a (Å)	5.43	5.65	4.36	3.57	
Density (g/cm^3)	2.33	5.31	3.21	3.52	
Melting point (°c)	1420	1238	Sublimes above 1800	Turn to graphite above 1200	
Johnson 's figure of merit (ratio to silicon)	1.0	6.9	1137.8	8206.0	
Keyes 's figure of merit (ratio to silicon)	1.0	0.5	5.8	32.2	

Table 2.1 Comparison of semiconductor properties for Si, GaAs, SiC, natural diamond and polycrystalline diamond [2][9][22][45][46]

For example p-type diamond results if boron, from column-III of the periodic table, is introduced as an impurity which substrates for carbon atoms in the diamond lattice. Boron doped diamond is found in nature (although rarely). Boron can also be introduced into natural or synthetic diamond by ion implantation [3] [17] [21] or can be incorporated into diamond films by adding boron during the CVD process. The resistivity of boron doped diamond can be on the order of 1 Ω-cm or less.

Interestingly, many CVD diamond films are found to be p-type even without the introduction of column-III impurities such as boron. The resistivity of such films is substantially lower than insulating diamond, but not as low as diamond which has been heavily doped with boron. The origin of this p-type behavior has been the subject of speculation. One view is that it is associated with the role of hydrogen in the films. The effects of atomic hydrogen in passivating inter-band states in various semiconductors, such as amorphous silicon and polycrystalline silicon, have been well established. In case of natural diamond crystals and CVD diamond films, Landstrass and Ravi [47] postulate that the resistivity of hydrogenated diamond is governed by shallow acceptor levels, whereas removal of the hydrogen activates deep donors, pinning the Fermi level and giving rise to high resistivity.

In contrast to the situation for p-type diamond, creation of n-type diamond has been extremely difficult. Column-V dopants are generally not effective as n-type dopants in diamond because the donor levels that they introduce are far removed from the conduction band edge. Although some researchers have reported the achievement of n-type diamond, the quality of the doping is at best much less than for p-type diamond.

Therefore, bipolar devices that require both n and p-type doping would be difficult to achieve at this time entirely in diamond. Most device work has focused on uni-polar or majority carrier devices including Schottky diodes or Field Effect Transistors (FET's). This dissertation focuses on the former. A brief review of previous works on diamond Schottky barrier diodes follows.

2.7 Diamond Schottky barrier diodes

Both ohmic and rectifying contacts are required in Schottky barrier diode fabrication. The electrical properties of metal-to-diamond film contacts depend strongly on the properties of the diamond film and surface treatment (such as heat treatment, and chemical cleaning). For example, Grot et al. [48] have shown that surface preparation plays an important role in determining the characteristics of metal contacts on diamond surface. They reported that exposure of boron-doped diamond CVD film surface to a hydrogen plasma resulted in ohmic I-V characteristics of the Au/diamond contacts regardless of the doping level.

In many reports, silver paint or a damaged surface have been used for establishing ohmic contacts on semiconducting diamond. In some cases, the contacts were annealed to reduce contact resistance. Moazed et al.[45] [49] studied the formation of Ti, Ta, Mo, and Mo/Ni contact on natural boron-doped diamond. A layer of 100-150 Å of the metal followed by a 1500 Å layer of protective Au was employed. An ohmic contact was obtained following an anneal at 885 °C for 8-16 minutes in a hydrogen ambient. Geis [2] found that In forms ohmic contacts to diamond without high-temperature processing or

ion implantation. However, the low melting temperature (156 °C) of In makes it impractical for high-temperature devices. In the case of polycrystalline CVD diamond deposited on silicon wafers, there are reports by Grot et.al [50], Gildenblat et al. [40] and Huang and Reinhard [43] that the silicon wafer also acts as an ohmic back contact to the polycrystalline CVD diamond.

For films with high doping [2] or high defect densities [43], contacts are basically ohmic because any depletion layers at the contact are sufficiently thin to allow adequate tunneling current. Geis [51] observed that ohmic contacts can be obtained on heavily boron-doped (10^{21} cm^{-3}) natural diamond with several metals. Similar results have also been reported for polycrystalline diamond films. For films of higher purity, however, the depletion layer is larger allowing the formation of electrical samples with rectifying characteristics.

Rectifying contacts have been reported forming on naturally occurring semiconducting diamond crystals [17], on synthetic boron doped crystal [19], on CVD grown homoepitaxial films [40][48][52], and on CVD grown polycrystalline films [40][50][53]. These contacts have been formed by using point contacts [95] or by evaporation of films of various metals, e.g. Pt[17], Al [13][53][54], and Au [50][52], provided the contact area is small (typically less than 1 mm^2). The defective nature of typical CVD diamond films is thought to lead to excessive leakage across Schottky barriers when contact areas are significantly larger than this, giving rise to (poor) ohmic characteristics [52][55].

Varying reports exist for diamond-metal barrier height values. Hicks [56] and Gildenblat [20] have measured barrier heights of 1.13 eV for Al contacts on

polycrystalline undoped diamond films using internal photoemission spectroscopy. Other groups also reported a similar result on Au [20][50][57]. Trew [9], however, noted that the height of the potential barrier is essentially independent of the metal due to surface pinning and has value in the range of 1.3-1.7 eV. It should be pointed out that barrier heights are difficult to determine from current-voltage (I-V) or capacitance-voltage (C-V) measurement on undoped CVD diamond films since the contacts deviate widely from ideal behavior as a result of high bulk resistivity [15][58]. To reduce the high series resistivity, Ebert et al. [59] successfully used a p^+-doped diamond substrate for the homoepitaxial growth of the p-doped active layer. The structure of metal/undoped diamond/p-doped diamond has also been reported by Kang et.al [15].

Diamond Schottky barrier diode dc characteristics have been studied by several researchers. These tests have demonstrated diamond Schottky diode to be capable of operating under very high temperature up to 1000 °C [52][60][61]. A high breakdown voltage of 400 V has been reported by Jeng and Tuan [13] for Al/polycrystalline CVD films. Gildenblat et al. reported that the breakdown voltage exceeded 200 V at 300 K on Au/CVD films. An example of dc I-V characteristic of an Au/ polycrystalline CVD diamond is shown in Figure 2.16.

By using the thermionic emission / diffusion model, Hicks [56] and Jeng [13] reported an ideality factor of 1.8 and 1.85 at room temperature for Al/CVD diamond respectively. However, at an elevated temperature of 1000°C, Vescan et al. [61] reported an ideality factor close to unity (η=1.01) on Au / CVD diamond film, clearly showing thermal emission dominated the forward I-V characteristics. This has been confirmed by the reduction of ideality factor from 1.8 to 1.1 while the temperature was elevated from

100 to 500 °C reported by Ebert et al. [16] on Au / p-doped CVD diamond. Kang et al. [15] also reported the reduction of ideality factor from 2.4 to 1.1 while the temperature increased from 25 to 300 °c on Au / undoped diamond/ p-doped diamond structures.

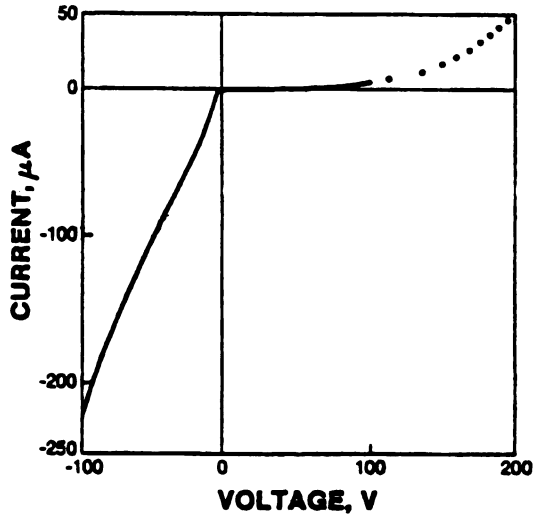

Figure 2.16 Current-voltage characteristics of an Au/CVD diamond Schottky diode [20]

2.8 Time varying signal response of diamond Schottky barrier diodes

When a small-signal voltage is applied to an electrical sample such as a diamond Schottky barrier diode, the resulting current is characterized by both an amplitude and by a phase relative to the applied voltage. The results may be expressed mathematically by a complex admittance (ratio of current to voltage) where the real part corresponds effectively to a measured small-signal sample conductance and the imaginary part corresponds effectively to a measured small-signal sample capacitance.

Small-signal capacitance versus voltage (C-V) methods have been used by several groups to study the small-signal responses in semiconducting diamond [15][17][18][19] [20][21][62][63]. Glover [19] did a thorough analysis of the reverse-biased C-V behavior of Schottky diode form on natural, single-crystal type IIb diamond. He found an anomalous frequency dependence of the capacitance versus voltage and derived a model, which included both deep level traps and bulk resistivity effects, to explain the phenomenon. He found that the results could be represented by a series circuit consisting of two capacitors C_j and C_f and two resistances R_f and R_B as shown in Figure 2.17.

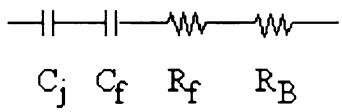

Figure 2.17 Glover's Schottky barrier diode model is represented by combination of C_j, C_f, R_f and R_B.

Comparing this model to the simple model of Figure 2.6, C_B is now missing because for Glover's bulk samples, C_B is negligible. Also Rj is not included by Glover because for his reverse biased samples it is very large. Thus C_B and R_j are replaced by open circuits in Glover's model. The elements C_j and R_B in Glover's model are the depletion layer capacitance and bulk diamond resistance as in Figure 2.6. In addition to these, Glover added C_f and R_f as additional elements. C_f and R_f were included to model hole emission from slowly responding deep levels.

From a theoretically analysis, Glover found that C_f is proportional to $\omega^{-1/2}$. He expressed his measured capacitance, C_m, as

$$C_m(V,\omega,T) = \frac{C_T}{1+(\omega R_T C_T)^2}$$

$$\frac{1}{C_T} = \frac{1}{C_j(V)} + \frac{1}{C_f(\omega,T)} \qquad (2.17)$$

$$R_T = R_f(\omega,T) + R_B(T)$$

The simulation result of his work is shown in Figure 2.18. According to his model it could be seen that at low frequency, measurement capacitance C_m approaches C_j. However, at high frequency two cases could be distinguished depending on the value of R_B. When R_B is small, the term $\omega R_T C_T \rightarrow 1$, so that $C_m = C_f/2$, therefore the measurement C_m falls off with frequencies as $\omega^{-1/2}$. When R_B is large, however, the second term of C_m in Equation 2.17 dominates, so C_m depends on frequency as $\omega^{-3/2}$.

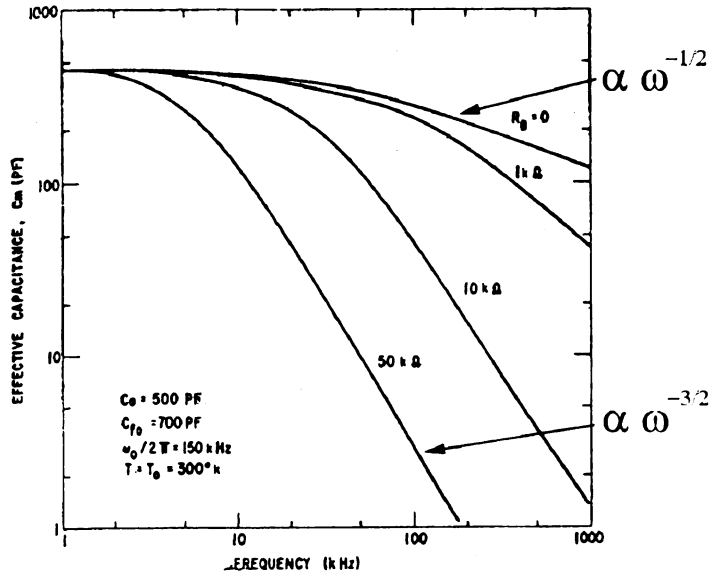

Figure 2.18 Model plot from Glover's publication [19]

Kang et al. [15] applied Glover's equations to their experiment on metal/undoped diamond/p-doped polycrystalline diamond structures with a modified term in

$$\frac{1}{C_T} = \frac{1}{C_I} + \frac{1}{C_j(V)} + \frac{1}{C_f(\omega, T)}$$

where C_I was needed to account for the contribution of the capacitance by the undoped diamond layer. No fitting comparison between model and experimental results have been made but the $\omega^{-1/2}$ and $\omega^{-3/2}$ fall off were confirmed by their experimental results. They also concluded that the fall off in capacitance at high frequency was due to the high series resistance of the diode.

Gildenblat et al. [18][20] obtained a very similar frequency dependence to that obtained on single crystal diamond by Glover for their Schottky diodes fabricated using

Au and Al contacts on thin CVD polycrystalline diamond films. A model for the equivalent circuit was proposed by the authors (see Figure 2.19), very similar to that of Glover, which agreed qualitatively with their experimental results. Because of the thin film nature of their samples, it was necessary to add the component C_g due to the contribution of geometric capacitance from the bulk part of the sample. Note that in Gildenblat's model, C_O and Cg correspond to C_j and C_B in Figure 2.6.

C-V characteristics of Schottky diodes, fabricated using sputter-deposited Ag contacts on boron doped polycrystalline diamond thin films grown by hot filament CVD, were studied by Zhao et al. [64]. The results obtained for these diodes were very similar to those of Schottky diodes fabricated using a single-crystal diamond substrate by Glover.

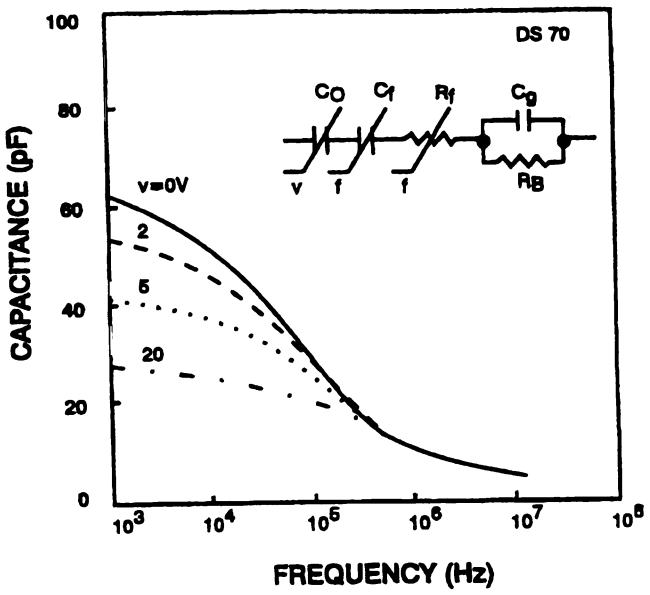

Figure 2.19 Frequency dependence of the capacitance of Au/CVD diamond contact for different reverse biases giving an equivalent circuit as in the insert; Gildenblat [18]

The frequency dependence in the C-V measurements of both type IIb naturally boron-doped crystals and polycrystalline diamonds were investigated by von Windheim et al. [21] using good ohmic back contacts, achieved by B ion implantation followed by an Ag paste contact. The authors observed that the frequency dependence significantly reduces after back contact implantation. From the analysis of their experimental results they concluded that a poor back contact has a strong effect on high frequency measurements and may be at least partially responsible for the frequency dependence observed on diamond by Glover [19] as opposed to trapping effects. This view argues against the use of R_f and C_f in a circuit model.

Differential C-V measurements as a function of frequency were also performed on Al and Pt rectifying contacts on natural type IIb diamonds by Venkatesan et al. [17]. The sample preparation was very similar to that of Glover. However, in some samples, the backsides of the diamond are exposed to B ion implantation. Again, the effects of back contact capacitance and resistance, the size and shape of the Schottky contact, and the bulk resistance of diamond on the frequency dependence of the measured capacitance of rectifying contacts were reported. The authors observed a frequency-dependent capacitance that decreased significantly after reducing the back contact impedance. A circuit model without deep level traps was proposed by the authors to explain the phenomenon as in Figure 2.20.

In the circuit of Figure 2.20, C_S is the specific capacitance of the Schottky barrier, R_B is the series bulk resistance of the diamond. The effects of the ohmic contact were represented as a parallel combination of C_c and R_c. However, the C_c-R_c combination was,

according to authors, negligible and only C_S and R_B were used to model the sample with reduced back contact impedance.

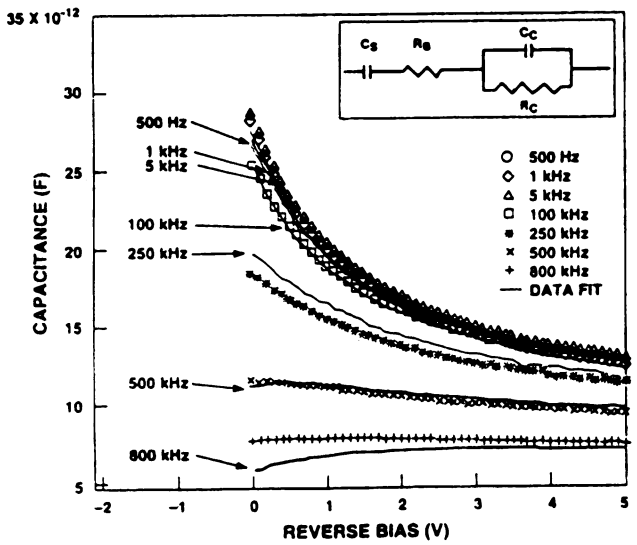

Figure 2.20 Frequency dependence of the capacitance of Al/natural diamond contact for different reverse biases giving an equivalent circuit as in the insert; Venkatesan [17]

To summarize the small signal C-V studies on diamond Schottky barrier diodes, some studies (e.g. Glover's) indicate that traps play an important role in understanding the experimental results, requiring the addition of R_f and C_f to the circuit model. Other results (e.g. Venkatesan) indicate that such elements are not necessary and indicate that the model of Figure 2.6 should apply. In this study the issue is explored further by investigating the entire small signal admittance, not just capacitance, at both reverse and forward bias.

Finally, in terms of large signal ac response, the author is not aware of previous studies. The results of this investigation on large signal (switching) responses of diamond Schottky barrier diodes are described later in this dissertation.

CHAPTER 3

Experimental Methods

3.1 Chapter overview

This chapter presents the details of how samples were grown, electrically contacted and characterized. It starts by describing the substrate preparation prior to the diamond film deposition. The microwave plasma–assisted chemical vapor deposition system and process is briefly described and typical process parameters for the diamond growth are given. The formation of ohmic and rectifying contacts on the samples is then discussed followed by the probe system setup description. The last three section of this chapter give details on equipments, measurement setup and processes for electrical dc characteristics measurement, small signal response and large signal response of diamond Schottky barrier diodes.

3.2 Substrate preparation for diamond growth

Diamond has been reported to be successfully grown on several substrates such as diamond (homoepitaxy), Si, nickel and sapphire (polycrystalline) [40] [66] by other researchers. Consequently, there are a number of candidate substrates for a study of this

type. Ready availability, the ability to form a back ohmic contact with the diamond polycrystalline film, and adequate mechanical support for the thin film diamond made silicon (Si) a good choice of substrate for this study. Due to the low nucleation density on non-diamond substrate ($\sim 10^4$ cm^{-2}), the silicon substrate was treated to enhance nucleation density. There are several techniques to enhance and control nucleation density on Si wafers described in the literature such as diamond photo-resist coating [67], abrasion seeding [68], ultrasonic agitation technique [69], and bias enhanced nucleation [70]. However, only first two methods have been utilized to nucleate the Si substrate in this study.

Before Si substrates were seeded for the diamond deposition, they were first cleaned and weighed. The Si substrates were cleaned by rinsing the substrates with acetone followed by methane and finally with de-ionized water. Each rinsing step took approximately 2 –3 minutes to ensure the thoroughness. The substrates were then dried with a nitrogen blowgun. The weight gain of the substrates after the deposition compared to before the deposition was used to approximate the average thickness of the deposited diamond films. The Si wafers were either 2-inch or 3-inch diameter and were p-type, (100) orientation, and with resistivities in the range of 0.01 – 20 Ω-cm

3.2.1 Nucleation by the diamond photo-resist

Diamond photo-resist seeding was developed at Michigan State University by Masood et.al. [67] [71] as a method of patterning or selectively seeding desired areas of the substrate with diamond powder. The process basically consists of the following steps:

(1) diamond powder is mixed in the photo-resist solution, (2) the solution is spun on the substrate using wafer spinner, and (3) the substrate is baked in an oven. If needed, the photo-resist can be patterned by lithographic processing to selectively remove diamond seed from the substrate afterward.

In this study, ultra virgin natural diamond 0-1/10 μm powder from Amplex Corp. was utilized with Shipley 1813 photo-resist and type-P Shipley photo-resist thinner in order to seed a few of the earlier samples by the author and Khatami [72]. However, all of the later samples were prepared by abrasion seeding described in next section.

3.2.2 Nucleation by diamond powder abrasion seeding

The general technique of abrasion seeding or "scratch-treatment" on Si substrates to control nucleation density involves abrading the substrate with micron-sized diamond particles and following a debris removal process. Sufficient nucleation density to produce fine-grain continuous diamond films has been reported by H. Windischmann [68]. In Windischmann's process, a small amount of 1 μm diamond powder was sprinkled on the substrate. The substrate was then polished by hand with a laboratory paper tissue (Kimwipe^{TM}). The excess diamond powder was rinsed away with methanol.

One possible reason why diamond nucleates on the diamond scratched surface is that during the scratch-treatment, small amounts of diamond particles are left on the surface. Work by S. Iijima et.al [73] showed that tiny (less than several tens of nanometers) clumps of sp^3 carbon may remain after the debris removal. However, it has been demonstrated that diamond nucleation is also possible on substrate that are

scratched with non-diamond powders [74]. Another study by P. A. Dennig [75] concluded that diamond nucleation can be linked to the modification of the silicon surface.

In this study, adequate nucleation density to yield continuous diamond films were successfully obtained on Si substrates by scratching with ultra virgin natural diamond 0-1/4 μm powder from Amplex Corp. The scratching process was accomplished by the author and Ulczynski [76] by rubbing the substrates, which are sprinkled with diamond powder, with Kimwipe^{TM} tissue. After approximately 2-3 minute of thoroughly rubbing in a circular motion on the substrate surface, the remaining diamond powder was wiped away and blown clean with a nitrogen gun. The seeded substrates were then rinsed with acetone followed by methane and finally with de-ionized water. Each rinsing step took approximately 2 –3 minutes to ensure thoroughness. Finally the rinsed substrates were blown dry with a nitrogen blow gun.

As mentioned earlier, only a few earlier samples were seeded by the photo-resist process, all later samples were fabricated using scratch-treatment since the scratch-treatment is somewhat simpler for nucleating our un-patterned Si wafers. Another advantage of scratch-treatment is that nucleation occurs from structures created on the silicon substrate [74] [75] or from very small sp^3 fragments rather than from relatively large diamond particles which could themselves be defective from the start. Scratch-treatment nucleation can also avoid question of the contamination effects from photoresist etch during diamond deposition. It was also noted that the scratched seeding give finer-grain films than that of photo-resist seeding films.

3.3 Diamond growth

All diamond films used in present research were prepared by the microwave plasma–assisted chemical vapor deposition (MPACVD) process. Details of the MPACVD process for the diamond deposition in the microwave cavity plasma reactor (MCPR) have been described by Huang [46], Zhang [77], Kuo [78], Khatami [72], and Ulczynski [76]. The MCPR acronym is commonly applied to a particular variation of Asmussen [79] reactors. This research used samples grown by Khatami, by Ulczynski, and by the author. The main features of the deposition system and process used by the author are briefly described here.

Figure 3.1 shows the simplified schematic diagram of the deposition system constructed by Ulczynski [76]. The body of the MCPR's cavity is a brass cylinder with water cooling on the base plate. The upper end of the cylinder is terminated by a movable sliding short with the end-feed microwave-coupling probe. Microwave energy is introduced into the system via this probe. The length of the probe inside the cavity is adjustable. The length of cavity can also be varied by the sliding short. These features make it possible to match the impedance of the cavity to the microwave power source. A perforated stainless steel screen is affixed to the base plate in the bottom part of the cavity to terminate the cavity and still allow gas to flow through.

The plasma is contained inside a quartz bell jar, which is vacuum sealed to the base plate. The stainless steel sample holder is placed on top of two cylinder quartz tubes with an insert stainless steel disk between the tubes.

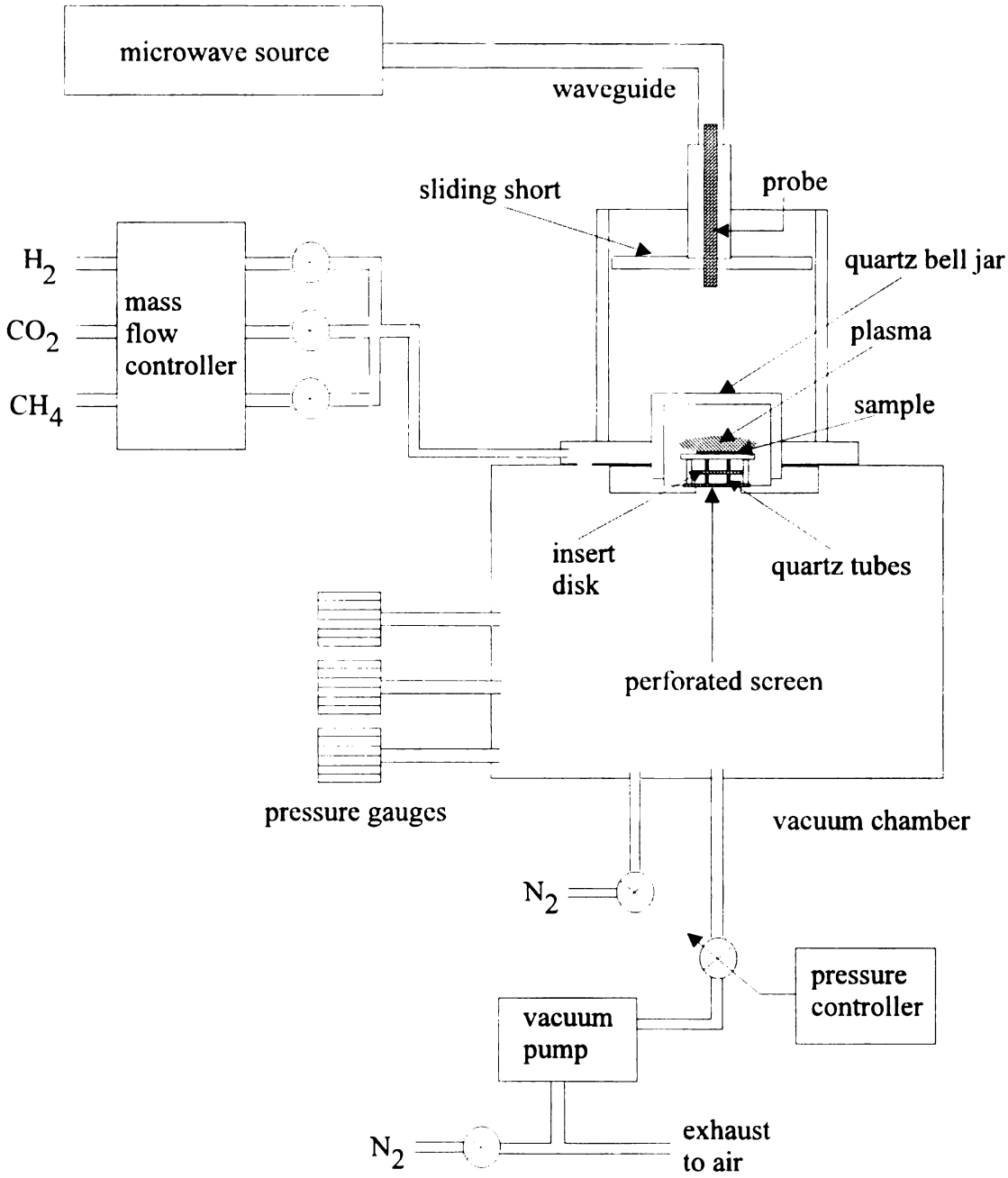

Figure 3.1 The simplified schematic diagram of the microwave plasma–assisted chemical vapor deposition (MPACVD)

The mixture of H_2, CH_4 and optional CO_2 is uniformly distributed to the system through a common gas inlet in the base plate. The flow rate of all gases is precisely adjustable by a computerized mass flow controller. The sample can be accessed to be loaded/unloaded from the large stainless steel vacuum chamber below the base plate and the quartz bell jar. The pressure measurement within the vacuum system is performed through a system of four vacuum gauges. Each gauge is set to measure pressure in different range, ranging from mTorr vacuum to above an atmosphere.

The pressure level in the system is adjusted by a computerized throttle valve controller which is connected to a mechanical pump. The pump is filled with Acatel 200 oil, which is safe for pumping hydrogen and methane gases. Due to the explosive nature of H_2 and CH_4, nitrogen gas is mixed into the exhausted gases before releasing them to the atmosphere. Nitrogen is also used to purge and backfill the vacuum chamber after the deposition process.

It should be noted that a leak/outgas check was not performed for every deposition run in this research. However at various times, the leak/outgas rate of the entire system (approximately 70 liters in volume) was between 0.1 to 1 mTorr/min. To find the effective flow rate of leak/outgas in the system, let us consider the following flow unit conversion [80] [81]

sccm	=	1 cm^3/min at standard pressure 760 Torr and standard temperature 300 K (STP)
scc/sec	=	1 cm^3/sec at STP
mTorr	=	0.001 Torr = 1 μ Hg (or μ) (very nearly)

μ liter/sec = liter/sec at a pressure of 1 μ

Thus, 1 scc/sec = 760 μ liter/sec.

For a leak rate of 1 mTorr/min in a 70 liter chamber, the flow rate of leak in the system becomes

$$\frac{1\ \text{mTorr}}{\text{min}} \times 70\ \text{liter} = \frac{1\mu \times 70\ \text{liter}}{60\ \text{sec}} = 1.17\ \frac{\mu\,\text{liter}}{\text{sec}}$$

$$\frac{1.17\ \dfrac{\mu\,\text{liter}}{\text{sec}}}{760\ \dfrac{\mu\,\text{liter}}{\text{sec}}} = 1.54 \times 10^{-3}\ \frac{\text{scc}}{\text{sec}} = 9.2 \times 10^{-2}\ \text{sccm}$$

or roughly 0.1 sccm. Thus, leak rate 0.1 to 1 mTorr/min corresponds to effective leakage of approximately 0.01 to 0.1 sccm. As a result a non-negligible amount of gases such as N_2 and O_2 in the atmosphere are also incorporated into at least some of the samples used in this research.

Throughout this research, the range and typical values of deposition parameters used by the author were varied or fixed as in table 3.1 to explore variation in electronic quality of the diamond films. In addition, some higher temperature samples grown by other investigators were also used in this study. The thickness of diamond films used in this research was from 0.3 μm to 8 μm.

Gas composition	CH_4:H_2 = 1.5 – 5 % CO_2:H_2 = 4% (optional)
Gas flow rate	H_2 = 200 sccm CH_4 = 3 – 10 sccm CO_2 = 0, 8 sccm
Operation pressure	7 – 25 Torr
Microwave power	1000 W
Substrate temperature	470 – 520 °C

Table 3.1 Typical deposition parameters used in the diamond film deposition process.

3.4 Diamond film characterization with Raman Spectroscopy

Raman Spectroscopy has been widely used to characterize diamond quality. A sharp narrow peak at 1332 cm^{-1} is characteristic of diamond and often interpreted as an indication of high quality diamond film. Graphitic carbon produces a broad band Raman signal centered around 1580 cm^{-1}. However, it should be noted that the ratio of intensities of the diamond peak to the graphitic carbon centered is not proportional to the ratio of the diamond to non-diamond components in the films. This is because the Raman scattering efficiency is typically 50 times greater for sp^2 bond (graphitic carbon) than sp^3 (diamond).

The Raman analysis system in this study most often used an Argon laser with a wavelength of 514 nm. The configuration and operation of this Raman system is well documented by J. Mossbrucker [82]. In some samples, the Raman spectroscopies were also obtained using a Kaiser Optical System Inc. Raman system. This second system uses the 532 nm doubled Nd:YAG laser. The Raman spectrum of a polycrystalline film is shown in Figure 3.2. The spectrum shows a distinct peak around 1332 cm^{-1}, which is the signature of crystalline diamond. The broad characteristic arch between 1350 and 1580 cm^{-1} of graphitic carbon is almost absent from the spectrum. This indicated a good quality diamond thin film on the Si substrate.

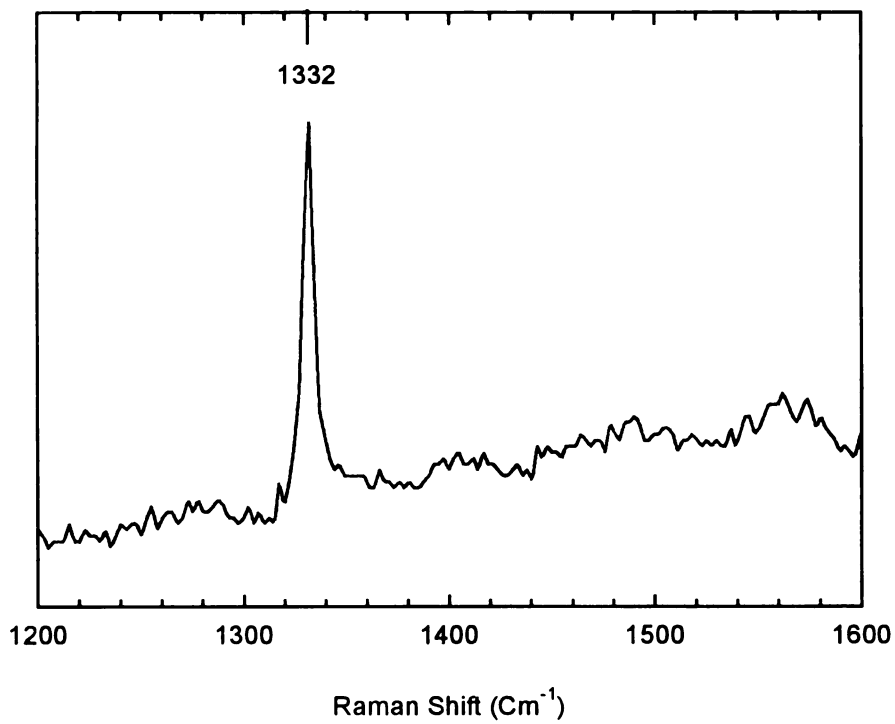

Figure 3.2 Raman spectrum of a polycrystalline diamond film on Si substrate, BC4 observed by 532 nm Nd:YAG laser.

3.5 Metalization

Metalization on diamond surfaces has been studied by many researchers due to its importance in electrical characterization of diamond films. As mentioned in chapter 2, two general categories of metals have been used by researchers in this area, namely carbide and non-carbide forming metals. Carbide forming metals such as Ti, Ta and Mo were shown to give ohmic contacts while non-carbide forming metals tend to give rectifying contacts on diamond surface.

Schottky barrier diodes require one ohmic contact and one rectifying contact. In this research, Schottky diodes are generally fabricated in a sandwich structure with the diamond film between a back ohmic contact and a top rectifying contact (see Figure 3.3).

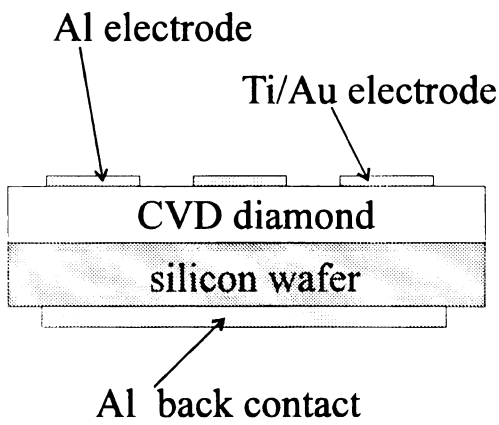

Figure 3.3 Drawing show cross-section view of one example of a diamond Schottky diode structure

The silicon wafer acts as an ohmic back contact [83] [50] as well as giving the mechanical support to the diamond thin films. After diamond deposition was performed on the Si wafers surfaces, aluminum was thermally evaporated onto the whole bottom side of the substrates as a conduction path. This allowed electrical measurements to be made in the direction perpendicular to the diamond surface.

The top rectifying contacts were formed by thermally evaporated aluminum [13] [17] [18] [20] [50] [52] [84] electrodes (1200 - 1800 Å thick) on the diamond film surface through a shadow mask. The rectifying contact area evaporated on diamond surfaces were between $4x10^{-4}$ to $2x10^{-3}$ cm^2.

Alternatively, in some samples, 100 - 200 Å of titanium followed by 1200 - 1600 Å of gold as a protective layer are deposited through a shadow mask forming the ohmic contacts [45] [49] [52] [58] on the top diamond surface with contact areas of $4x10^{-4}$ - $5x10^{-2}$ cm^2. All evaporation in current study was done under 10^{-6} torr vacuum. The metal deposition rates on the sample were controlled to be 12 - 18 Å/sec for Al and Au and 5 - 8 Å/sec for Ti. The samples were hold in the water-cooled substrate holder to prevent sample heating during the evaporation.

Although research suggests that annealing processes can improve the quality of diamond as observed by Raman spectroscopy [40] [85], there was no annealing performed before or after the metalization process in this study in fear of increasing the resistivity of diamond films. Landstrass [47], Vandersande [11] and Sugino et.al. [85] [86] showed that annealing process could cause a several order increase in resistivity of polycrystalline diamond film. The study of McKeag et.al. [55] also showed a reduction in rectification ratio on diamond Schottky barrier diode after 400 °C heat treatment in air.

3.6 Probe station setup

All of the electrical measurements on diamond Schottky barrier diodes in this study were performed on a Signatone S-1160 station. The S-1160 is a general-purpose analytical probe station designed for probing various geometries down to 1 μm in size. To protect the measurements from any photo-conductive noise signal, the probe station was shielded within a Signatone light-tight box model PSDB-1160. Eight feed through BNC connectors were attached on the side of the light-tight box to provide high frequency electrical access from the test equipment outside.

In order to test devices under different temperature, the probe station was equipped with a Signatone QuieTemp temperature-controlled chuck model S-1060 and a NESLAB re-circulating chiller model CTF-33. A measurement temperature from 10 to 350 °C can be achieved with this setup. Under the normal measurement process, a circular quartz disk, 3 mm thick, was placed on the top surface of the temperature-controlled chuck. This allowed heat transfer between chuck and samples placed atop, while the samples were isolated from the electrical circuit and noise of the chuck below.

Special high-speed microprobes, GGB model 10, were used with this probe station to conduct measurements up to approximately 1 MHz. The limitation range of operation for these microprobes is dc to 3.5GHz.

3.7 DC characteristics measurement setup

A Hewlett Packard model 4145B semiconductor parameter analyzer was used to measure the dc current-voltage characteristic of the diamond Schottky diodes. It is equipped with four programmable Source/Monitor units (SMU's). Each SMU can be set up to function as a voltage source/monitor, current source/monitor, or source common. A simplified circuit diagram of a SMU is illustrated in the Figure 3.5. By setting one SMU as a variable voltage source and another SMU as a common current source; the dc current-voltage characteristic of the diodes can be obtained by two-point probe measurement. The HP4145B can monitor current resolution as low as 0.05 pA with the maximum range of ±105 mA.

In this study, all dc measurements are conducted in the light-tight box. Figure 3.6 shows a schematic diagram of the measurement setup. SMU3 is used as a variable voltage source, and SMU1 is used as a common current return path.

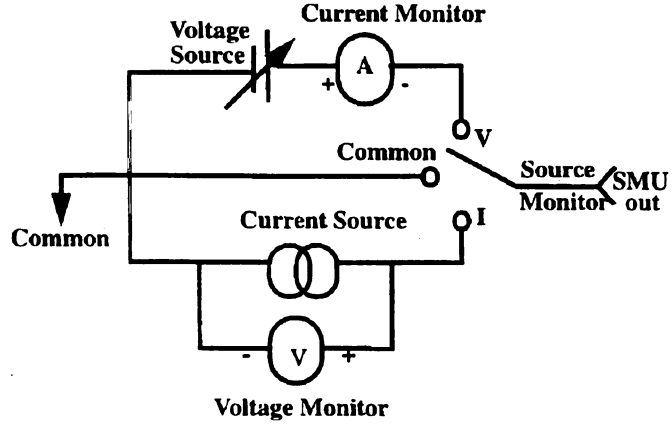

Figure 3.5 A simplified circuit diagram of a SMU unit of HP4145B

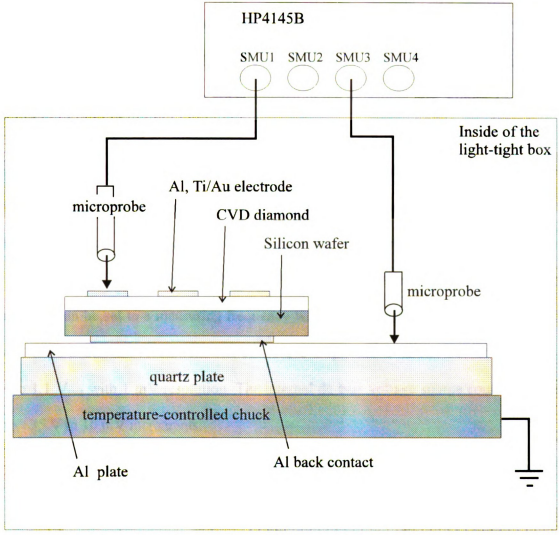

Figure 3.6 Schematic diagram of dc measurement setup

3.8 Small signal response measurement setup

The ac small signal responses of the Schottky barrier are measured by a HP4192A LF impedance analyzer and a HP4284A precision LCR meter; both controlled by a computer. Again all measurements are conducted in the light-tight box. Figure 3.7 shows the schematic diagram of the measurement setup.

The Hewlett Packard model 4192A LF impedance analyzer was primarily used earlier in this research to measure the small-signal response in terms of capacitance, C and the resistance, R of diamond Schottky diodes at various frequencies and bias voltages. The internal frequency synthesizer of HP4192A provides a sinusoidal wave test signal that can be set to a measuring frequency which may range from 5 Hz to 13 MHz with 1 mHz maximum resolution. The sine wave amplitude level can be varied from 5 mV to 1.1 V_{rms} with 1 mV resolution. The internal dc bias voltage source could provide up to ±35 V in 10 mV increments.

The HP4192A provides measurement in two equivalent circuit models, the parallel or the series modes. The instrument has four terminals, two current terminals: H_{CUR}, and L_{CUR}, and two potential terminals: H_{POT}, and L_{POT} The test signal is output from the H_{CUR} terminal as shown in the Figure 3.8. The purpose of the current terminals is to cause a measurement signal to flow through the sample, and the potential terminals are used to detect the voltage drop across the sample.

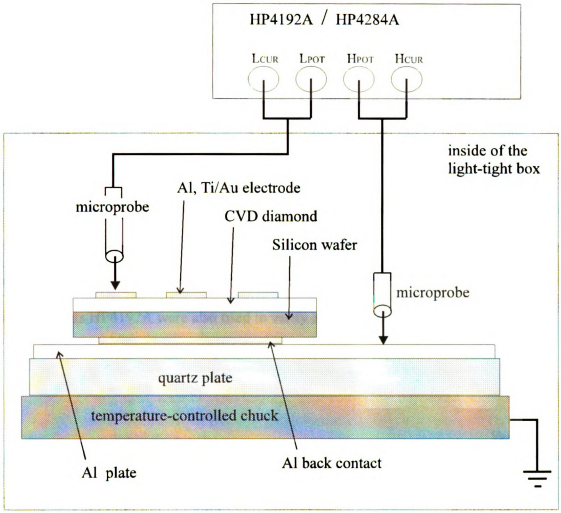

Figure 3.7 Schematic diagram of the small signal measurement setup

In this research, to compose a measurement circuit loop in a four-terminal pair configuration, the H_{CUR} and H_{POT} , L_{POT} and L_{CUR} terminals were connected together respectively and, in addition, the shields of all conductors were also connected together as shown in Figure 3.8. This four-terminal method provided the shielding required for high-impedance, high-frequency measurements. Since the same current flow through both the center conductors and the outer shield conductors (in opposite directions, hence canceling each other), no external magnetic fields are generated around the conductors.

As mention above, the HP 4192A LF impedance analyzer was used earlier in this research. Later measurement were performed by the HP4284A precision LCR meter due to convenience of use and simpler computer controlled capability. However, in selected measurements HP4192A were also used to verify and cross-check the experimental data.

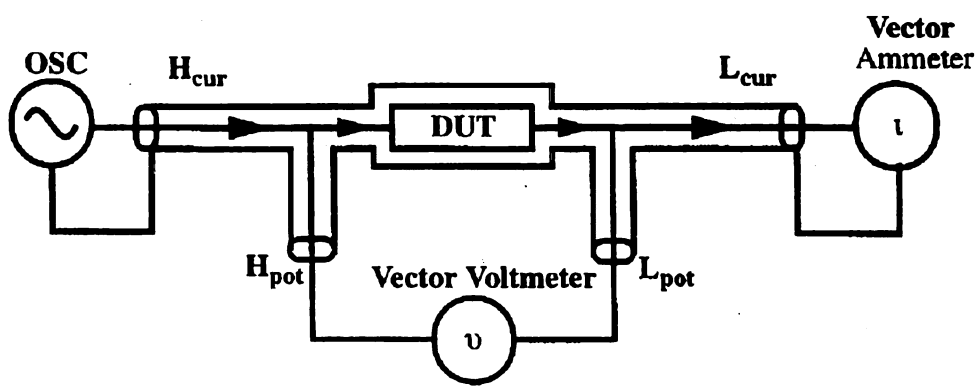

Figure 3.8 A simplified circuit model of four-terminal pair configuration of HP4192A

The Hewlett Packard model 4284A performs similar to the HP4192A. It measures the capacitance, C and the resistance, R of diamond Schottky diodes over a wide range of frequencies (20 Hz to 1 MHz) and test signal level (5 mV to 20 V_{rms}, 50 μA to 100 mA_{rms}). The HP4284A offers C-R measurement with a basic accuracy of ±0.05% at all test frequencies. The measurement ranges of C and R for this instrument are 0.01fF to 9.99999 F and 0.01 mΩ to 99.99MΩ respectively. Similar to the HP4192A LF Impedance Analyzer, the HP4284A offers two measurement modes, the parallel and series equivalent circuit models. Also, this instrument employs the four-terminal pair configuration : the H_C , H_P , L_P and L_C as shown in Figure 3.9.

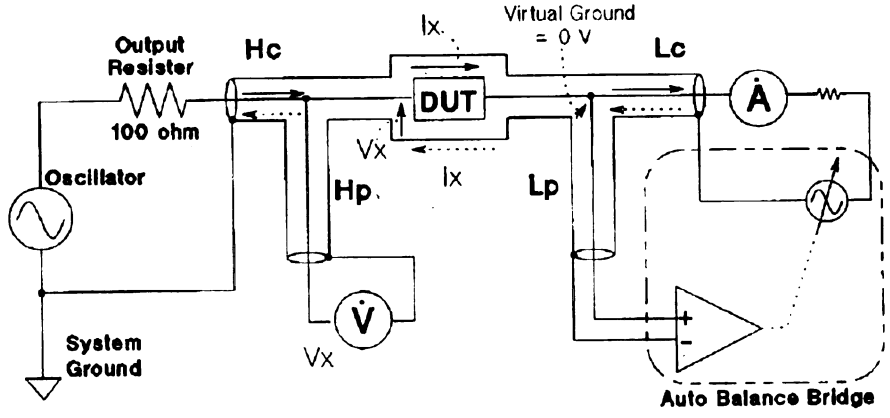

Figure 3.9 A simplified circuit model of four-terminal pair configuration of HP4284A

In this research, the instrument test frequency was increased systematically from 100 Hz to 1 MHz in each test. The center dc bias was also varied within –10 V to + 10 V, while the oscillation level was fixed at 0.1 mV. The values of resistance and capacitance of the Schottky diodes under test were measured and stored into data files. Both instruments operate so as to measure the resistance and capacitance versus frequency in both parallel (C_P, R_P) and series (C_S, R_S) equivalent circuit models.

3.9 Large signal response measurement setup

To study the diode responses to a large switching signal, a Hewlett-Packard model 8116A programmable pulse/function generator was used to generate 20 V peak-to-peak input sine waves for the test. The input signals passed through a coaxial microprobe to the test wafer. The responses of diamond Schottky diodes were then probed by the HP54200D and/or Tek11401 oscilloscopes in parallel with load resistance. The schematic diagram of the measurement setup is shown in Figure 3.10.

The specification of The Tektronix model 11401 is the following. Its main unit has a vertical accuracy of 1.0% of the volts/division setting and a time-base accuracy of 0.01% of the time/division setting. Combined with the 11A32 plug-in unit, this system provides 200 MHz bandwidth with a risetime of 1.8 ns. The 0.9% amplitude accuracy as well as 100 ps ± 0.002% horizontal time-base accuracy can be achieved at all test ranges (1mV to 10V full-scale, 20 ns to 1000 s full-interval). However, since the 11A32 plug-in unit only has input channels with 50 Ω impedance (shunted by approximately 15 pF), it is difficult to probe weak output signal from the high resistance diamond diodes.

Therefore, the Hewlett-Packard model 54200D digitizing oscilloscope was also used to investigate the large-signal switching response. This oscilloscope has two input channels with input impedance of 1 MΩ ±2%, shunted by approximately 14 pF. This much higher impedance makes it easier to detect signal from the high resistance samples. The instrument is a dedicated, multi-channel, simultaneous, waveform acquiring digital storage oscilloscope with full GPIB programmability. It has digital storage bandwidth of 50 MHz (200 megasamples/second sampling rate) with ±2% full-scale gain accuracy. The horizontal time-base measurement accuracy of the instrument is ±2 ns.

Note that a load resistance is introduced into the measurement setup to adjust the input impedance of the oscilloscope to the suitable value. It has been found that the 1 MΩ (shunted 14 pF) input impedance of the HP 54200D gave too large an RC time constant to detect the weak signal from the diamond Schottky barrier diode without distortion. The load resistance used in this research was varied between 10 KΩ to 50 KΩ. The effects of load resistance will be further described in detail in chapter 6.

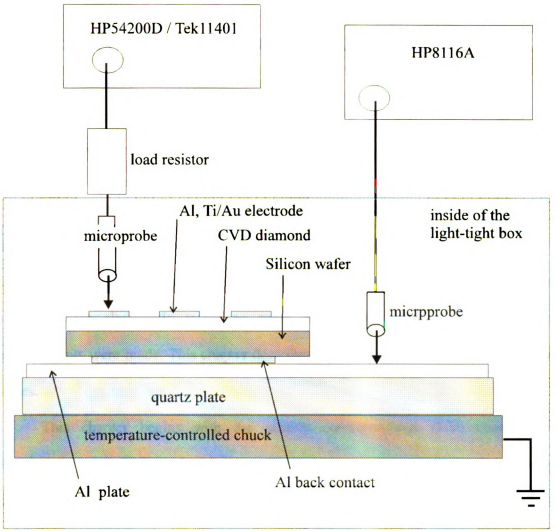

Figure 3.10 Schematic diagram of large signal switching response measurement setup

CHAPTER 4

DC characteristics of diamond Schottky barrier diodes

4.1 Chapter overview

During the course of this research, Schottky diodes were formed on over 30 different diamond substrates that were deposited under a variety of CVD conditions. On each substrate, approximately 34 diodes were formed. At least 10 diodes on each substrate were electrically tested to some extent. On selected diodes, extensive measurements were made. This chapter describes the results of dc measurement on these diodes.

This chapter begins with the general current-voltage (I-V) characteristics observed for contacts formed with two different type of metals; Ti/Au and Al contacts. Next, the diode parameters, which are ideality factor η, saturation current I_O, and bulk resistance R_B, are extracted from the dc characteristics at room temperature. The dc characteristics obtained at different temperatures are then used to yield two additional parameters; barrier height ϕ_B, and activation energy E_A. The following sections explore the roles of methane concentration in the CVD growth process, and the effects of diode area and film thickness on the dc characteristics of diamond Schottky diodes. Finally, the experimental I-V characteristics are compared with computer simulation (SPICE) results.

4.2 General Characteristics

As described in detail in chapter 3, the dc device current-voltage (I-V) characteristics are obtained by using the HP4145B semiconductor parameter analyzer. All measurements are conducted in a light-tight box. Typical I-V characteristics of the Ti/Au-diamond film-Si-Al and Al-diamond film-Si-Al structures at room temperature are shown in Figure 4.1 and Figure 4.2 respectively.

For low voltages less than 8 V, the I-V characteristics of Ti/Au are nearly linear and symmetric, as shown in Figure 4.1, as would be expected for top and bottom ohmic contacts. This shows that both the Si substrate and the Ti/Au metalization provide ohmic contacts to the diamond. For a film thickness of 0.91 μm (based on weight gain), 8 V corresponds to an electric field of 8.8×10^4 v/cm. This indicates that for electric fields below about 10^5 V/cm, the sample exhibited predominantly ohmic behavior with a resistivity that is independent of the applied voltage. Taking a film thickness of 0.91 μm and a contact area of 4.91×10^{-4} cm^2 into account, the resistivity of the diamond sample is then determined to be 72×10^6 Ω – cm.

On the other hand, for the Al-diamond structures, the results show a rectifying characteristic, indicating that the rectifying property is a result of the Al-diamond interface. This is consistent with earlier work which attributed the rectifying property to the band bending at the top contact-diamond interface [18] [46].

When two coplanar Ti/Au contacts are used to contact the diamond film, almost identical I-V characteristics are obtained regardless of the distances between the Ti/Au contacts as shown in Figure 4.3. This indicates that the current passes via the first Ti/Au-diamond ohmic contact through the diamond film to the silicon ohmic contact, through

the silicon and back up through the diamond film to the second Ti/Au ohmic contact. The resistance of the doped silicon path is negligible compared to that of diamond path. The current is, as expected, approximately half that of figure 4.1 because the path length through diamond is twice as long. This also indicates a lack of appreciable surface conduction between contacts to the diamond film.

Figure 4.4 shows the I-V characteristic between two coplanar contacts with one contact being the evaporated Al circle and the other being the Au circle. In this case, Schottky barrier diode characteristics with less forward current than the one in Figure 4.2 are observed because of the longer (essentially double) path length through the diamond film.

However, it should also be noted here that not all Al or Ti/Au contacts on the sample give exactly the same I-V data (comparing the same type of metal), despite the fact that all contacts for a given sample are fabricated under identical processing conditions. This is probably due to variation in film thickness, and in some cases, variation in the diamond quality across the wafer.

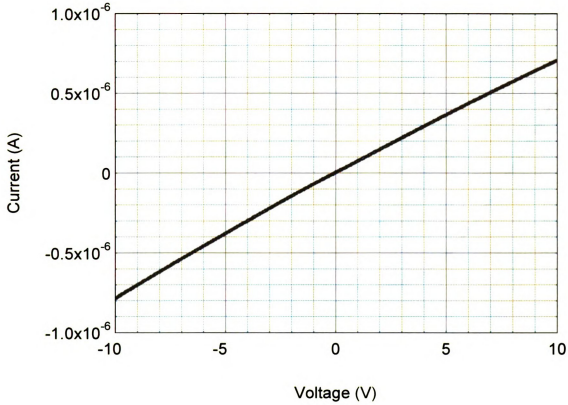

Figure 4.1. The I-V characteristic of the Ti/Au-diamond film-Si-Al samples show ohmic behavior. The above results are at room temperature.

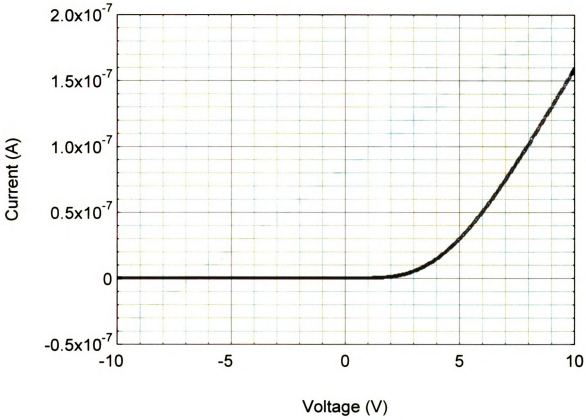

Figure 4.2. The I-V characteristics of Al-diamond film-Si-Al samples show Schottky barrier diode behavior. The above results are at room temperature.

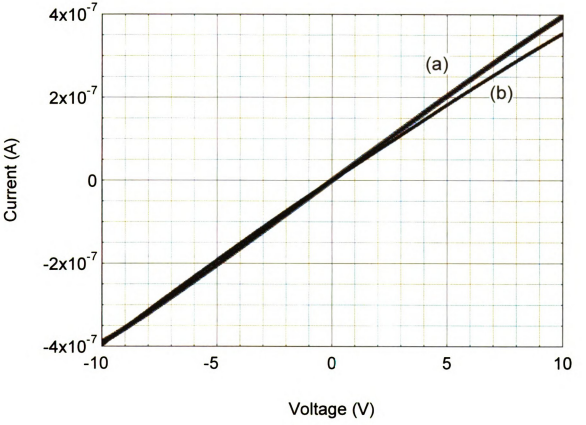

Figure 4.3. The I-V characteristics of samples with coplanar Ti/Au surface contacts show ohmic behavior. Curve (a) corresponds to 1.5 mm between two contacts and (b) 4.5 mm between the Ti/Au contacts.

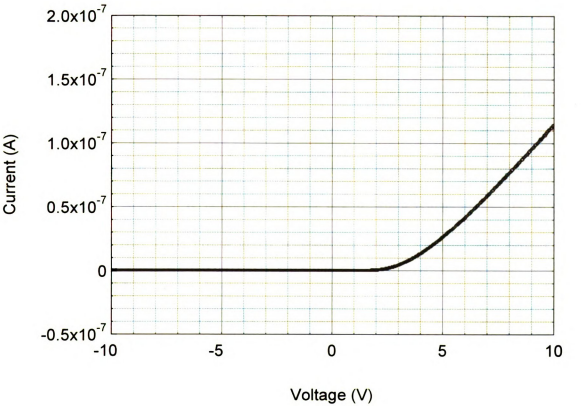

Figure 4.4. The Schottky barrier diode characteristics of a diode with coplanar surface contacts. One contact is Al and the other is Ti/Au contact.

The rectification ratio of the diode samples fabricated in this study at ±10 volt, 27 °C is found to be between 10^4 to $1.8x10^5$. This range of values is comparable to the best results previous reported [13] [83] [84], although recently Al/diamond Schottky diodes with rectification ratios greater than 10^6 have been reported [16] [87].

The current-voltage results of each diode can be analyzed by considering the device current as a function of both the voltage across the depletion-layer region, and the voltage across the bulk region. From the diode equation (Equation 2.1) in forward bias

$$I \approx I_O \exp(qV_j/\eta kT) \qquad (4.1)$$

Here V_j is the junction voltage across the depletion-layer region (junction region), η is the diode ideality factor, T is temperature, k is Boltzmann's constant, and I_O is the saturation current [22] [27]. For a given forward current, I, the junction voltage is therefore found to be

$$V_j = (\eta kT/q) \ln(I/I_O) \qquad (4.2)$$

And the bulk voltage V_B is subsequently found from

$$V_B = V - V_j$$

where V is the applied voltage. In Equation 2.3, V_B is expressed as IR_B. The value of I_O and η can be determined from the linear portion of a plot of log I versus applied voltage as shown in Figure 4.5 for a particular representative Al-diamond film-Si-Al sample BC4. At 27 °C, the ideality factor η and the saturation current I_O of sample BC4 are found to be 2.43 and 1.82 pA respectively. η values in a range from 2.4 to 4.6 were obtained for all other diamond diode samples in this study. The literature has reported a wide range of η values for diamond Schottky barrier diodes [13][15][16][56][88]. The resistivity of the bulk diamond, obtained from the plot between bulk voltage V_B and

current I of sample BC4, as shown Figure 4.6, is approximately 1.13 MΩ. Note that the value of R_B in Figure 4.6 is obtained at high bias voltage, at which the current should only be limited by the bulk resistance. R_B values in a range from $1.1x10^6$ to $5x10^{10}$ Ω-cm were obtained for all other diamond diodes in this study. This range of values is also comparable to the values in as-grown diamond reported by several others [47] [50] [85] [86] [89] [90] [91] [93] but substantially less than values of 10^{15} to 10^{16} reported by Vandersande and Zoltan [11].

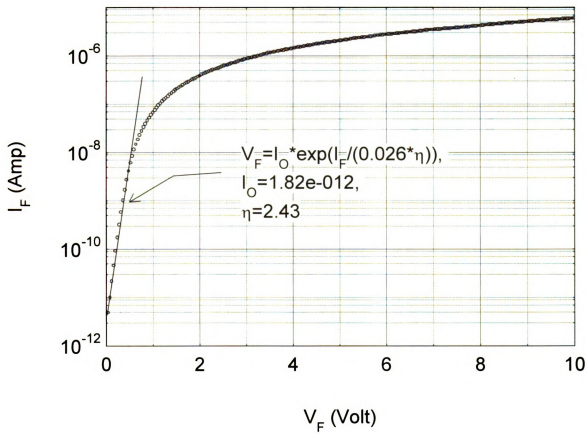

Figure 4.5 Semi-log plot of forward I-V characteristic of sample BC4. The solid line represent the least square fit of the linear portion of log (I) versus the applied voltage (V_F). The value I_O=1.82e-012 and η=2.43 result from the curve fit.

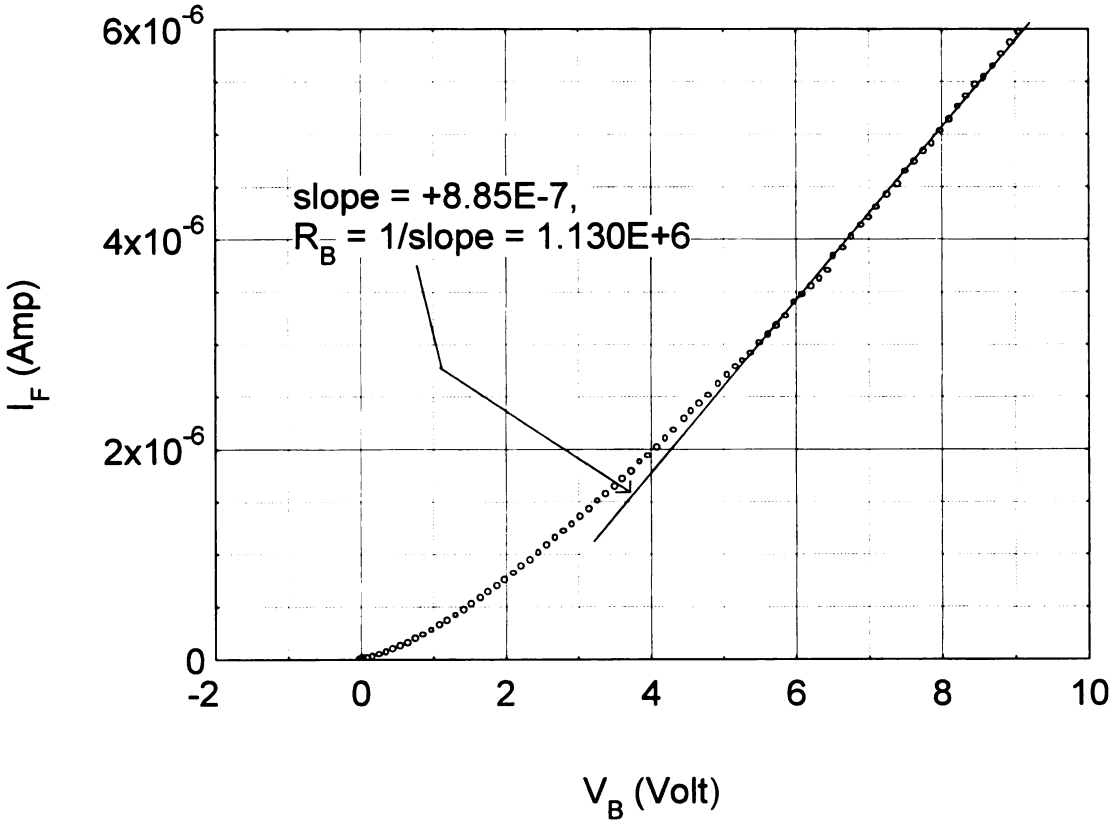

Figure 4.6 A plot of forward current versus bulk voltage of sample BC4. The solid line represents the linear least square fit at high bias portion of the bulk voltage (V_B). The value $R_B \approx 1.13$ MΩ results from the inverse value of the slope.

According to Equation 2.4, the barrier height of the Schottky diode can be determined if the value of effective Richardson's constant is known. Actually if we account only for thermionic emission, for a p-type Schottky diode

$$A^{**} = 120 \cdot \left(\frac{m^*_{lh} + m^*_{hh}}{m_o} \right)$$

where m_o is the free electron mass and m^*_{lh} and m^*_{hh} are the effective masses for light and heavy holes, respectively. To the extent that diffusion effects in the space charge layer are important, the A** theoretical values is further modified to account for an effective diffusion velocity.

However, since ϕ_B is not very sensitive to the choice of A** (see section 2.3), one can, as a first approximation, assume the theoretical value of A** based on thermionic emission theory with an effective mass of unity, that is 120 A cm^{-2} K^{-2} [15] [23]. The barrier height on BC4, using Equation 2.4, is then calculated to be 0.926 eV. The barrier height of all the samples in this research, assuming the ideal value of A**, are calculated to be between about 0.72 to 1.08 eV. Reported values in the literature for barrier height range from approximately 0.85 to 2 eV. As a point of reference, if surface states were negligible and the diamond electron affinity were zero, then the theoretical barrier height would be about 1.4 eV. However, surface states in diamond are reported to play an important role.

4.3 Temperature dependence of device parameters

The experimental current-voltage characteristics of BC4 were obtained at five temperatures for the Al-diamond film-Si-Al structure. These temperature dependent I-V characteristics of BC4 are shown in Figure 4.7. Table 4.1 contains the extrapolated saturation current axis intercept I_O, ideality factor η, and bulk resistance R_B obtained from each I-V curve (each temperature) in Figure 4.7.

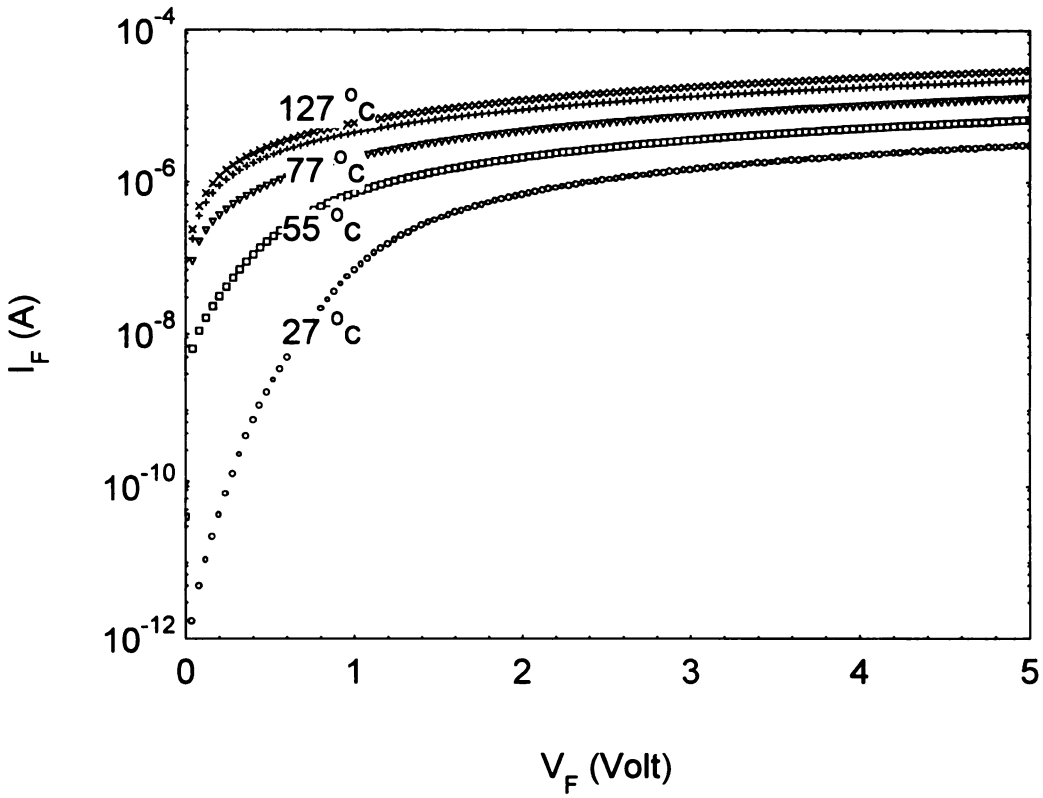

Figure 4.7 Forward I-V characteristics of BC4 in the temperature range from 27 °C to 127 °C.

Temperature (°C)	I_O (A)	η	R_B (Ω)
27	1.80×10^{-12}	2.43	1.13×10^{6}
52	2.58×10^{-11}	2.16	624×10^{3}
77	6.16×10^{-11}	2.20	356×10^{3}
102	8.14×10^{-9}	2.16	218×10^{3}
127	1.48×10^{-8}	2.06	168×10^{3}

Table 4.1 Experimentally determined saturation current, I_O, and ideality factor, η and bulk resistance R_B of BC4 at different temperature.

As can be seen in Table 4.1, the reduction of ideality factor at increased temperature reported by Ebert [16] and Kang [15] is also observed in the course of this study. As established earlier, the potential barrier height based on the theoretical A** calculation of BC4 is 0.926 eV. As described in chapter 2, the barrier height can also be determined from a Richardson plot of $\ln(I_O/T^2)$ versus (1/T). According to Equation 2.5

$$\ln\left(\frac{I_O}{T^2}\right) = \ln(A_c A^{**}) - \frac{q\phi_B}{k}\left(\frac{1}{T}\right)$$

The slope of the plot yields the value of barrier height and the intercept on the axis gives the value of the effective Richardson's constant. Figure 4.8 shows the Richardson plot for sample BC4.

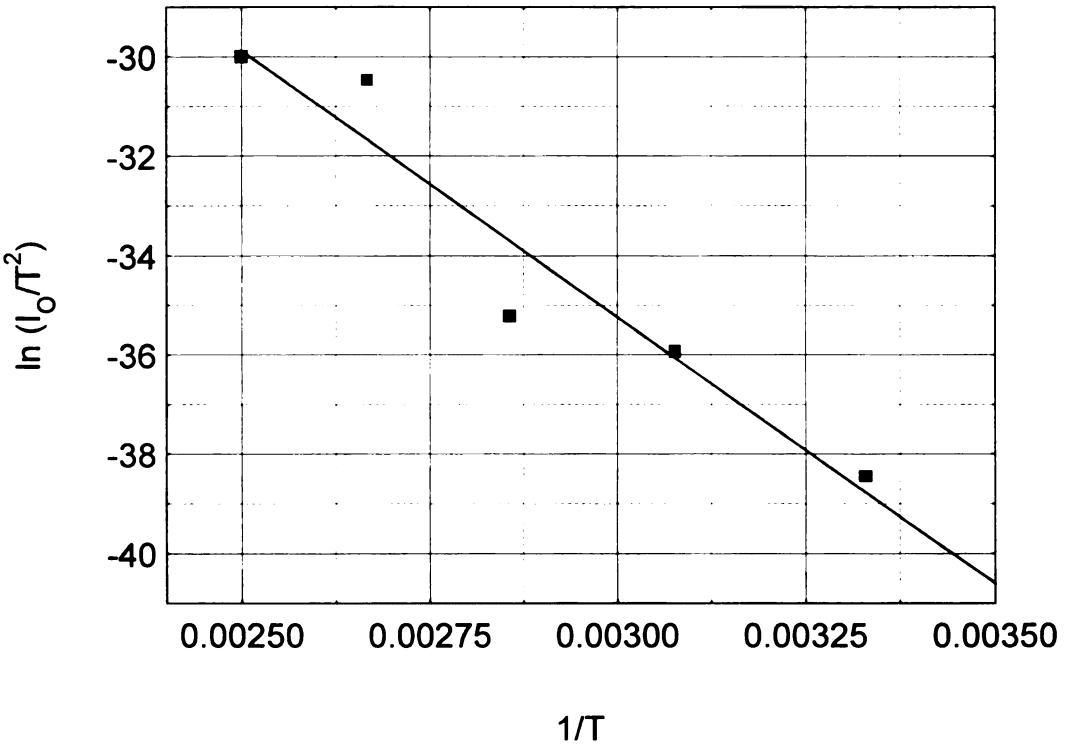

Figure 4.8 Richardson plot of BC4 over the temperature range of 27 °C to 127 °C.

The barrier height determined from the slope of best-fitted straight line is 0.923 eV. This value is close to the estimate of 0.926 eV established earlier. Given the diode area of 4.91×10^{-4} cm^2, the extrapolated interception of the plot on the vertical axis yields an A** value of 92. In comparison, H.Kiyota et.al. [28] observed an A** value of 84 for a diamond Schottky barrier diode which corresponds to a combined effective hole mass value of 0.7. It is interesting that, based on cyclotron resonance experiments [93], m^*_{lh} = 0.7 m_0 and m^*_{hh} =2.1 m_0 which would predict a larger value of A** than obtained either in this research or by Kiyota.

As described in section 2.3, a plot of $\ln(R_B)$ versus (1/T)should be linear and the slope would correspond to the activation energy (E_A) of the semiconductor. Such a plot for sample BC4 is shown in Figure 4.9. The activation energy of sample BC4 obtained from the slope of plot in Figure 4.9 is approximately 0.21 eV (above the valence band) which implies the presence of acceptor-like impurities or defects. E_A values between 0.17 to 0.24 were also obtained in other samples in this research.

For boron doped CVD diamond, the activation energy has been reported to be a strong function of the deposition conditions and the doping levels, varying between 0.013 eV, in the case of extremely heavy doping (boron concentration about 10^{20} cm^{-3}), to 0.41 eV for very lightly doped films [15] [18] [20] [92] [94] [95] [96]. The reported E_A for undoped polycrystalline diamond can range from 0.2 to 1 eV or higher depending on deposition conditions [21] [90] [96] [97]. Although the diamond films in this research were not intentionally doped, the activation energy E_A of the tested samples are at the lower end of the undoped diamond range and were in the range of doped CVD diamond.

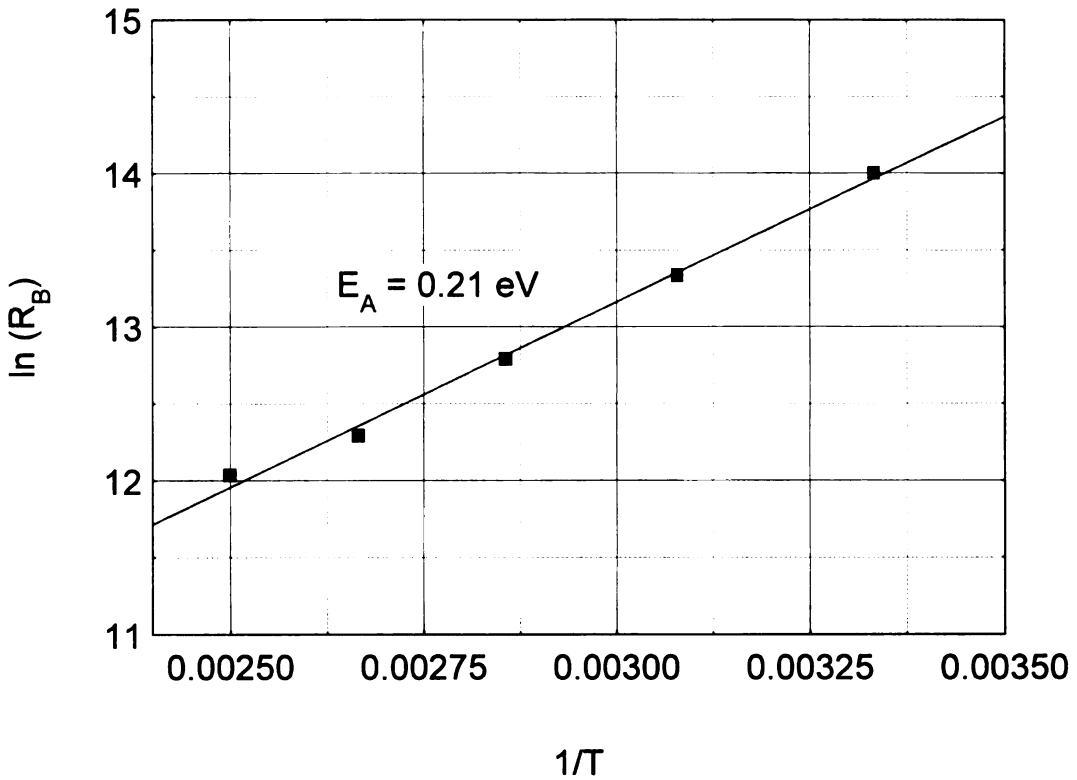

Figure 4.9 Plot of ln(R_B) versus 1/T for sample BC4 over the temperature range of 27 °C to 127 °C.

4.4 Influence of deposition chemistry on diode characteristic

Although a number of studies have been carried out to investigate the correlation between deposition parameters and morphology/quality/growth-rate of CVD diamond film [72] [78] [98], the effects of deposition parameters, such as CH_4 concentration, on diamond Schottky diode I-V characteristics have not been studied to the knowledge of the author.

For the reason that will become clear later in chapter 5, the bulk resistance of the diamond diode is preferred to be as small as possible in this research. There appear to be few reports on CH_4 concentration effect on CVD diamond resistivity. It was shown by A.T. Collins [99] that the concentration of defects increases as the concentration of methane (CH_4) increases, therefore, increasing CH_4 concentration in the CVD process should reduce film resistivity. However, film grown with CH_4 concentration higher than 5% is usually lower quality diamond based on Raman analysis [72] [78], or cauliflower-like. Such material does not produce good Schottky barriers. This research studied the role of CH_4 concentration for undoped diamond Schottky barrier diode fabrication.

For this purpose, 10 diamond films grown on silicon substrates were studied. The 10 diamond films were organized into three sets. Each set included films grown at the same H_2 flow rate, pressure, microwave input power and substrate temperature. The CH_4/H_2 concentration in each set was varied between 1.5 to 5 %. Tables 4.2 through 4.4 show the deposition parameters and some other key properties of the samples. All films were prepared for measurement in a similar way as describe earlier in chapter 3. Al is used to form the top surface contacts (contact area = 4.91×10^{-4} cm^2). Al is also thermally evaporated on to the whole backside of the sample, the silicon wafer side, to form the

ohmic contact. The I-V measurements were performed on random Al contacts of each sample in the direction perpendicular to the surface of the film.

Sample	Seeding Method	H_2 flow rate (sccm)	CO_2 flow rate (sccm)	CH_4 Flow rate (sccm)	Substrate temp (°C)	Film thickness (μm)
BC17	Scratched	200	0	3	518	1.432
BC15	Scratched	200	0	5	514	1.501
BC14	Scratched	200	0	8	514	1.446
BC13	Scratched	200	0	10	518	1.474

Table 4.2 Deposition parameters and other properties of diamond Schottky barrier diodes in set A.

Sample	Seeding Method	H_2 flow rate (sccm)	CO_2 flow rate (sccm)	CH_4 flow rate (sccm)	Substrate temp (°C)	Film thickness (μm)
S83	Photoresist	200	0	5	471	2.372
S84	Photoresist	200	0	8	470	2.498
S78	Photoresist	200	0	10	473	2.428

Table 4.3 Deposition parameters and other properties of diamond Schottky barrier diodes in set B.

Sample	Seeding method	H2 flow rate (sccm)	CO_2 flow rate (sccm)	CH_4 flow rate (sccm)	Substrate temp (°C)	Film thickness (μm)
S89	scratched	200	8	3	476	0.814
S92	scratched	200	8	5	470	0.912
S100	scratched	200	8	8	470	1.180

Table 4.4 Deposition parameters and other properties of diamond Schottky barrier diodes in set C.

In contrast to the Fujimori [42] result on B-doped film, which reported poor diode characteristics in low CH_4 films and good diode characteristics in high CH_4 films, it is found in this study that all measured contacts on each as-grown undoped film of every sample sets showed fairly good Schottky diode characteristics. For instant, Figure 4.10 shows I-V characteristics of one contact from each sample; BC17, BC15, BC14, and BC13 in set A. The bulk resistances of the diodes were extracted from the I-V data of each contact as describe in section 4.2. Figure 4.11 shows the graph of the bulk resistivity of the diodes in set A for the CH_4 flow rates ranging between 3 sccm and 10 sccm (1.5 – 5% CH_4/H_2 concentrations) while the H_2 flow rate, the gas pressure and the substrate temperature were held constant. The graph shows that for CH_4 flow rates below 2.5% the measured bulk resistivity of diamond Schottky diodes appear to decrease as the CH_4 concentration increase as one might expect. However, for percentages of CH_4 higher than

2.5%, the bulk resistivity of diamond Schottky diodes seems to increase as the CH_4 concentration increase. This phenomenon of increasing values of resistivity was unanticipated since higher CH_4 concentration was expected to give a higher graphitic concentration and lower film resistivity. An alternate hypothesis is that increasing CH_4 gave more defects and more scattering, increasing resistivity.

Similar result of decreasing then increasing values of resistivity are also observed in sample set B and C as shown in Figure 4.12. However the differences in bulk resistivity of sample set B are less than in sample set A. It should be note that higher resistivity of CVD diamond film grown with higher CH_4 concentration (6%) than that of film grown with lower CH_4 concentration (0.5%) was also observed by Fujimori [42]. However, it is an opinion of the author of this research that the different in resistivity of Fujimori' s films may result from the much different morphology of his diamond films. In Fujimori's experiment, film grown with higher CH_4 concentration has flat smoother surface while sample grown with lower CH_4 concentration exhibited rougher surface and bigger grain size. Interestingly, contrary to one's expectations, Fujimori's film with smoother surface demonstrates higher film resistance than a film with a rough surface.

In this regard, the SEM (Scanning Electron Microscopy) photos of the films in set B from M. Ulczynski [76] are shown in Figure 4.13. Although, there appears to be somewhat more twinning in the film grown with higher CH_4 concentration, the photos generally show that all films consist of polycrystalline diamond with very similar morphology. Also there is not much different in resistivity of the films in this set. It appeared that the different diode bulk resistivity in this sample set B should not result from the different film morphology.

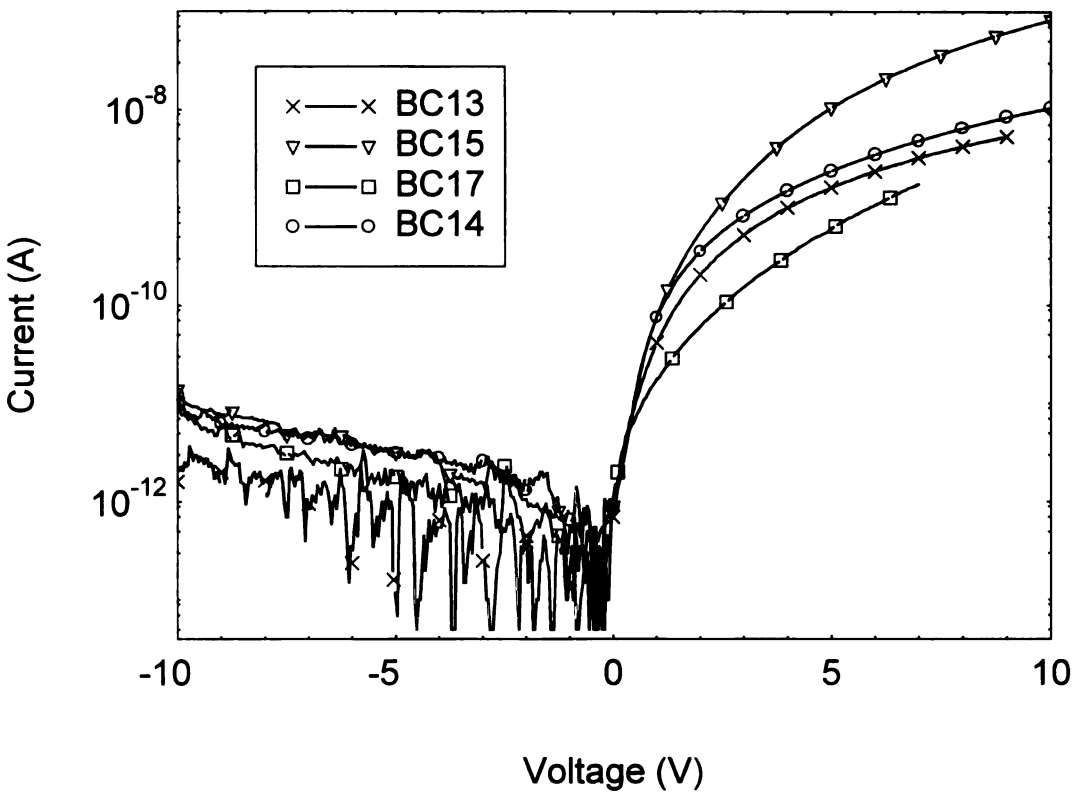

Figure 4.10 The plot shows absolute value of current versus bias voltage on sample BC17 (1.5%-CH_4), BC15 (1.5%-CH_4), BC14 (1.5%-CH_4), and BC13 (1.5%-CH_4). A significant noise level showed under reverse bias is possibly due to equipment limit of HP4145B.

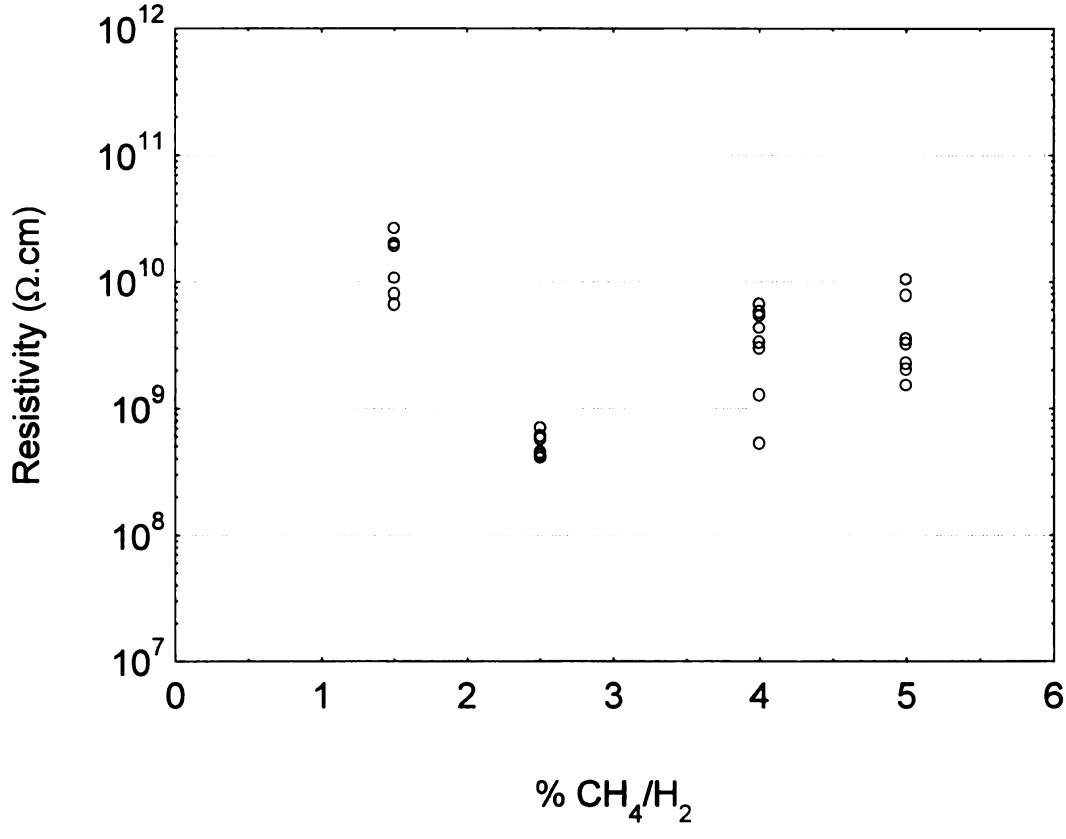

Figure 4.11 Effect of CH_4 concentration in growth process to the bulk resistivity of diodes in sample set A. (see Table 4.2)

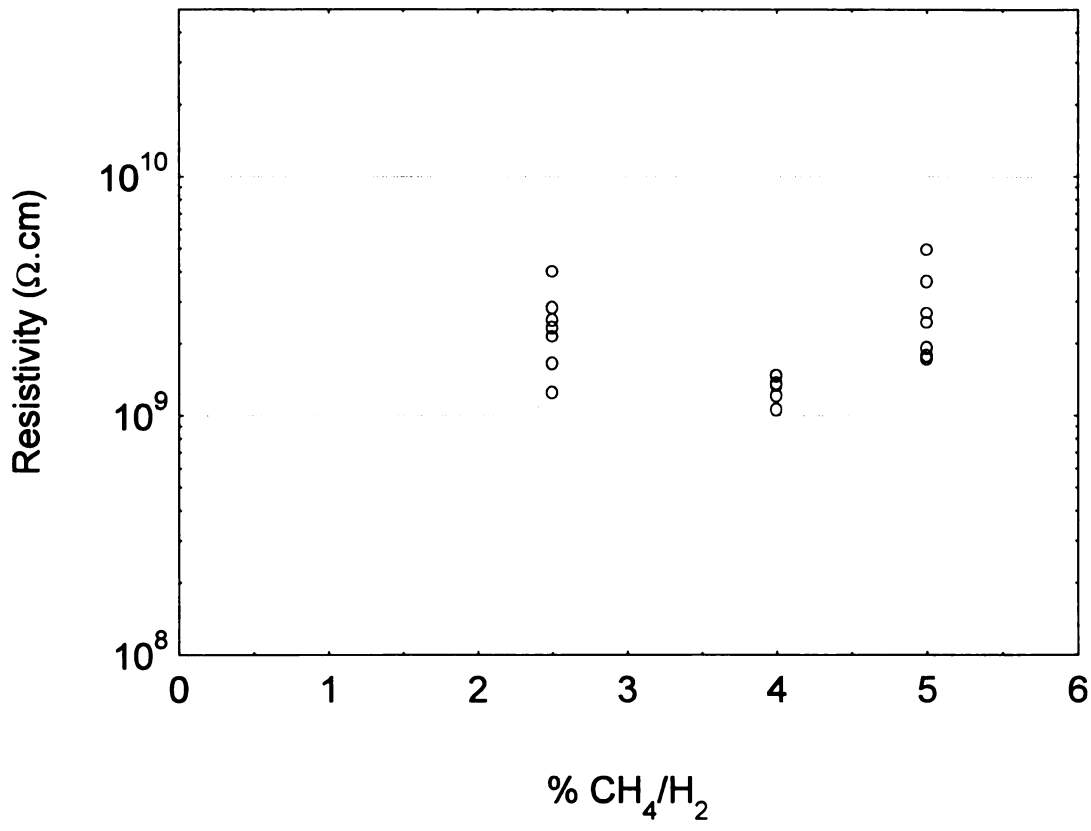

Figure 4.12 Effect of CH_4 concentration in growth process to the bulk resistivity of diodes in sample set B. (see Table 4.3)

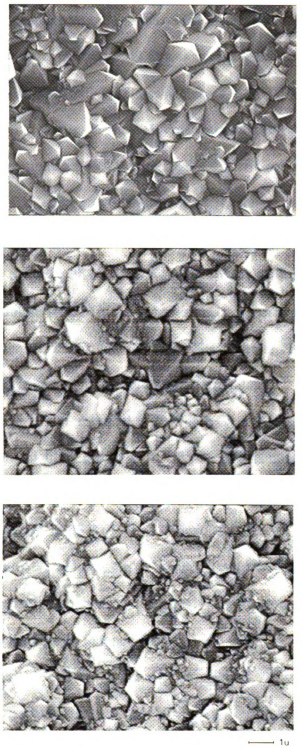

Figure 4.13 SEM photos of diamond sample S83, S84, and S78. Copyright by Ulzcynski [76], used with permission.

In sample set C, CO_2 was added during the CVD process. The flow rate of CO_2, as the O_2 source, in sample set C was maintained at 8 sccm. Again, as shown in Figure 4.14, the bulk resistivity of diodes decreases as the CH_4 concentration increase from 1.5% to 2.5% then increases as the CH_4 concentration increase from 2.5 to 4%. When the SEM photos of samples in set C, as in Figure 4.14(b), are examined, it shows that, under the present of CO_2, film grown with higher CH_4 concentration give much smaller grain than film grown with lower CH_4 concentration. In contrast with one might expect, the resistivity of film with smallest grain and smoothest surface, S100, is highest among the 3 films in sample set C. This observation is in agreement with Fujimori's result mentioned earlier. It is still inconclusive whether the different diode bulk resistivity in this sample set C result from the difference in film morphology.

H. Lux [100] reported that without O_2 in the growth process, volume resistivity of CVD diamond films grown with 1.25 % CH_4 is approximately an order of magnitude lower than that of films grown with 0.63 % CH_4. However, with O_2 addition in the growth process (0.25-0.63%), he found an increasing in volume resistivity of CVD diamond film with increasing CH_4 concentration (1.25-3.13%). According to Lux, adding O_2 to the reactive gas is a key to yields high volume resistivity of the CVD diamond.

In summary, undoped films grown with CH_4 concentration between 1.5 to 5% yielded fairly good Schottky diode characteristics. However, increased CH_4 concentration in the film growth process does not necessarliy reduce the bulk resistivity of diamond diode as one might expect, in fact, CH_4 concentration higher than 2.5 – 4% in the growth process increased the bulk resistivity of the diode. The reason for this is not yet understood.

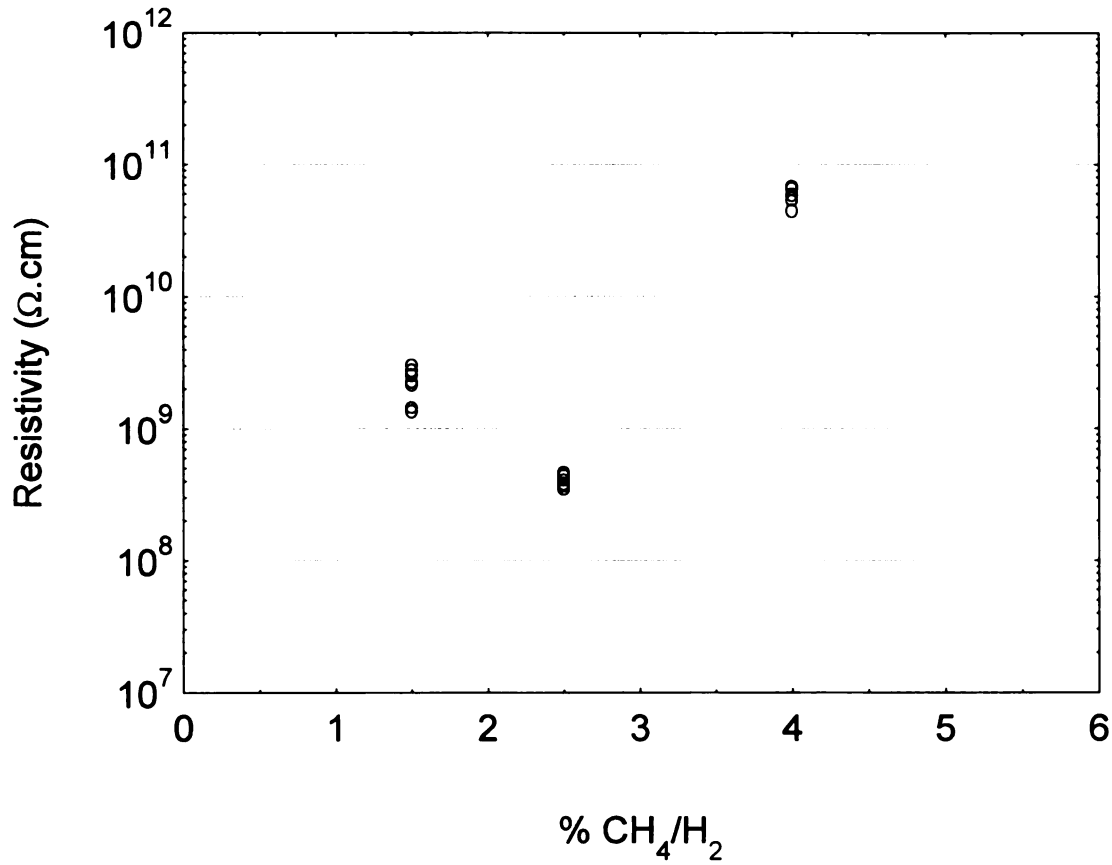

Figure 4.14 Effect of CH_4 concentration in growth process to the bulk resistivity of diodes in sample set B. (see Table 4.4)

S89

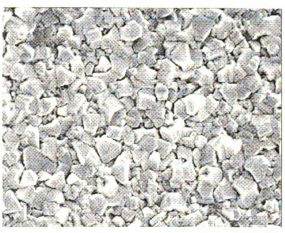

S92

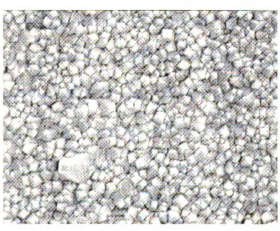

S100

Figure 4.15 SEM photos of diamond sample S89, S92, and S100. Copyright by Ulzcynski [76], used with permission.

4.5 Effects of contact area and film thickness on I-V characteristic

From the fact that the bulk resistance of the semiconductor material can be reduced simply by making the metal contact area larger or by making the diamond film thinner, the effects of contact area and film thickness on diamond film were also studied. Diamond Schottky diode samples were prepared on silicon wafers as described in chapter 3. Aluminum was thermally evaporated to cover the whole backside of silicon wafer forming the ohmic contact. Aluminum was also used to form the top diamond surface contacts with different contact areas on the same sample.

Figure 4.16 shows the I-V characteristics of sample SK7 with top surface contact areas of 4.91×10^{-4} cm^{-2}, 4.45×10^{-2} cm^{-2}, and 7.91×10^{-2} cm^{-2} denoted as SK7-Y, SK7-C, and SK7-D respectively. As can be seen in Figure 4.16, the forward bias current of the diodes improves as the Al contact area become larger. However, the reverse leakage current also becomes much more significant with larger contact area. In fact, the reverse leakage current rises at a higher proportion to the diode area than forward current. This substantially reduces the rectification ratio of large area diode. For SK7-Y, the rectification ratio at 10 V is approximately 5×10^{4}, which is reduced to approximately 292 in SK7-C, and finally to only about 18 in SK7-D.

Similar results were obtained with other diamond Schottky diodes. Therefore, the smaller contact area of 4.91×10^{-4} cm^{-2} was utilized regularly on all other measurements to ensure good rectifying characteristics. McKeag [55] suggests that metal contact areas of less than $\sim 1 \times 10^{-2}$ cm^{-2} are typically required to provide good rectifying characteristics.

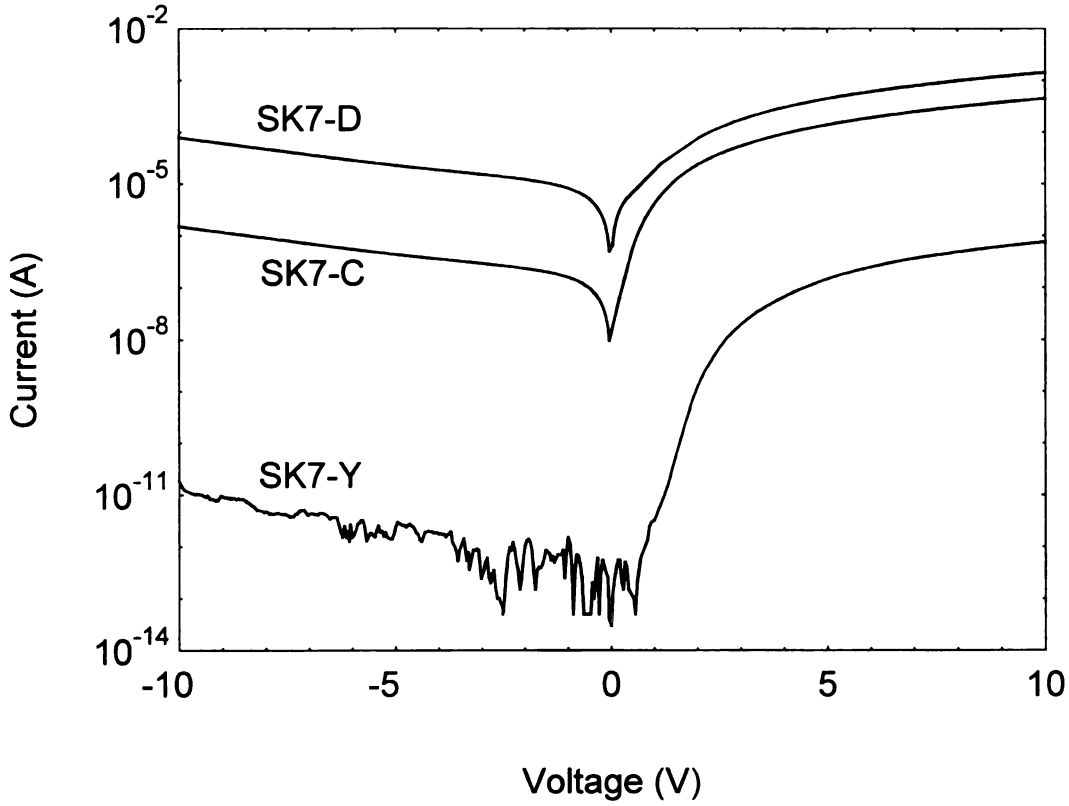

Figure 4.16 I-V characteristics of sample SK7 with top surface contact area of 4.91×10^{-4} cm^2, 4.45×10^{-2} cm^2, 7.91×10^{-2} cm^2 labeled on the plot as SK7-Y, SK7-C, and SK7-D respectively.

The defective nature of as-grown CVD diamond films is thought to lead to excessive leakage across the barrier when significantly larger than this, giving rise to poor reverse current characteristics.

The question of film thickness is linked to the space charge layer thickness. As described previously in chapter 2, a region of space charge (or depletion layer) exists in a semiconductor just inside of a metal-semiconductor interface when the potential barrier is non-negligible. To calculate this space charge width associated with the Al/diamond contacts in this study, we start with Equation 2.7 for the dependence of the space charge width on the applied voltage. As a rough estimation, we use the middle range value of 10^{14}-10^{18} cm^{-3} reported hole concentration on natural type IIb diamond [21] [101], which is 10^{16} cm^{-3}, a dielectric constant for diamond of 5.5, and use the Schottky barrier height as an upper bound for the built-in potential V_{bi}. Reported Schottky barrier diode height for most metals on diamond range from approximately 0.85 to 2.0 [56] [97] [102] [103] [104] [105] [106] and is believed to be relatively independent of non-carbide forming metal type or metal work function due to the pinning of Fermi level by surface states. The barrier heights of all the samples in this research are between 0.72 to 1.08 eV (see section 4.2), therefore, a value of 1.08 eV will suit as an upper limit for the built-in potential.

For those values given above, the space charge region width in the diamond is approximately 0.25 μm at room temperature. This means that space charge region may extend a considerable distance into the diamond film which is of special concern if diode samples are fabricated on a very thin diamond film. To avoid running into the question of space-charge-limited current or a punch-through effect, our diodes were usually fabricated on film with thickness of 0.4 μm or higher.

However, one set of samples, which were prepared for measurement in a similar way as described earlier in chapter 3, was used to study the effect of film thickness on the I-V characteristics. Al was used to form both the top surface contacts (contact area = 4.91×10^{-4} cm^2) and the whole backside ohmic contact. Tables 4.5 shows the deposition parameters and some other key properties of this set of samples.

Sample	Seeding method	H2 flow rate (sccm)	CO_2 flow rate (sccm)	CH_4 flow rate (sccm)	Substrate temp (°C)	Average thickness (μm)
BC5	Scratched	200	0	5	476	0.309
S106	Scratched	200	0	5	439	0.604
BC12	Scratched	200	0	5	502	1.081
BC15	Scratched	200	0	5	514	1.501
S83	Photoresist	200	0	5	470	2.372

Table 4.5 Deposition parameters and other properties of diamond Schottky barrier diodes with different film thickness.

Again, the I-V measurements were performed on random Al contacts of each sample in the direction perpendicular to the surface of the film. All contacts of each sample yield fairly good rectifying characteristic except sample BC5 which have very high reverse leakage current. Figure 4.17 shows the values of forward and reverse current of each sample at ± 10V. As expected, the plot indicates that although the bulk resistance

of the diode can be reduced by making the diamond film thinner, thereby increasing the forward current, the reverse leakage of the device became large for the two thinnest samples. In fact, the I-V characteristic of the very thin diamond film sample BC5 resembles poor ohmic contacts with non-linear effects.

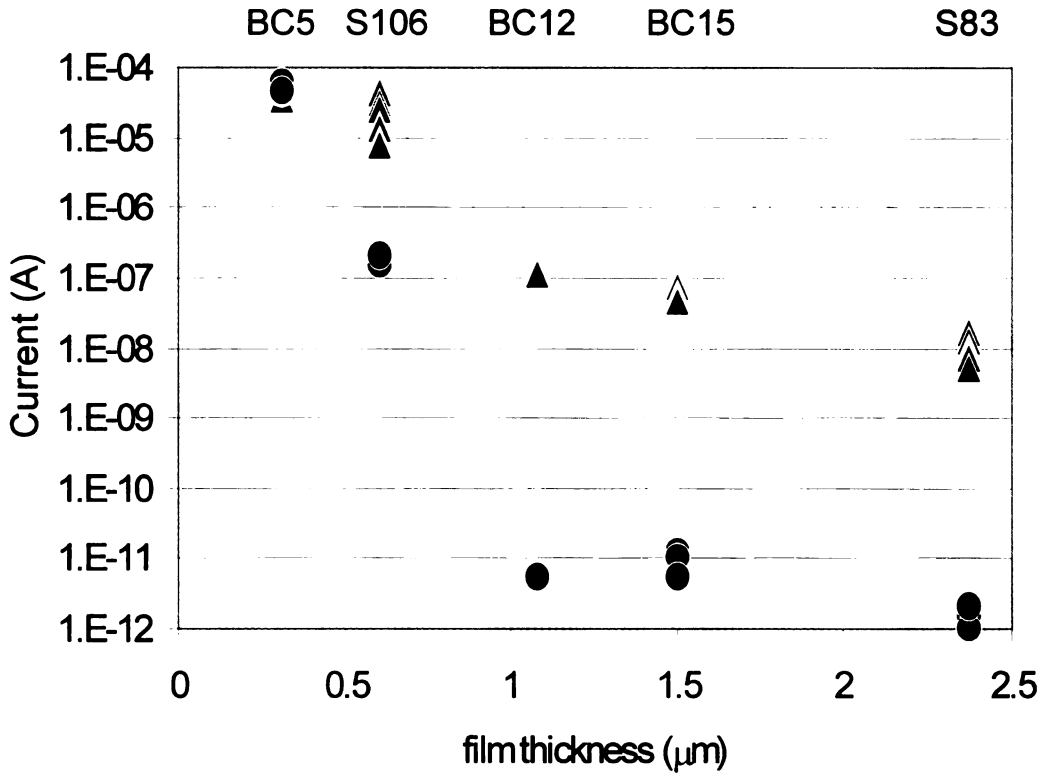

Figure 4.17 The forward current at +10V forward bias (triangle marks) and reverse leakage current at −10V reverse bias (circle marks) versus diamond film thickness.

4.6 Variation with time and sample history

It has been observed that the dc I-V characteristics of the many diamond Schottky barrier diodes investigated in this study often exhibited some variation from one test to another. Two types of change were observed in the experiments: (1) a change in bulk resistance of the film (shown in Figure 4.18 and 4.19), and (2) a change of ideality factor η and saturated current I_O of the junction (shown in Figure 4.20).

Changes such as shown in Figs. 4.18, 4.19 and 4.20 were observed under a variety of test conditions. These include (1) exposure to light, (2) electrical testing at high temperatures (greater than 100 °C), and (3) prolonged (several hour) testing involving dc biases. The literature [89] [107] [108] [109] [110] indicates that the electrical conductivity of CVD polycrystalline diamond is strongly affected by states fairly deep in the gap (an eV or more from the valence band edge). These states include both acceptor type and donor type states. The acceptor-like states dominate, causing the CVD diamond material to be p-type in nature. However, the donor states are also important because they act to compensate the acceptor states. Changes in population of either can cause substantial changes in the valence band hole concentration and, because the states are deep lying, non-equilibrium population of these states can persist for long periods of time, including several days.

Changes in the population of deep lying states can therefore cause an increase or decrease in the bulk resistivity. Changes in the barrier height and space-charge layer, on the other hand, are also strongly affected by changes in the population of interface states, and near-interface states. Both bulk states and interface state populations can be changed by the three device test conditions described above.

Considering the case of exposure to light in Figure 4.18, the result of S100 shows that light exposure causes little or no change in the space charge layer properties (I_O and η remain essentially the same), however a significant decrease in the bulk resistance R_B. This is consistent with observations of Ashok et.al. [108] and Gonnon et.al. [110]. Ashok reported that change in I-V characteristic of their thin CVD diamond films, which were very sensitivity to illumination, resulted from the presence of exponential distributed traps in diamond. Gonnon et.al. observed a persistent photoconductivity in polycrystalline diamond after illumination. They explained the phenomena as follows. The illumination created electron-hole pairs. After illumination, electrons raised in the conduction band were trapped in deep-lying states below the conduction band. The population of free holes left in the valence band was believed to give rise to the persistent photoconductivity.

However prolonged exposure to an electrical bias has been observed in this study to sometimes cause an increase in bulk resistivity, as seen in Figure 4.19 for sample BC4 after a series of large signal switching experiments, indicating a decrease in the hole population. One possibility is that a portion of the donor-type levels are emptied (and therefore activated) by the bias, causing increased acceptor compensation. Alternatively, if injected electrons are trapped by deep-lying acceptors, the effective population of acceptors would be reduced, also increasing the bulk resistance. Our experimental observations do not distinguish between these possibilities.

It should be noted that observation of temperature induced long-term variations in bulk resistance as in Figure 4.19 were also reported by other researchers and were attributed to dissociation of hydrogen from the diamond surface which cause anomalous

or unstable conduction [47]. Hydrogen is believed to exist and passivate the deep traps in CVD diamond films [89] [111]. High temperature can cause hydrogen to out-diffuse resulting in an increase of trapping density leading to increased capture of holes, therefore, reduction in free carrier concentration and increasing resistivity of the film. However, the idea of increased bulk resistance in our sample caused by the out-diffused hydrogen is doubtful, since the lowest reported temperature, which may cause hydrogen dissociation, of 300 °C [85] [86] is much higher than our test temperature (27 – 127 °C). We did not anneal our samples because an increase in bulk resistance is contrary to good diode characteristics.

Finally, it was noted that long term electrical bias could also cause different test condition induced variations. For example, as shown in Figure 4.18, under prolonged dc bias conditions associated with small signal testing (chapter 5), BC7 showed changes in I_O and η but not R_B, indicating the changes involved interface states and band-bending, but not bulk properties. In contrast, BC4 showed only changes in R_B.

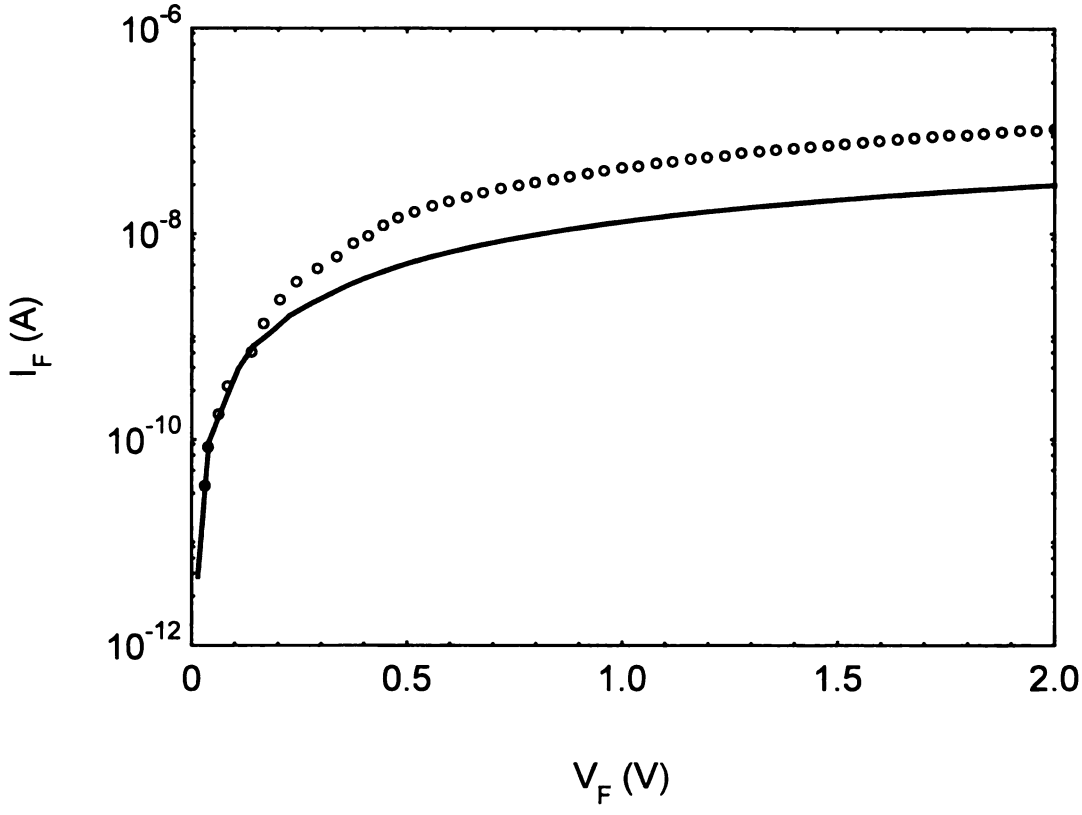

Figure 4.18 Change of I-V characteristics in sample S100. The solid-curve shows characteristics before and the dot-curve shows characteristic 5 minutes after sample was exposed briefly to bright light. Here I_O and η remain the same but R_B decreases.

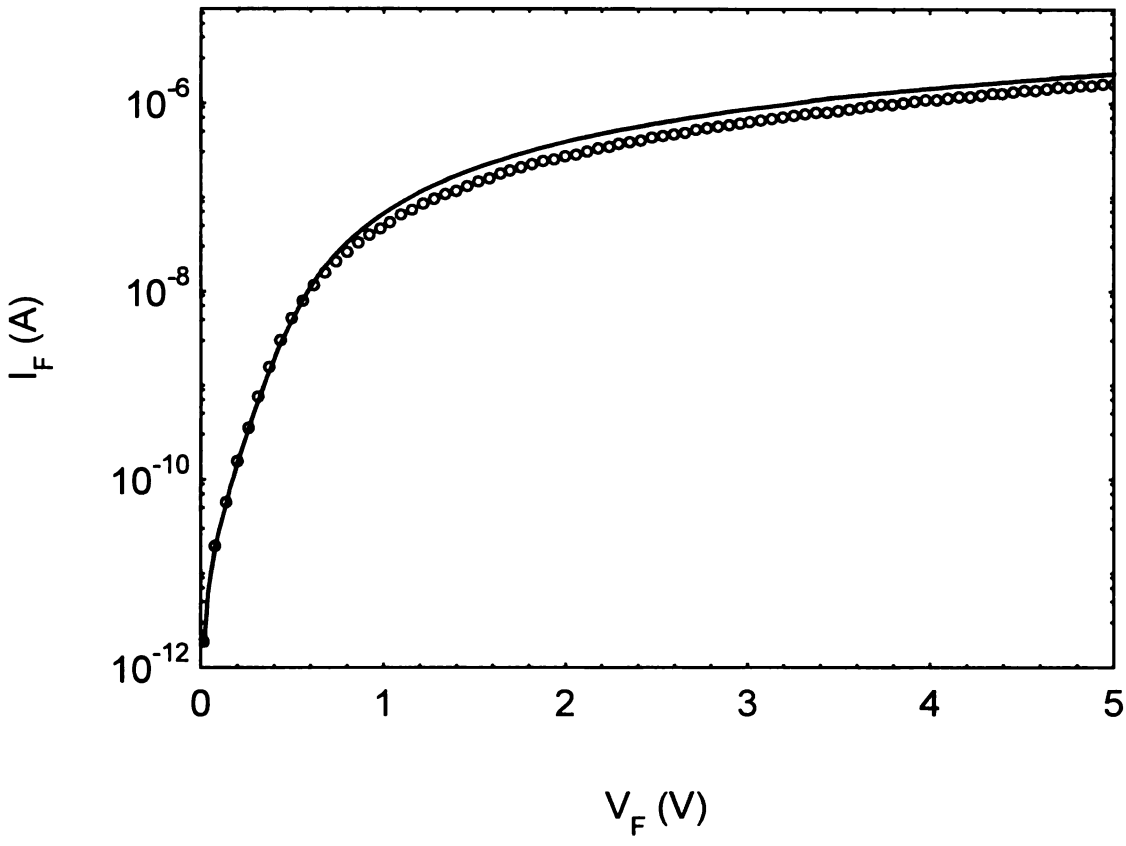

Figure 4.19 Change of I-V characteristics in sample BC4. The solid-curve shows characteristics before and the dot-curve shows characteristic after 1 hour of large signal test (see chapter 6). Here I_O and η remain constant but R_B increases.

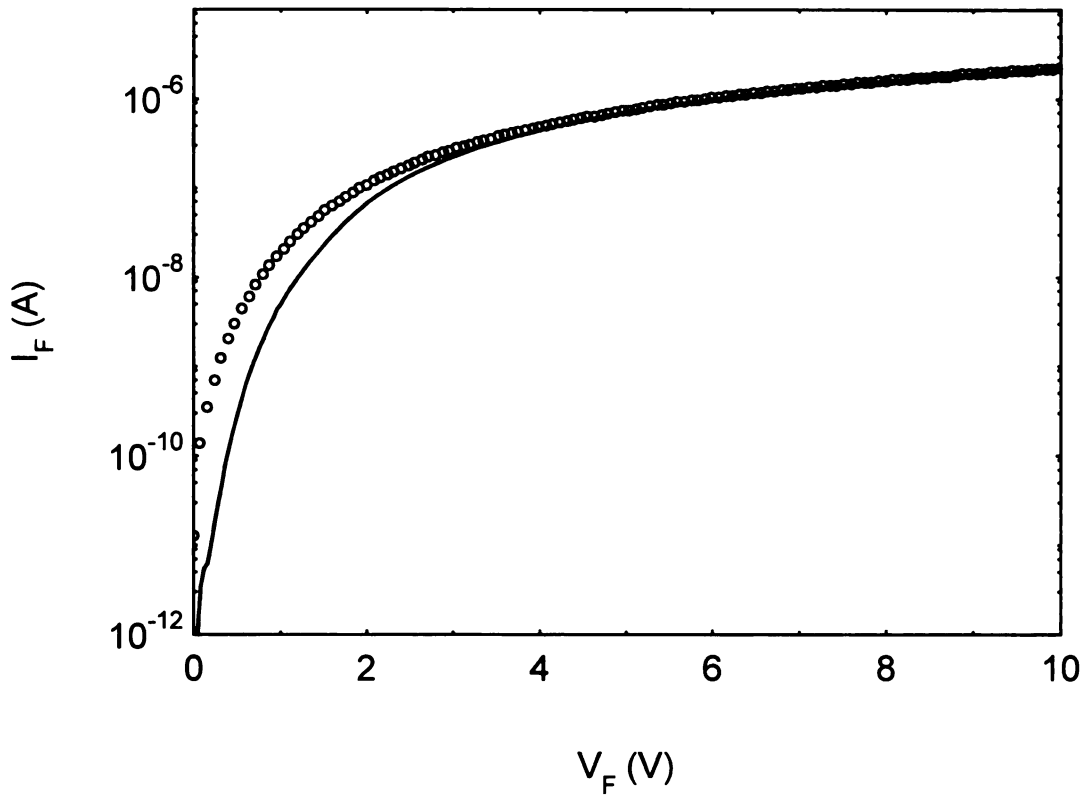

Figure 4.20 Change of I-V characteristics in sample BC7. The solid-curve shows characteristics immediately after a small signal test. The dot-curve shows characteristic 2 hour thereafter. Here R_B is constant but I_O and η change.

4.7 SPICE modeling and simulation for diode dc characteristics

The acronym SPICE stands for Simulation Program with Integrated Circuit Emphasis. It was developed originally at the University of California Berkeley, and has since effectively become an industry standard for device and circuit simulation [112]. The simulation tool PSPICE-6.3 [113] used in this research is a commercial version of SPICE. The PSPICE diode model allows for the input of up to 29 parameters to describe the device. Many of these parameters, however, are not relevant to the dc I-V characteristics modeling for the diode. Table 4.6 shows the PSPICE diode model parameters for dc simulation [26] [113].

SPICE parameter	Compared notation	Parameter description
IS	I_O	Saturation current
RS	R_B	Parasitic bulk resistance
N	η	Ideality factor, emission coefficient
IK		High-injection "knee" current
EG	E_g	Energy gap = 5.45 eV for diamond
ISR		Recombination saturation current
NR		Recombination current emission coefficient

Table 4.6 PSPICE diode model parameters for dc simulation

In SPICE, the dc characteristic of the diode under low-injection condition is modeled by a nonlinear current source that follows the Shockley equation (see section 2.2), rewritten for convenience in the SPICE implemented form

$$I = IS \cdot EXP\left[\frac{V}{N \cdot Vt}\right] \qquad (4.3)$$

where V is the voltage across the diode and Vt is the thermal voltage (=kT/q). However, the above equation is based on the assumption that the carriers are constant throughout the space charge layer. In reality some carriers may be lost in this region by the generation-recombination process. SPICE thus uses a different set of parameters to model this region as

$$I = ISR \cdot EXP\left[\frac{V}{NR \cdot Vt}\right]$$

Under high-injection/high current condition, it can be shown [26] that the observed diode current stops follow the Shockley form and approaches a modified form

$$I = IS \cdot EXP\left[\frac{V}{2 \cdot N \cdot Vt}\right]$$

For practical reasons, SPICE includes this effect by using the parameter IK to determine the onset of high-injection. Figure 4.21 shows each region in SPICE simulation.

By using the values of I_O, η, and R_B determined from section 4.2, and adjusting the remaining parameters to give the best fit to the experimental result, we can obtain the SPICE characteristic parameters for each diode. These parameters will be used as a basis for other parts of this study including time varying waveforms.

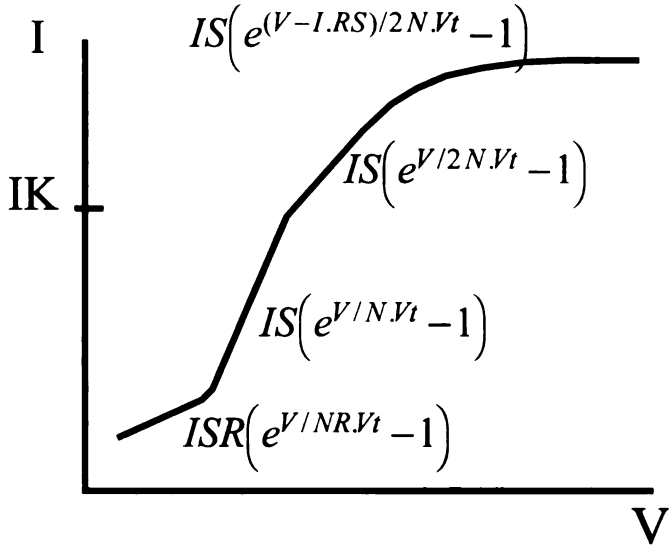

Figure 4.21 An exaggerated display of regions in SPICE diode modeling

Figure 4.22 shows the fitting between the experimental result and SPICE simulation for sample BC4. We obtain a very good fit between experimental data and SPICE simulation with IS = 1.8 pA, N = 2.40, RS = 1.2 MΩ, IK = 1.2 nA, ISR = 4.3 pA and NR = 3.06. However, in some samples especially those with high leakage current, a discrepancy between experimental data and SPICE simulation remains. Figure 4.23 shows the fitting of sample SK7-C. Good fit is obtained in forward bias part while reverse bias part shows appreciable difference. The best-fit SPICE parameters used in Figure 4.23 are IS = 48 nA, N = 4.47, RS = 17.95 kΩ, IK = 400 nA, ISR = 351 nA, and NR = 19.98.

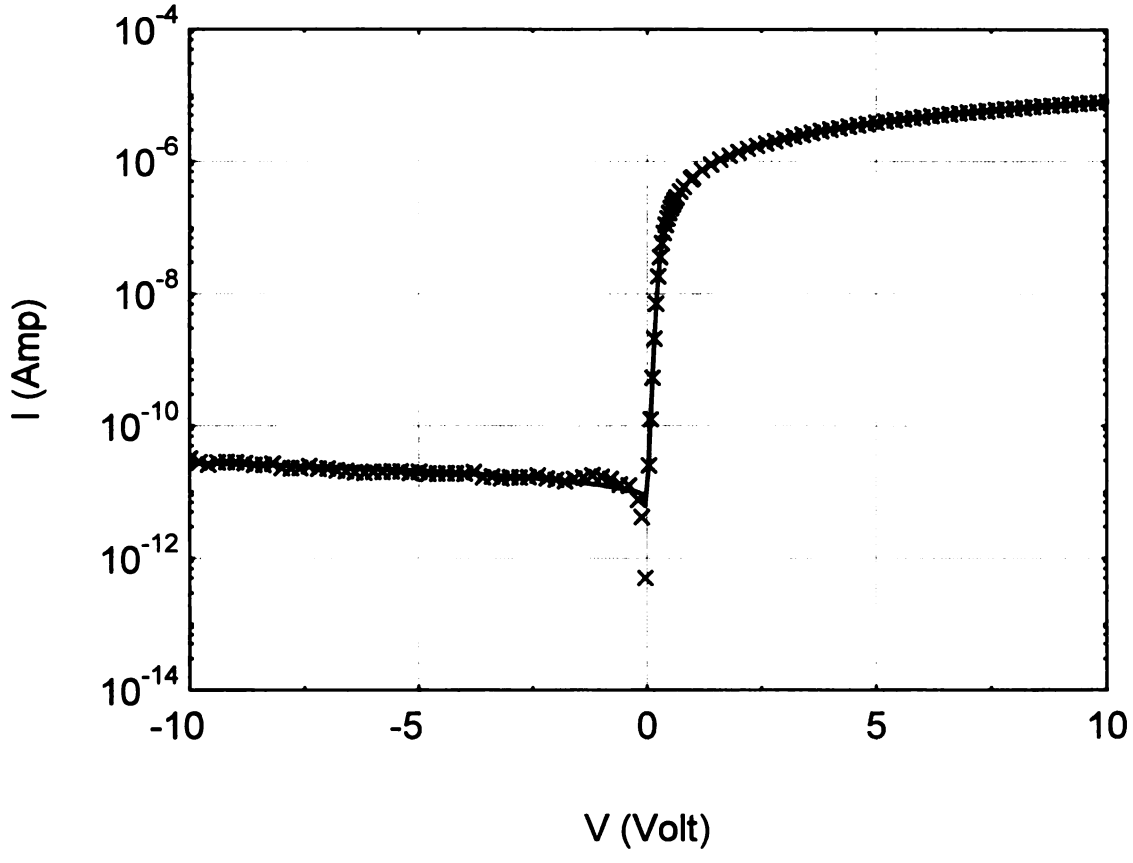

Figure 4.22 Comparison between the experimental I-V data (cross mark) and SPICE simulation result (solid line) on BC4

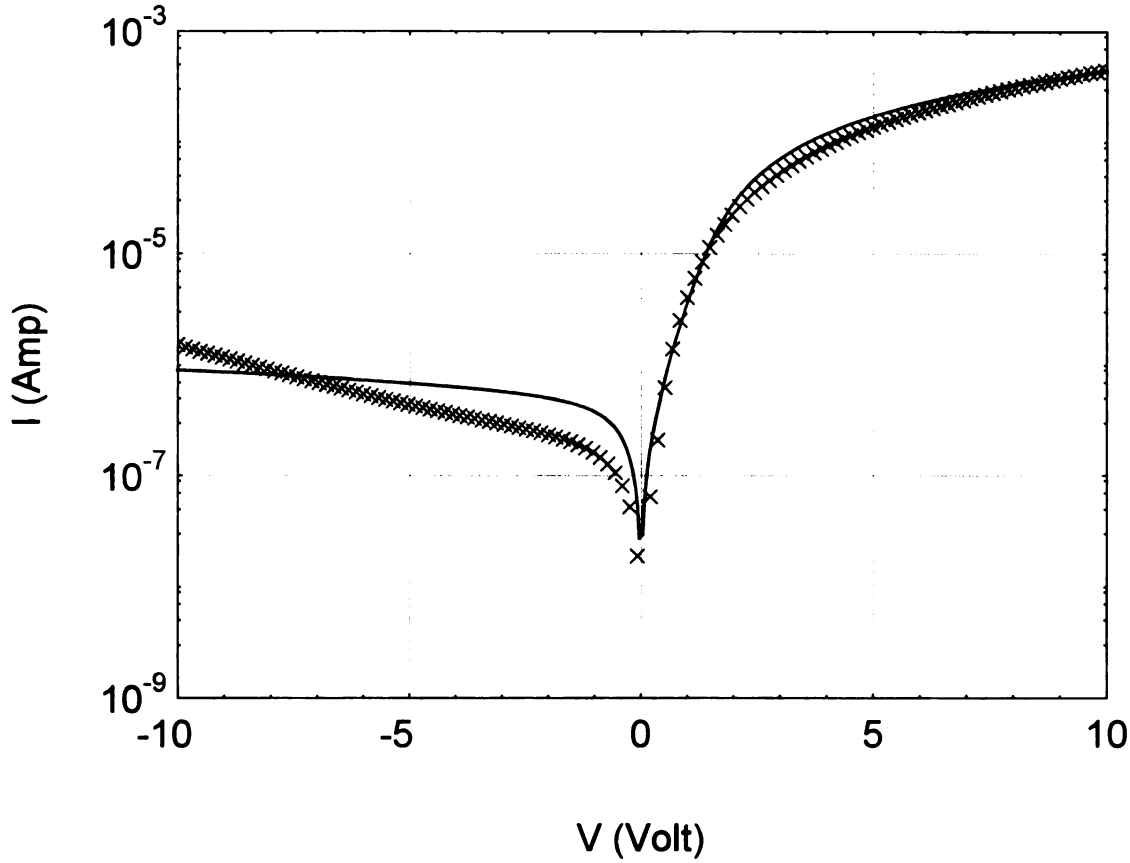

Figure 4.23 Comparison between the experimental I-V data (cross mark) and SPICE simulation result (solid line) on SK7-C

CHAPTER 5

Small signal response of diamond Schottky barrier diodes

5.1 Chapter Overview

This chapter presents the results of the investigation on the small ac signal responses of diamond Schottky barrier diodes. Immediately following this chapter's introduction section, the admittance results in both parallel (C_P, R_P) and series (C_S, R_S) equivalent circuit modes versus bias voltage and frequency are presented. The qualitative interpretation of the results is given. In the next section, C_P, R_P, C_S, and R_S experimental results are compared to three different models. These three models are: (I) a simple model that only includes the combination of junction capacitance-resistance and bulk capacitance-resistance as shown in Figure 2.6(a); (II) a simple model with an addition of a series contact resistance R_C; and (III) a model which includes the effect of trap states represented by a frequency dependent capacitance (C_f) and a frequency dependent resistance (R_f). The last section discusses the application implications of diamond Schottky diode in this study under small ac signal.

5.2 Experimental results and their basic interpretation

In this study, before each small signal test, the dc current-voltage characteristic measurement was performed on each diode at 27 °C. The diode parameters such as I_O, η, and R_B were then extracted from the dc current-voltage result as described in section 4.2. The values of these diode parameters were used in model calculation to compare with the experimental results.

As described in detail in section 3.8, the diode responses to a small signal were studied by using a HP4284A precision LCR meter. A HP4192A LF impedance analyzer was sometime used to verify and cross check the experimental data. All measurements were conducted at 27 °C in the light-tight box. The experimental results at difference ac frequencies and dc bias will be presented in this section along with some remarks. Under normal test conditions, the instrument (HP4284A/HP4192A) test frequency was increased systematically from 100 Hz to 1 MHz in each test. The center dc bias was varied between –5 V to + 5 V, while the oscillation level were kept fixed at 100 mV. The small signal resistance and capacitance values of the Schottky diodes were measured and stored into data files. Both instruments operate so as to measure the resistance and capacitance versus frequency in both parallel (C_P, R_P) and series (C_S, R_S) equivalent circuit models.

Figure 5.1 shows the frequency and bias dependence of capacitance and resistance in both parallel (C_P, R_P) and series (C_S, R_S) equivalent circuit modes for a diamond Schottky barrier diode (sample BC4).

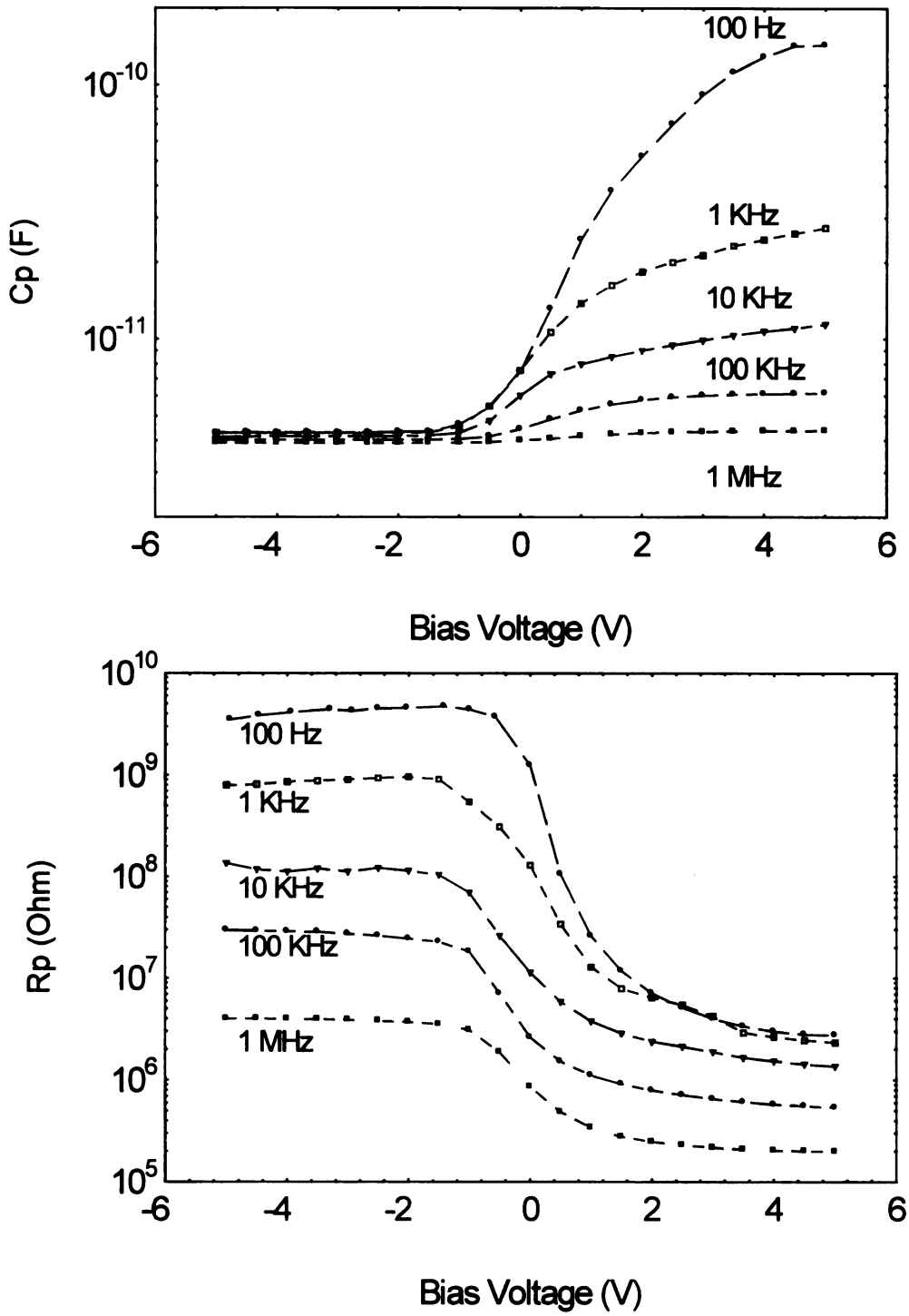

Figure 5.1 Plots of C_P, R_P, C_S, and R_S versus bias voltage at different frequencies of diamond Schottky barrier diode BC4. Negative voltage values indicate reverse biases.

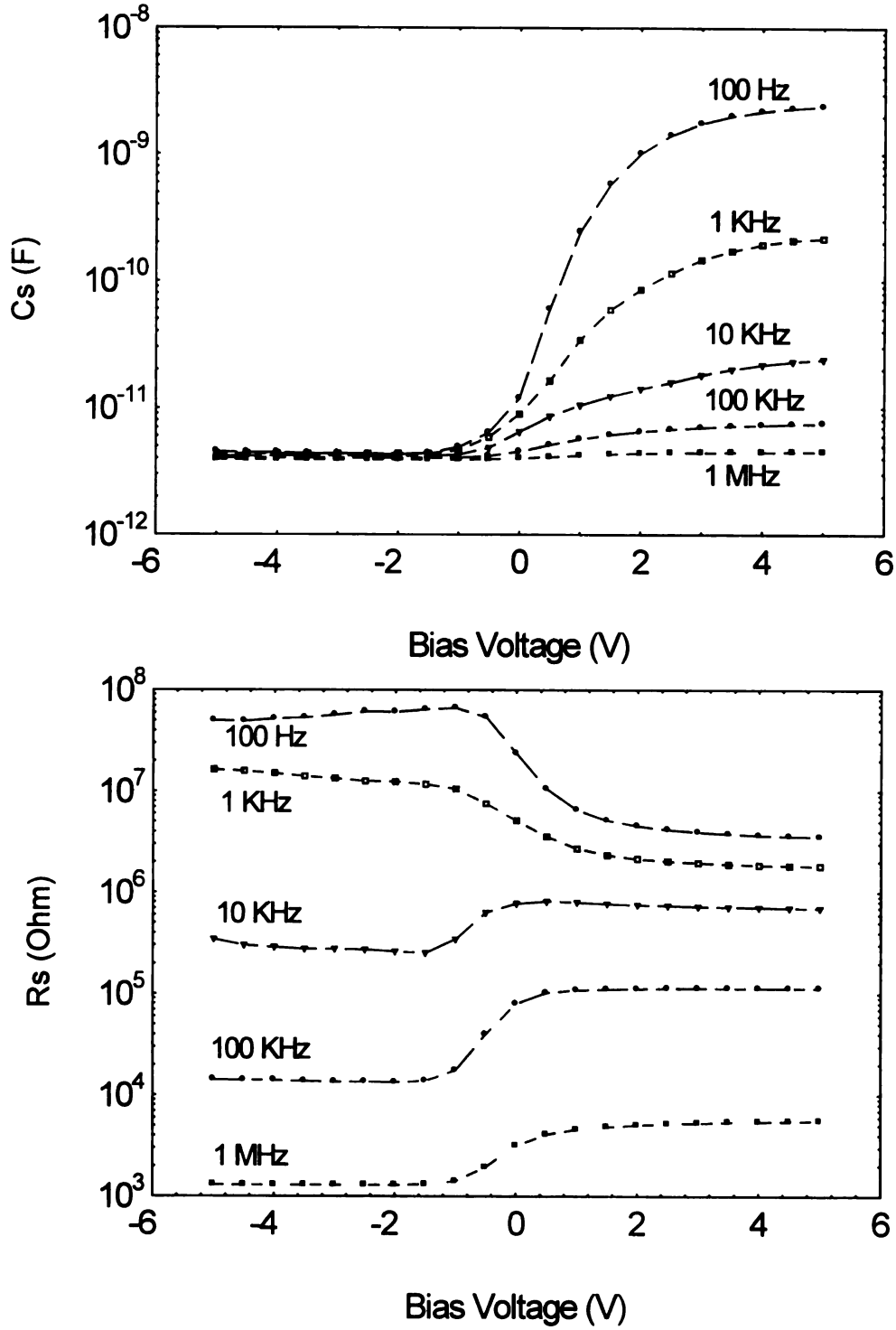

Figure 5.1 Continued

It is of interest to make a comparison of these experimental results with the small signal simple model discussion of section 2.4.Consider first the capacitance results. In both the C_S and C_P measurements, it is observed that at high frequencies (eg.1MHz) the results approach a saturation value for both forward and reverse bias. In comparison with Figure 2.8, this saturation value should be equal to $\varepsilon A/L$. Taking diode area of A = 4.91×10^{-4} cm^{-2}, the experimental results for C_P and C_S at high frequency indicate an L value of 0.54 μm. This compares to an L value of 0.56 um based on average weight gain measurements. At reverse bias, the expectation (as illustrated in Figure 2.8) is that the C_P value remains at $\varepsilon A/L$. This is also in agreement with the experimental results. However, for C_S in reverse bias, the experimental results show that the C_S value remains constant as frequency increased. Figure 2.10 indicates that at sufficiently low frequency, C_S should begin to increase. This increase was not observed experimentally for BC4. Now, considering capacitance results at forward bias, C_S is observed experimentally to increase as frequency decreases. This agrees qualitatively with the prediction of Figure 2.8. C_P also remain with decreasing frequency, however the experimental results do not show the eventually saturation in C_P that is predicted by the simple model.

Next, considering the resistance results, comparing Figure 5.1 with the prediction of Figure 2.9 and 2.11, at low frequencies, the reverse bias value of R_P is very large as expected, also at low frequencies, the forward bias value of R_P is in the order of R_B, again as expected qualitatively. At high frequencies, R_P decreases for both forward and reverse bias, again as expected from the simple model. For R_S again for the low frequencies, R_S is on the order of R_B for forward bias and much larger for reverse bias. At high

frequencies, R_S decreases for both forward and reverse biases, more rapidly for the later than the former as expected from Figure 2.12.

Therefore, from a qualitative point of view the results for C_P, C_S, R_P, and R_S as a function of frequency and bias seem to agree with expectation with two exceptions, namely, (I) C_P does not saturate in forward bias at low frequency, and (II) the increase in C_S with decreasing frequency in reverse bias is not seen.

It is also observed that in both capacitance and resistance measurement results for BC4, the responses monotonically change between forward bias values and reverse bias values for every test frequency. In contrast, Liu et al. [114][115], and Fox et al. [116] have observed a peak of capacitance and conductance versus voltage which moved with increasing frequencies in CVD diamond. They indicated that the interface states in diamond were the source for the peak. However, no peak of capacitance, resistance or conductance versus applied voltage is observed for any test frequency for BC4. It is suggested by Viktorovitch [36] that the absence of peak should indicate either that the density of surface/interface states is negligible or that their occupancy is controlled by the metal Fermi-level in such a way that they do not contribute to capacitance. Some of our samples show monotonic behavior as BC4, others do not.

Finally as stated by Rhoderick in his book [27] on Schottky diodes, the capacitance of a Schottky barrier structure under reverse bias obeys the relation as given in Equation (2.9) and (2.10). Thus, a linear relation can be obtained between C^{-2} and bias voltage. From the linear relation, the carrier (acceptor) concentration in the semi-conductor can be obtained.

For our experiment on diamond Schottky barrier diode BC4, both C_P and C_S spectroscopy at various frequencies are plotted in Figure 5.2 in the form of C^{-2} versus reverse bias voltage. However, no linear relationships were found in the plots. Kiyota et.al. [28] concluded in their study that a non-linear relation between C^{-2} versus bias voltage (C^{-2}-V) indicated that acceptor concentration, and therefore ionized states, were not uniform in their as-grown film. A non-uniform effective-acceptor concentration would, in fact, be expected if, as suggested by Hayashi et.al., Looi et.al. [117], and Gluche et.al.[84], the p-type nature is associated with near-surface hydrogenation.

With traditional silicon electronics, it is generally met in practice that a C^{-2}-V plot has a linear characteristic However, a non-linear relation between C^{-2} and bias voltage are often found in Schottky barrier diodes fabricated on other type of materials eg. GaAs, and ZnO even when the materials have uniform doping. These phenomena are currently not fully understood [118] and have been attributed to interface state [119], minority carrier injection [120], or non-zero free-carrier transit time in the space charge region [121].

For diamond Schottky barrier diodes, there are only a few articles which address the non-linear relation between C^{-2} and reverse bias voltage. One was by Kiyota on un-doped as-grown diamond Schottky diode as noted earlier. Liu et.al. [114][115] also observed such non-linear relations in their boron-doped diamond Schottky diodes. Since the doping conditions were kept unchanged in the sample growth, they concluded that the non-linear characteristic of C^{-2}-V in their boron-doped diodes should not come from non-uniform doping profile but rather from the interface states, deep level centers, and the series resistance in the diamond sample.

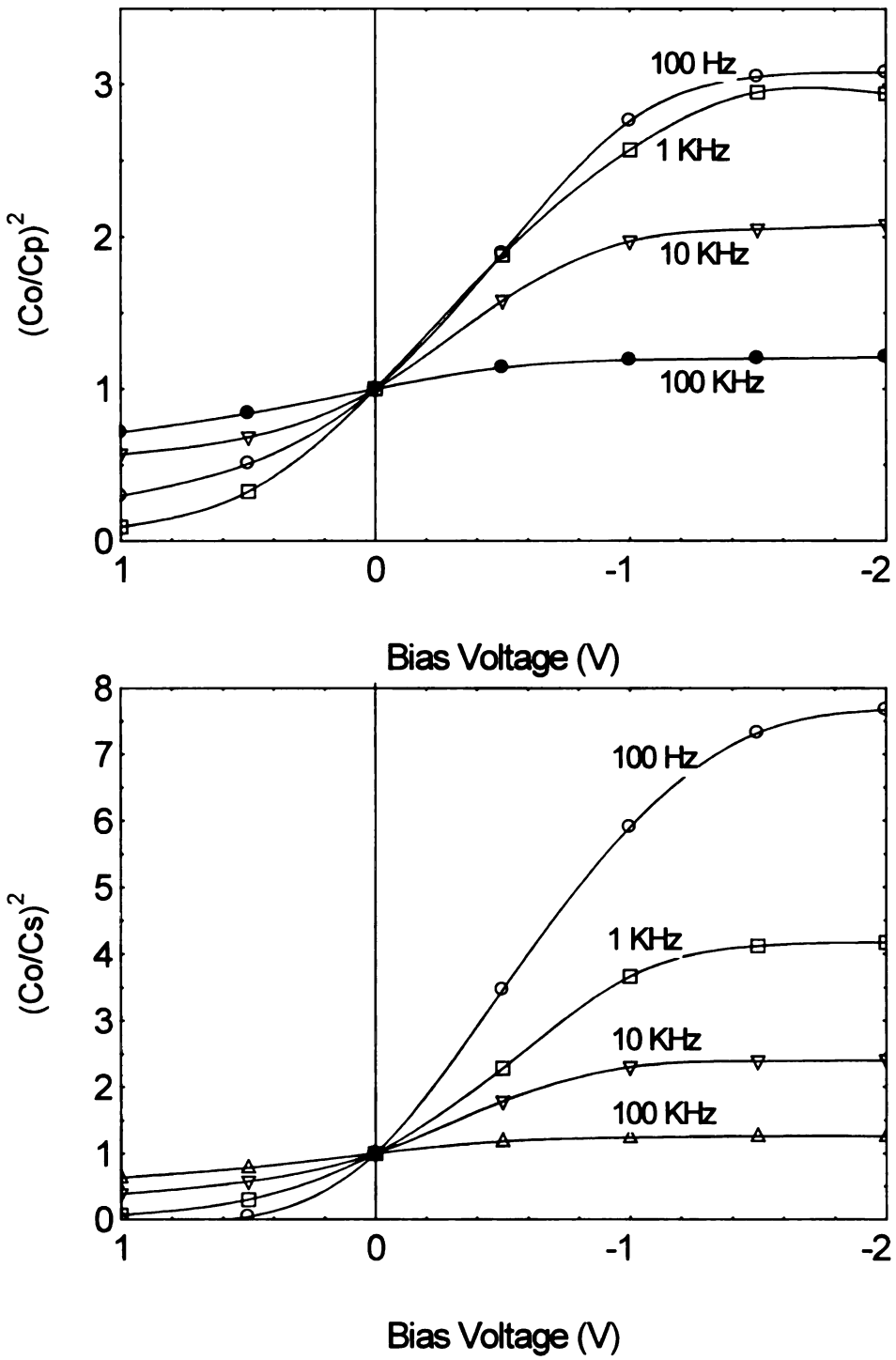

Figure 5.2 Plot of C_S and C_P in form of C^{-2}-V of sample BC4. The C_O is the capacitance value at zero bias at each test frequency. Negative voltage represents the reverse bias value.

5.3 Small signal model fitting results

This section describes the results of fitting the small signal experimental results with the models in chapter 2. In this section, models are applied to two diodes SK7-B, and BC4. Sample SK7-B is fitted to the models first. Later, sample BC4, which we already gave some results qualitative interpretations in the last section are considered.

Figure 5.3 shows C_P, R_P, C_S and R_S of diode SK7-B at different center bias voltage. As can be seen from the figure, the response of SK7-B is more complex than that of BC4. The non-monotonic behaviors i.e. peak of capacitance C_P and resistance R_P are observed. Such peak possibly indicates the presence of interface states in diamond [114][115][116]. However, compare Figure 5.3 to Figure 2.8 - 2.11, the responses of SK7-B qualitatively agree with most of the simple model predictions. Saturation of both C_P and C_S at high frequency regardless of bias is observed. At low frequency forward bias, C_P approaches saturation while C_S increases with decreasing frequency. The values of both R_P and R_S approach saturation under low frequency. At higher frequency R_P decreases and seems to approach a saturation value while R_S continue to decrease with the increasing frequency.

According to the equivalent circuit model in Figure 2.6(a), the impedance and the admittance of the circuit can be written as

$$Z = \frac{R_J}{1 + i \cdot \omega \cdot R_J C_J} + \frac{R_B}{1 + i \cdot \omega \cdot R_B C_B}, \text{ and } Y = \frac{1}{Z} \qquad (5.1)$$

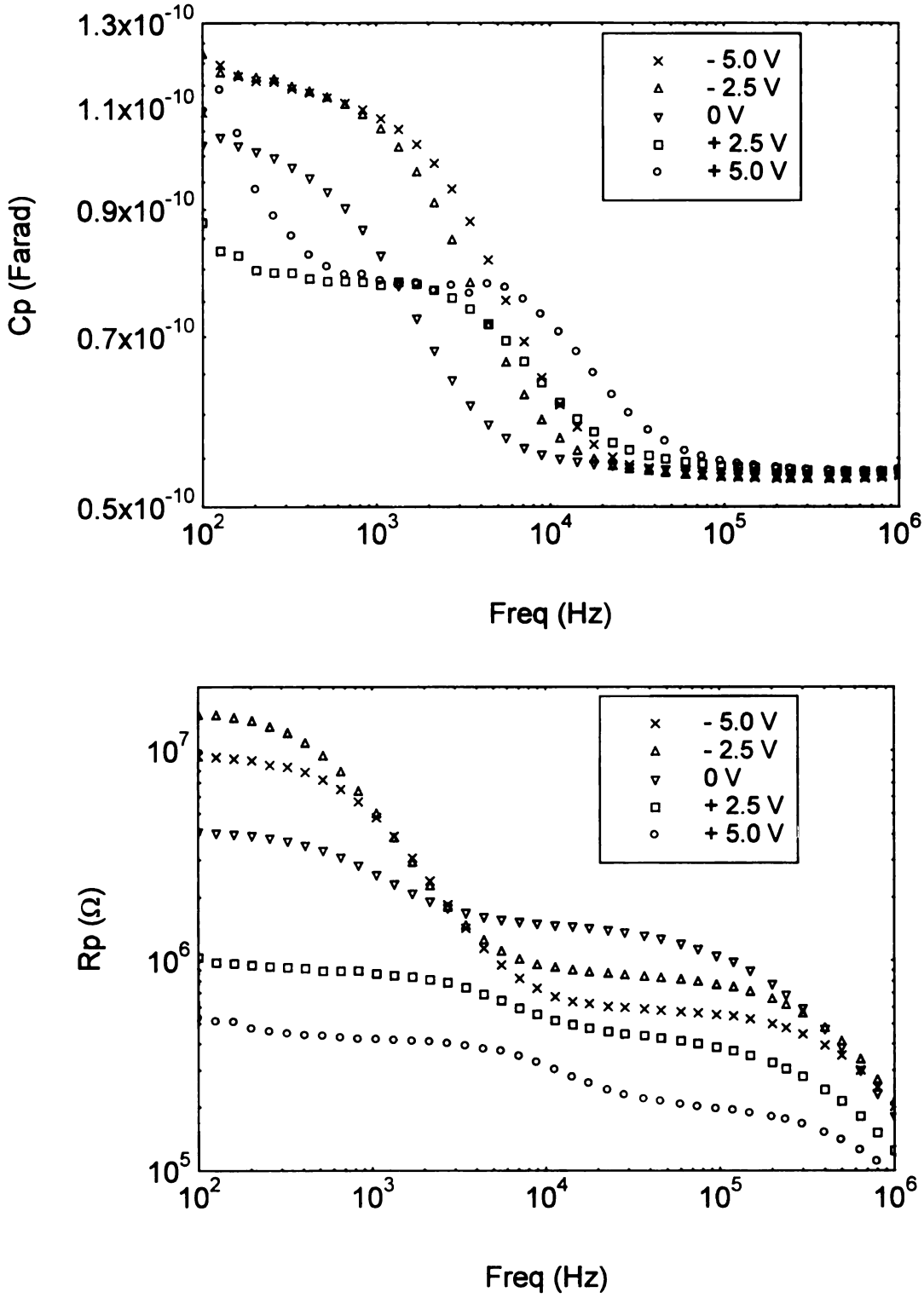

Figure 5.3 Experimental results of C_P, R_P, C_S and R_S measurement on sample SK7-B

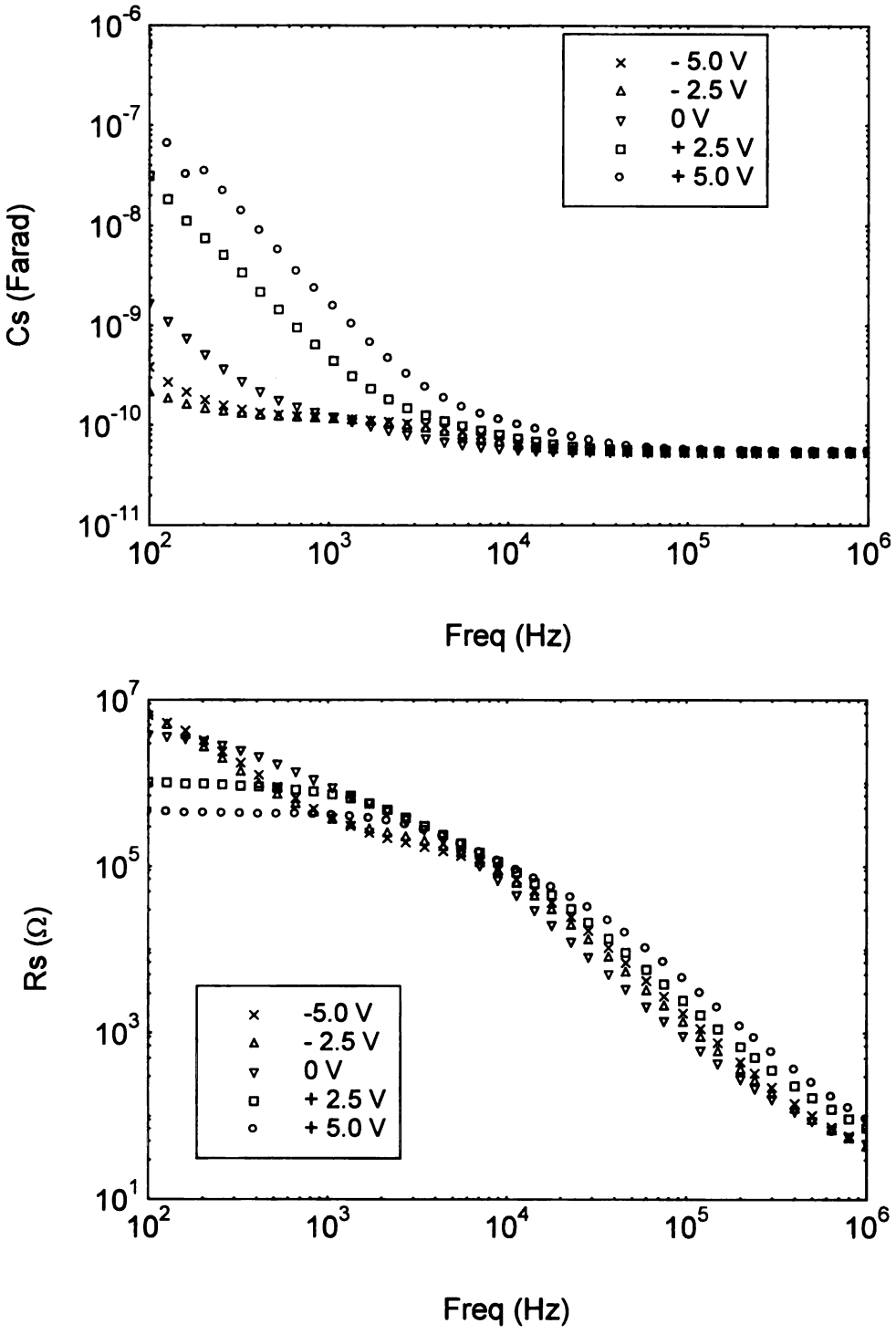

Figure 5.3 Continued

All the variables have the usual meaning as in section 2.4. The value of C_P, R_P, C_S and R_S can then be calculated from

$$C_P = \frac{\mathrm{Im}(Y)}{\omega} \quad , \quad R_P = \frac{1}{\mathrm{Re}(Y)} \quad , \quad C_S = \frac{1}{\omega \cdot \mathrm{Im}(Z)} \quad \text{,and} \quad R_S = \mathrm{Re}(Z) \qquad (5.2)$$

which will give the final expressions as in written in Equation 2.12 and 2.13.

In equation 5.1, there are four parameters - C_J, C_B, R_J and R_B. The value of C_J and C_B can be obtained from the sample thickness, L, and depletion layer width, w, as from the expressions in Equations (2.8) and (2.14). However, in both the C_S and C_P measurement, it is observed that at high frequency, the capacitance of the diode approaches a saturation value of 51 pF regardless of bias. According to the analysis in section 2.4, this value should equal to the geometrical capacity of the whole film, $\varepsilon A/L$. Taking the area of the diode 1.99×10^{-2} cm^2 into account, the thickness of the diode, L, is found to be 1.90 μm which is close to 2.02 μm based on weight gain. Also, the dc current-voltage characteristic measurement of this diode yields the value of R_B of 198 KΩ. However, since the thickness of the depletion layer is not constant but rather depends on the bias voltage, the value of R_B can be adjusted to reflect the change in depletion layer thickness. Under forward bias, value of the dynamic resistance R_J can be calculated from $\eta kT/I$, where I is the dc current at that specific bias voltage. From dc measurement, the ideality factor of SK7-B is 14.1 and saturation current is 58 nA. Under reverse bias, ideally R_J is very large (infinite), practically R_J can be obtained from dI/dV at specific reverse bias voltage of the dc measurement.

From the above discussion, one should be able to find a fit to all the C_P, R_P, C_S and R_S results at each different bias voltage by only adjusting the value of two variables, namely depletion layer width, w, and the bulk resistance, R_B. Figure 5.4 shows the results of the fitting between experimental data and simple circuit model. To obtain a fit to all bias voltage, the value of depletion layer width, w, was varied between 0.81 μm at 5 V forward bias to 0.94 μm at 5 V reverse bias. The value of bulk resistance, R_B, was also varied from 180 KΩ to 330 KΩ as shown in table 5.1.

From Figure 5.4, it can be seen that, although we can obtain a qualitatively acceptable fit between experimental and model results, discrepancies between experimental and model are remained in all plots, for example R_P and R_S at high frequency, and C_P at low frequency

Bias voltage	w (μm)	R_B (ohm)	R_J (ohm)
+ 5.0 V	0.81	330 K	48 K
+ 2.5 V	0.83	325 K	250 K
0.0 V	0.88	320 K	15 M
- 2.5 V	0.91	250 K	48 M
- 5.0 V	0.94	180 K	42 M

Table 5.1 The parameter values used in model fitting of the diode SK7-B in Figure 5.4.

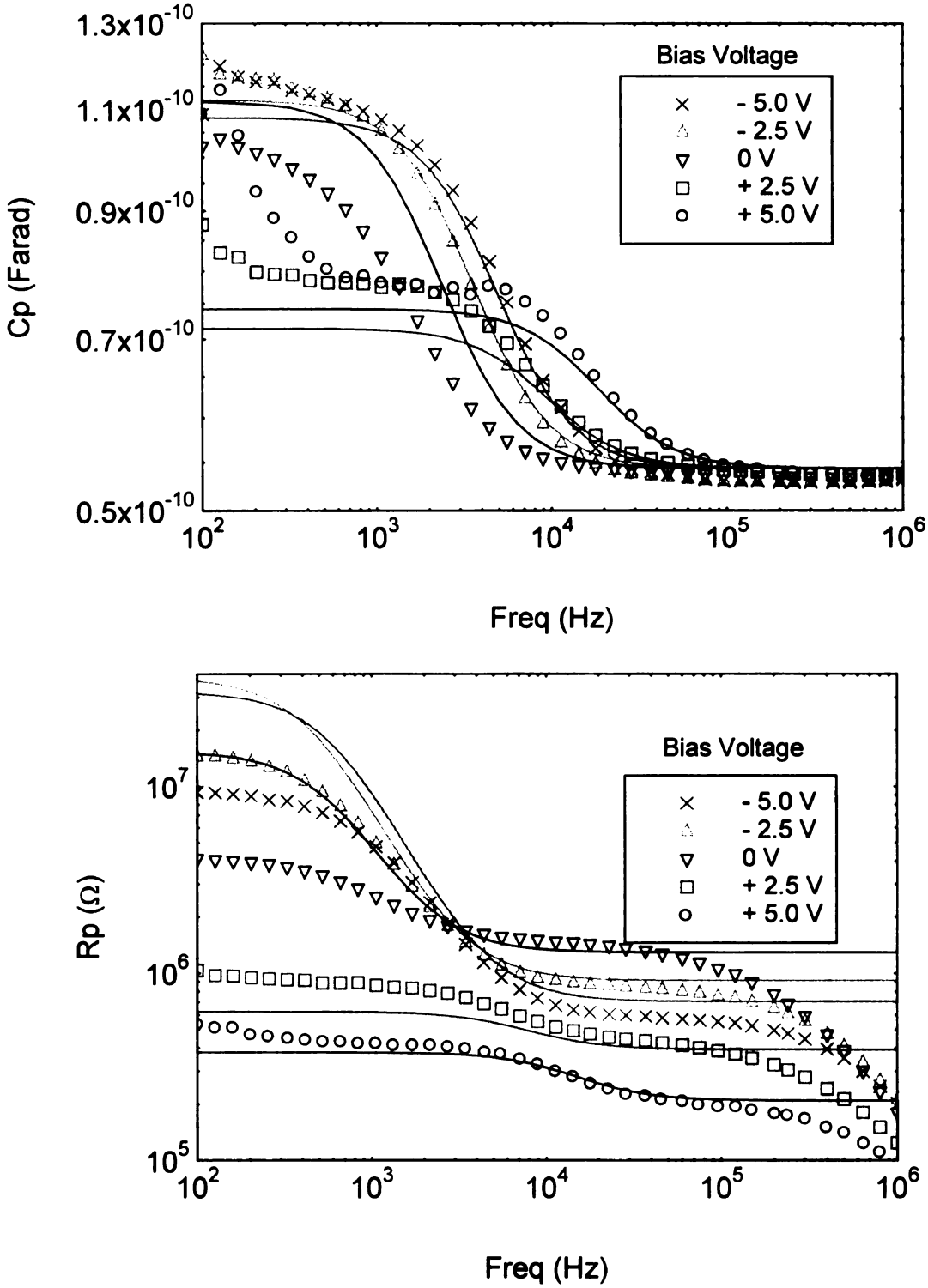

Figure 5.4 Fitting between the C_P, R_P, C_S, and R_S experimental and the simple model results. Solid lines represent model calculation at each bias.

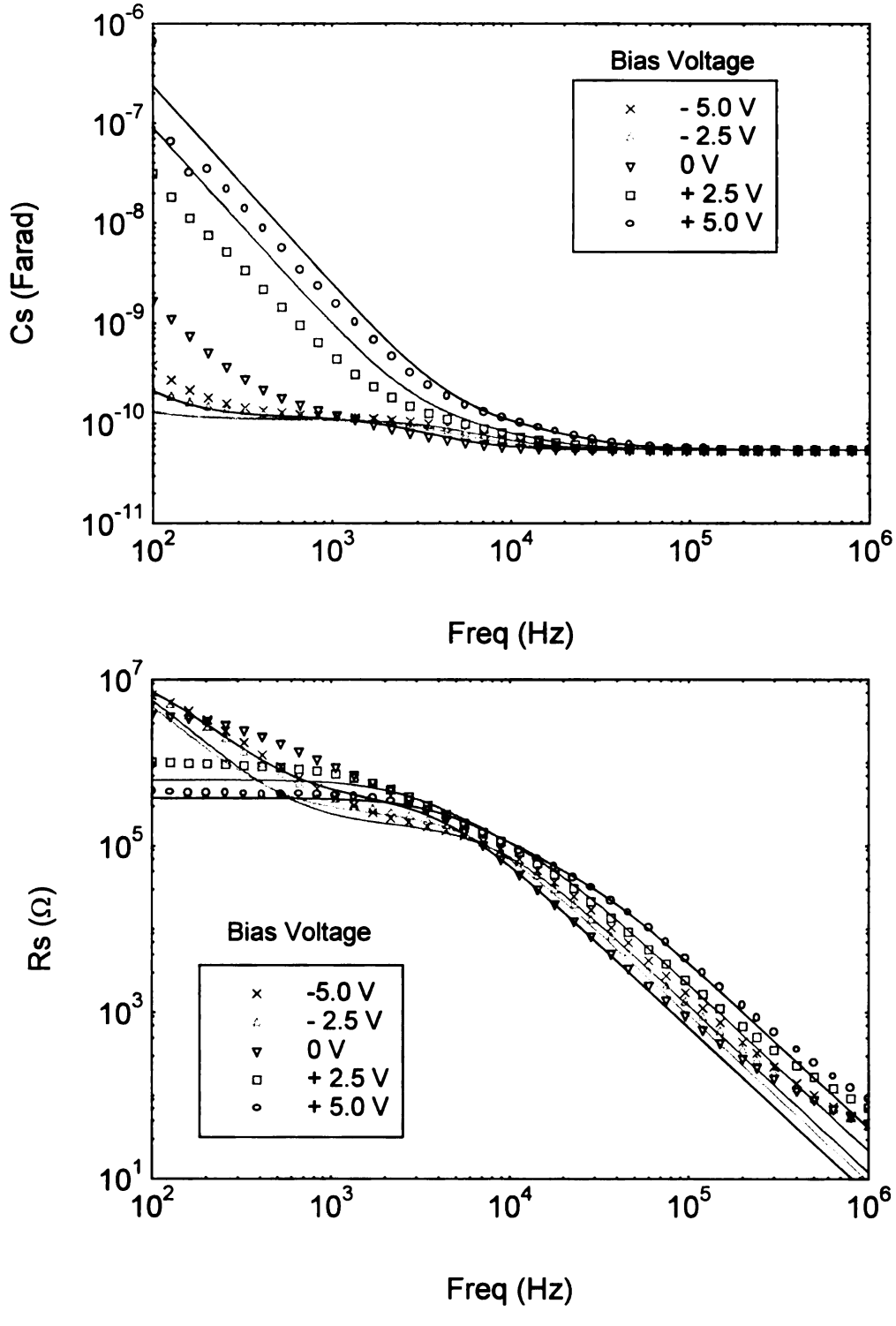

Figure 5.4 Continued.

Snell [37] observed a rapid rise in conductance (drop off in resistance) in the capacitance-conductance spectroscopy measurement on Au/Si Schottky barrier diodes at test frequencies higher than 10 KHz. He attributed such a rapid rise to a 40 Ω contact resistance. This may be expected since all metal-semiconductor contacts have a finite, non-zero, contact resistance. After taking the contact resistance effect into his model calculation, Snell observed perfect fit between his model and experimental results.

A study by Bataineh [122] on CVD diamond impedance spectroscopy suggested that although contact resistance is small it plays an important role at high frequencies and needed to be included into the equivalent circuit model. Studies by Venkatesan, and von Windheim et.al. [17] [21] on diamond Schottky barrier diodes also conclude that the frequency dependent capacitance of the sample is the results of the combination of junction capacitance, bulk resistance and back contact resistance. The authors observed that the frequency dependence significantly reduced after the back contact resistance was reduced.

In order to accommodate the contact resistance into our model calculation, Equation 5.1 is modified to include R_C as

$$Z = \frac{R_J}{1 + i \cdot \omega \cdot R_J C_J} + \frac{R_B}{1 + i \cdot \omega \cdot R_B C_B} + R_C \text{ , and } Y = \frac{1}{Z} \qquad (5.3)$$

Where R_C is the contact resistance. The value of C_P, R_P, C_S and R_S can then be calculated from Equation 5.2.

Figure 5.5 shows the fitting between experimental results and the model in Equation 5.3. Note that all the value of C_J, R_J, C_B and R_B were maintained at the same value as used in previous fitting between experimental results and model in Equation 5.1 (without R_C). With the addition of R_C=52 Ω in our model, the fall of at high frequencies of the resistances are observed in the model calculation. Now, a better fit in R_P and R_S than those in Figure 5.4 can be obtained.

As mentioned in section 2.8, there are two major interpretations of small signal C-V studies on diamond Schottky barrier diode. Some studies, e.g. Venkatesan's, indicate that the frequency dependent of capacitance can be simply model by the combination of the junction, the bulk, and the contact elements. Others, e.g. Glover, indicate that deep trap states in diamond play an important role in the interpretation of C-V results. It is important that we try to adapt Glover's model into our result interpretation.

Glover[19] models the effects of deep trap states with the combination of C_f and R_f as shown in Figure 2.17. Based on earlier work by Schibli [123], the values of C_f and R_f can be calculated from

$$C_f = \frac{B}{\sqrt{\omega}} \quad \text{,and} \quad R_f = \frac{1}{\omega \cdot C_f}$$

where

$$B = \sqrt{\frac{2e^2 \cdot N_a \cdot \varepsilon \cdot C_{CAP} \cdot P_1}{KT}}$$

N_a = acceptor concentration

C_{CAP} = capture probability

$$P_1 = \frac{N_R}{2} \exp\left(\frac{-E_A}{KT}\right)$$

N_R = valence band density of states

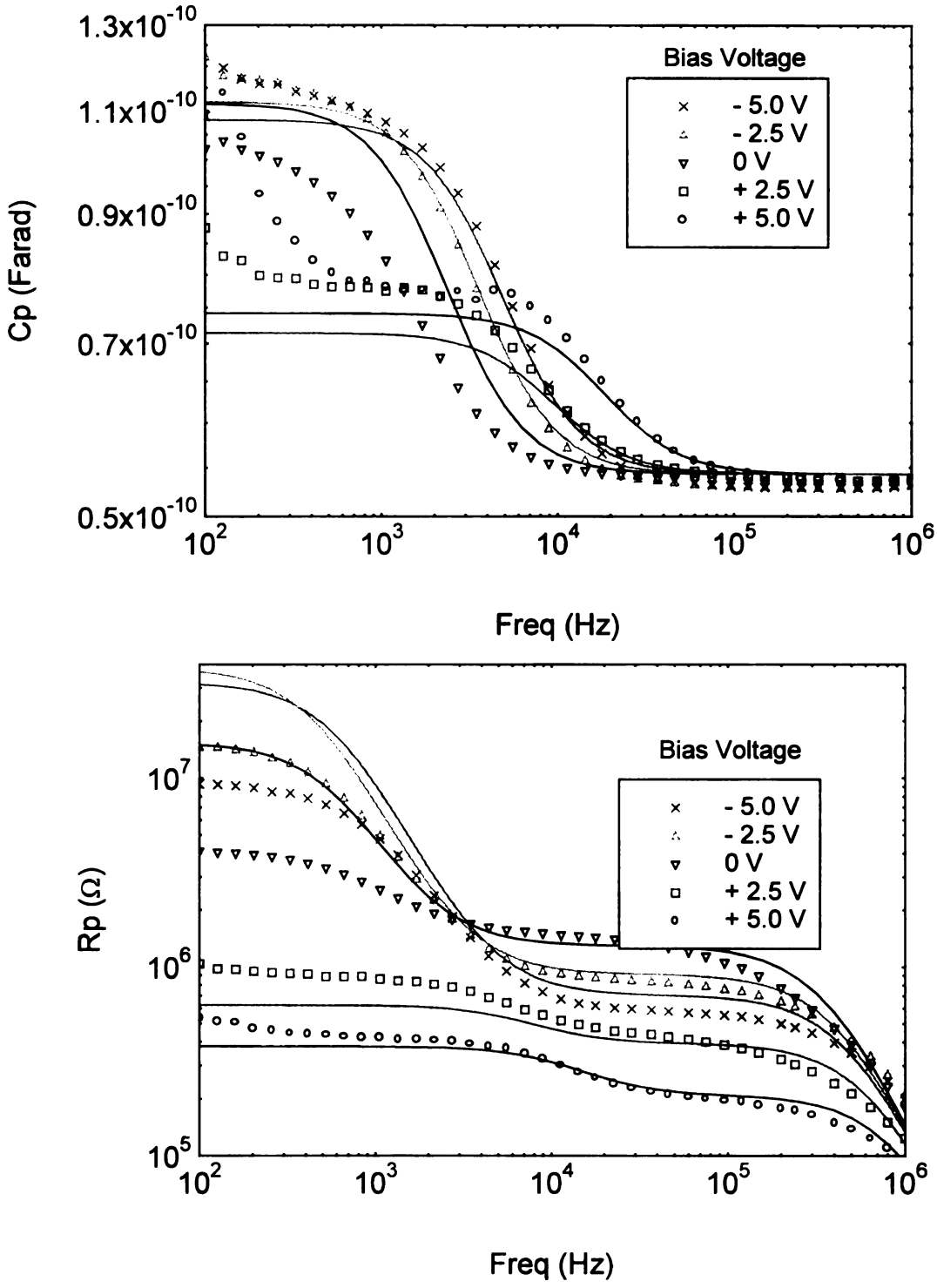

Figure 5.5 Fitting between the C_P, R_P, C_S, and R_S experimental results of SK7-B and the model which include the contact resistance effect.

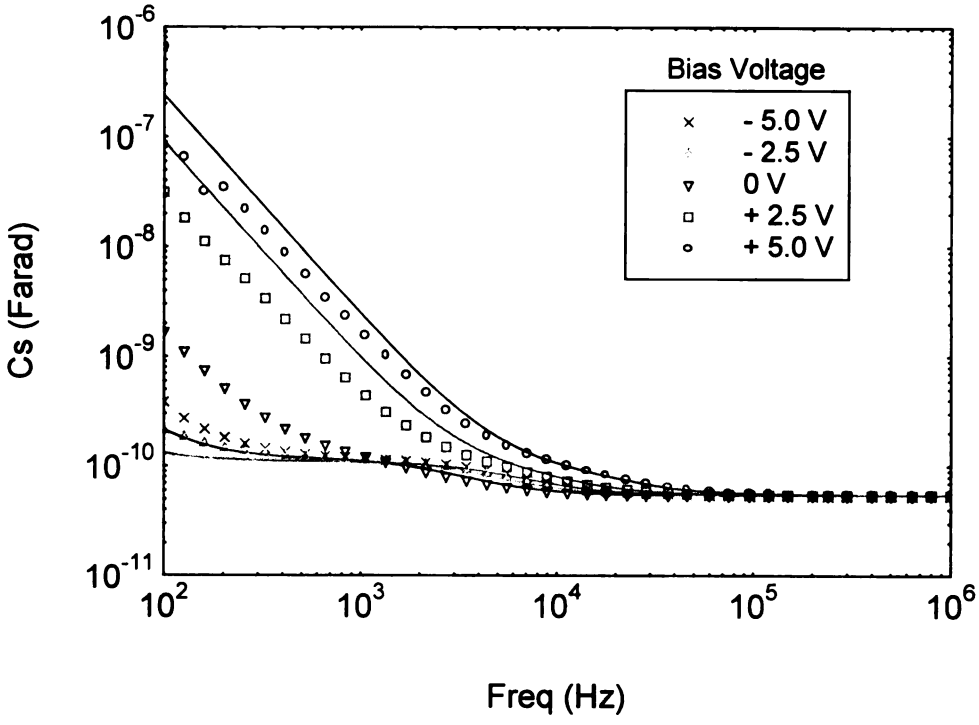

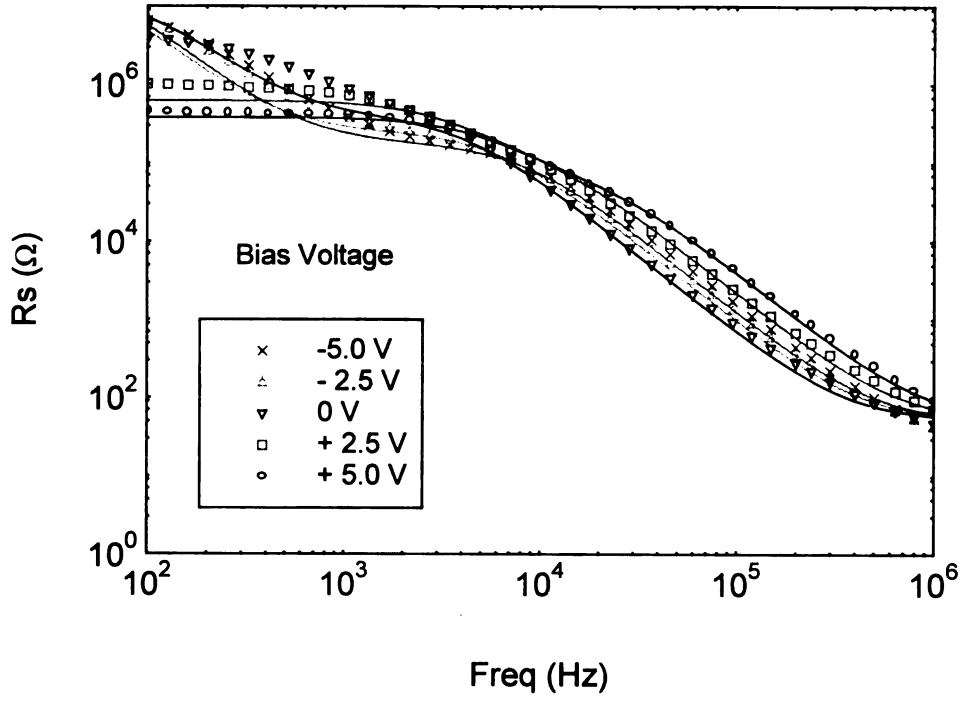

Figure 5.5 Continued

To obtain results which include Glover's C_f and R_f elements, our model Equation 5.1 must be re-written as

$$Z = \frac{R_J}{1+i\cdot\omega\cdot R_J C_J} + \frac{R_B}{1+i\cdot\omega\cdot R_B C_B} + \frac{1}{i\cdot\omega\cdot C_f} + R_f \qquad (5.4)$$

The value of C_P, R_P, C_S and R_S can then be calculated from Equation 5.2.

In order to obtain the value of B, one must have the values of N_a, C_{CAP}, and N_R. However, for the first approximation, we use the middle value of 10^{14}-10^{18} cm^{-3} reported acceptor concentration on natural type IIb diamond [21] [101], which is $N_a = 10^{16}$ cm^{-3}, a dielectric constant for diamond of 5.5, a valence band density of states $N_r = 10^{15}$ cm^{-3} [124], and use the activation energy of 0.21 eV obtained in section 4.3. Glover also reported the C_{CAP} value in the order of 10^{-10} cm^3/s for natural type IIb diamond.

For those values given above, the approximated value of B is in the order of 10^{-6} $F/(cm^2.sec^{1/2})$. Figure 5.6 shows the fitting between experimental results and the model in Equation 5.4. Note that all the value of C_J, R_J, C_B and R_B were maintained at the same value as used in previous fitting between experimental results and model in Equation 5.1 (without R_C). With B = 7x 10^{-6} $F/(cm^2.sec^{1/2})$ in our model, an improved fit in C_P, R_P, C_S and R_S can be obtained than that of simple model in Figure 5.4.

Let us now turn our attention to the admittance results of BC4 given in the last section. We also apply the models described above to BC4 results with the similar process. In both the C_S and C_P measurement, it is observed that at high frequency, the capacitances of diode BC4 approach a saturation value of 4.41 pF regardless of the bias.

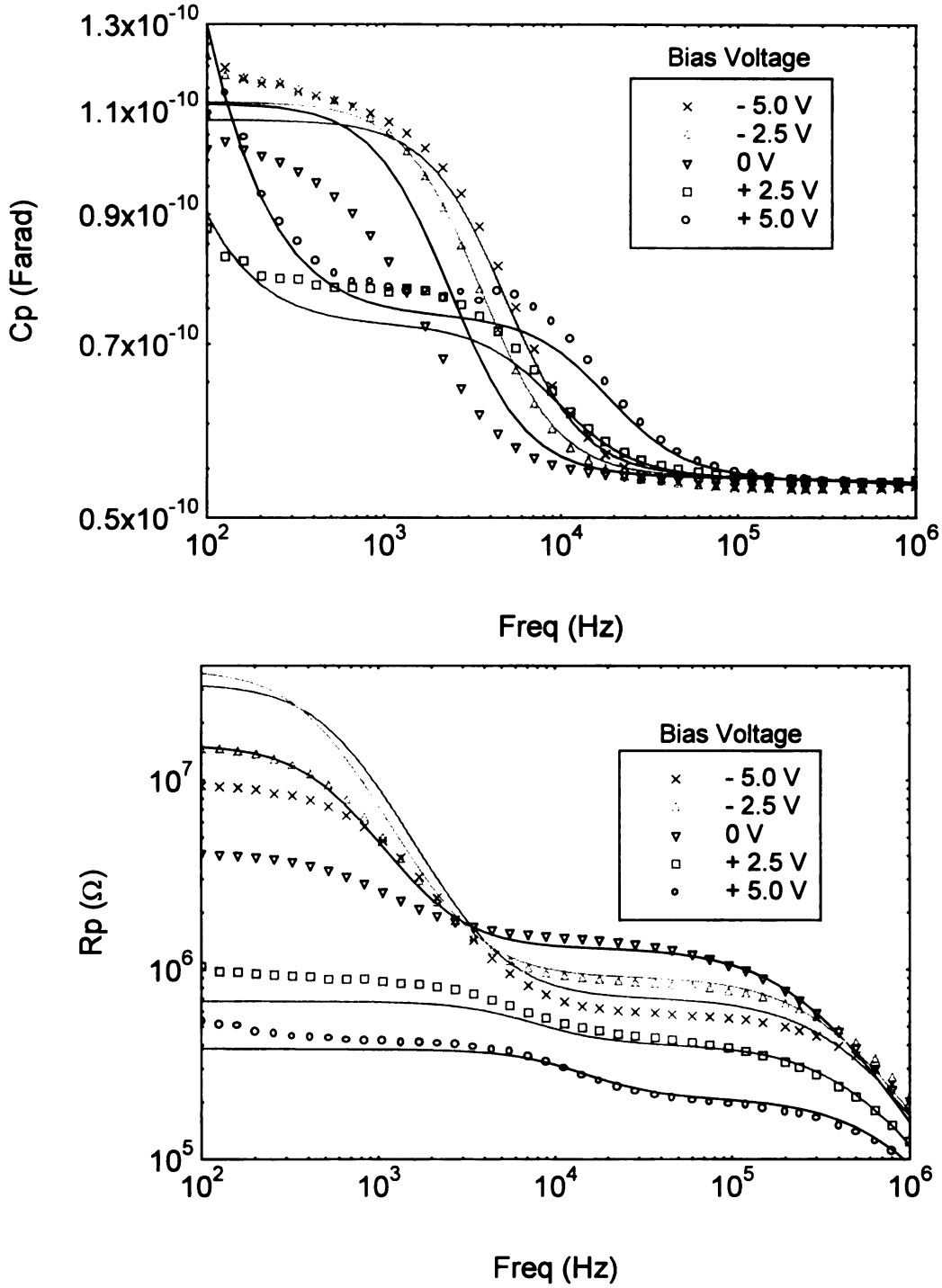

Figure 5.6 Fitting between the C_P, R_P, C_S, and R_S experimental results of SK7-B and the model which include Glover's element C_f and R_f.

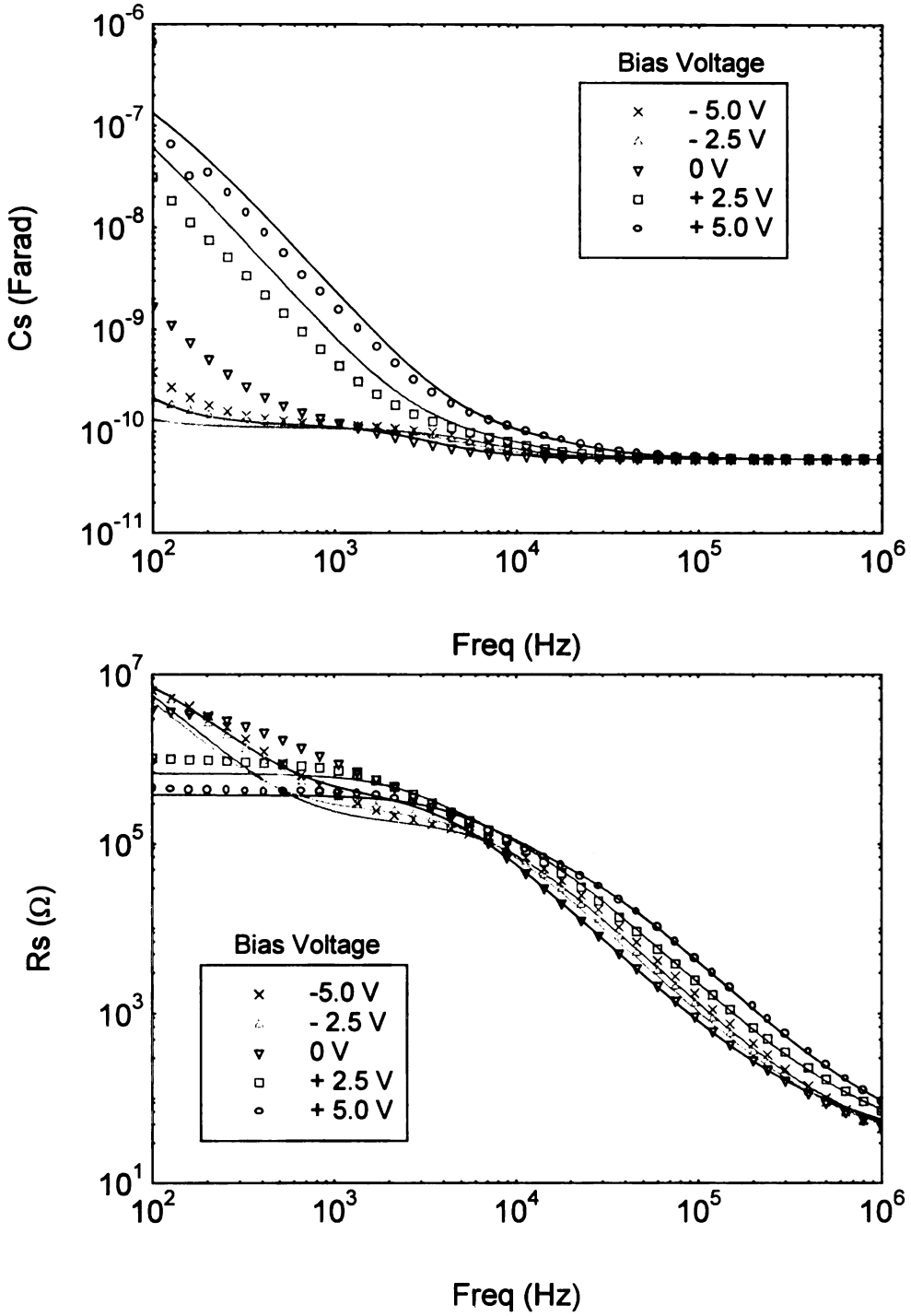

Figure 5.6 Continued.

According to the analysis in section 2.4, this value equals to the sample geometrical capacity, εA/L. Taking the area of the diode 4.91×10^{-4} cm^2 into account, the thickness of the diode, L, is found to be 0.54 μm. Also, the dc current-voltage measurement of this diode yields the value of R_B of 1.2 MΩ.

Under forward bias, value of the dynamic resistance R_J can be calculated from ηkT/I. From dc measurement, the ideality factor of BC4 is 2.4 and saturation current is 1.8 pA. Under reverse bias, ideally R_J is very large (infinite), in practice R_J can be obtained from dI/dV at a specific reverse bias voltage of the dc measurement. Again, by adjusting the value of two variables, w and R_B, we can find the fit for the simple model. Figure 5.7 shows the results of the fitting between experimental data and simple circuit model results at three different bias voltages. Table 5.2 shows parameters used in the fit. From the plot in Figure 5.7, it is shown that the simple model does not explain the characteristic of the responses of BC4. Furthermore, by adding contact resistance effect as in equation 5.3, we found that with the contact resistance up to 1 KΩ, there is no significant change in model calculation results.

Bias voltage	w (μm)	R_B (ohm)	R_J (ohm)
+ 5.0 V	0.81	330 K	48 K
0.0 V	0.88	320 K	15 M
- 5.0 V	0.94	180 K	42 M

Table 5.2 The parameter values used in model fitting of the diode BC4 in Figure 5.7.

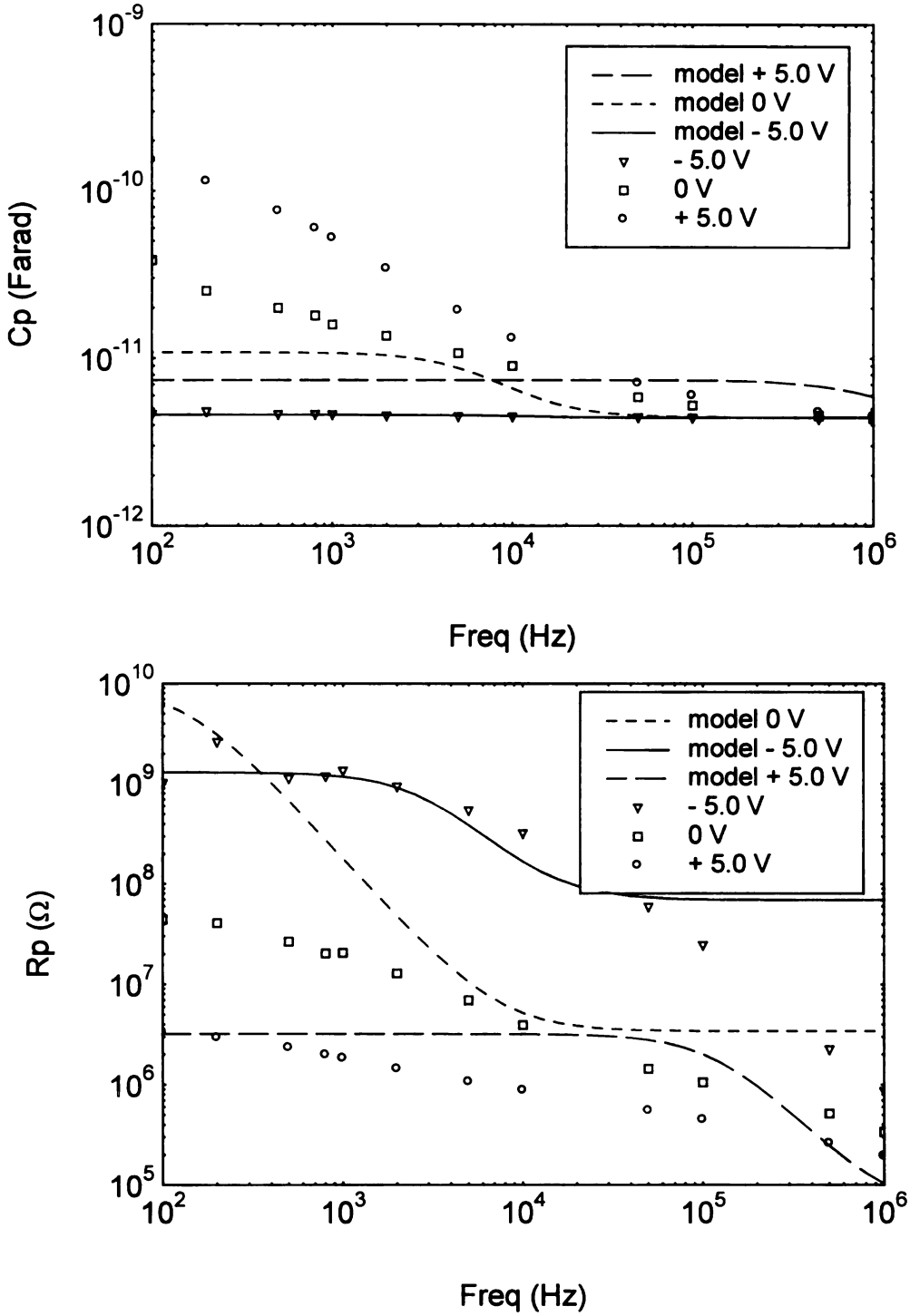

Figure 5.7 Fitting between the C_P, R_P, C_S, and R_S experimental results and the simple circuit model of sample BC4.

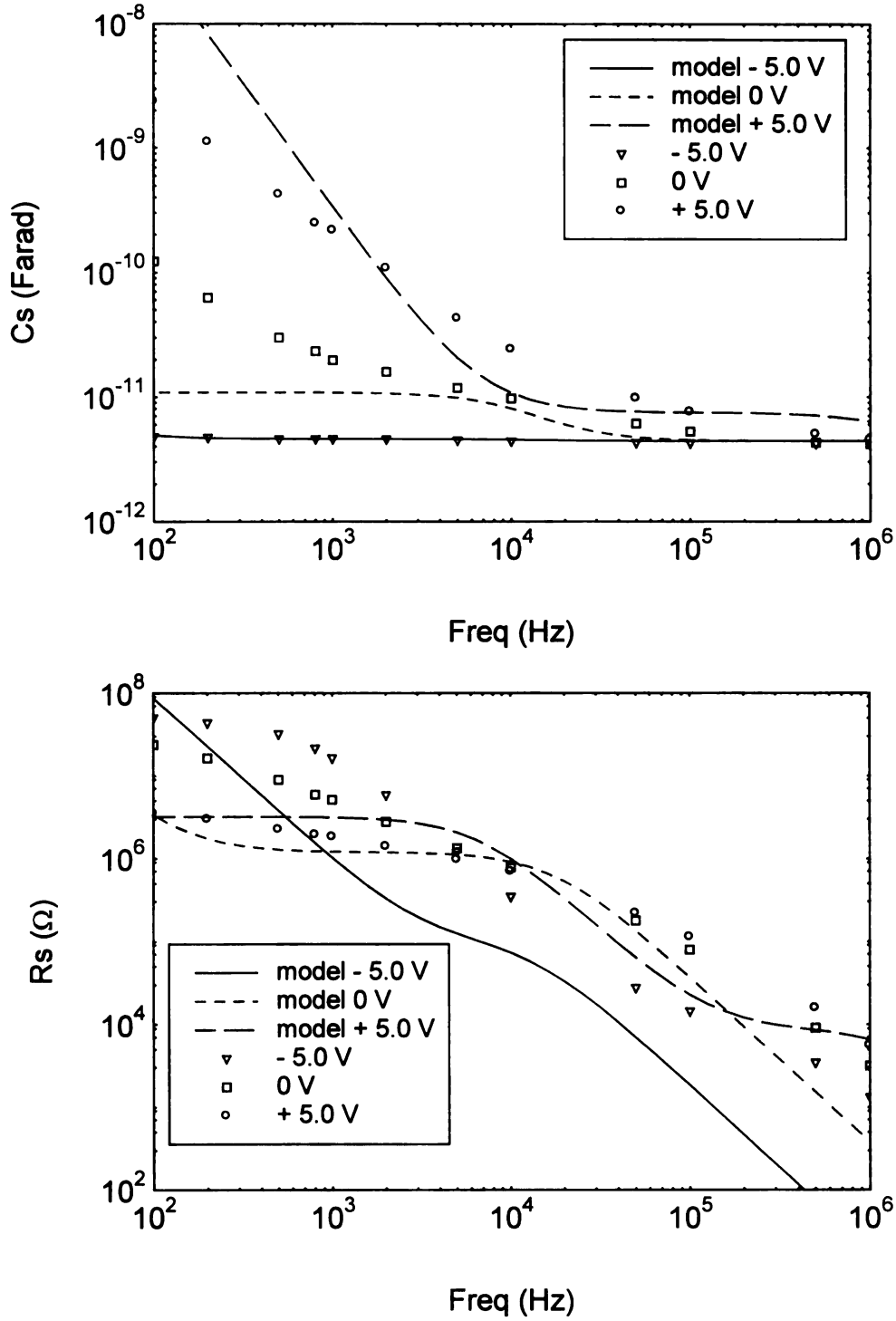

Figure 5.7 Continued.

Finally, the experimental results of BC4 are fitted with model that includes trap state effect. As can be seen from Figure 5.8, although there are some fitting improvement in the plot at high frequency over that of simple circuit model in Figure 5.7, the model still can not explain the admittance characteristics of BC4.

In conclusion, we have compared the experimental results with three types of models – (I) a basic model which only involves junction (C_J, R_J) and bulk (C_B, R_B) components, (II) a model which adds the effect of contact resistance R_C, and (III) a model which instead of R_C includes deep trap state effects. Some of our sample's small signal responses can be generally represented by models given above (e.g. SK7-B). However, the responses of other such as BC4 could not be explain by those three models. The comparison between those models and the experimental results of SK7-B show that the model with trap state effects give the best fit to C_P, R_P, C_S and R_S among the three models. However, it has been observed that the simulation results of model with contact resistance (R_C) and the model with trap state components (C_f ,R_f) gave a very similar results in R_P, C_S, and R_S simulations. The difference between those two models is in the results of C_P, which will not be observed if the experimental data are only taken in series mode (C_S, R_S). This has in fact often been the case in the literature. Furthermore, since the characteristics of both models are very similar, the real response of the diamond Schottky barrier diode is possibly affected by both the contact resistance and the deep trap state effects.

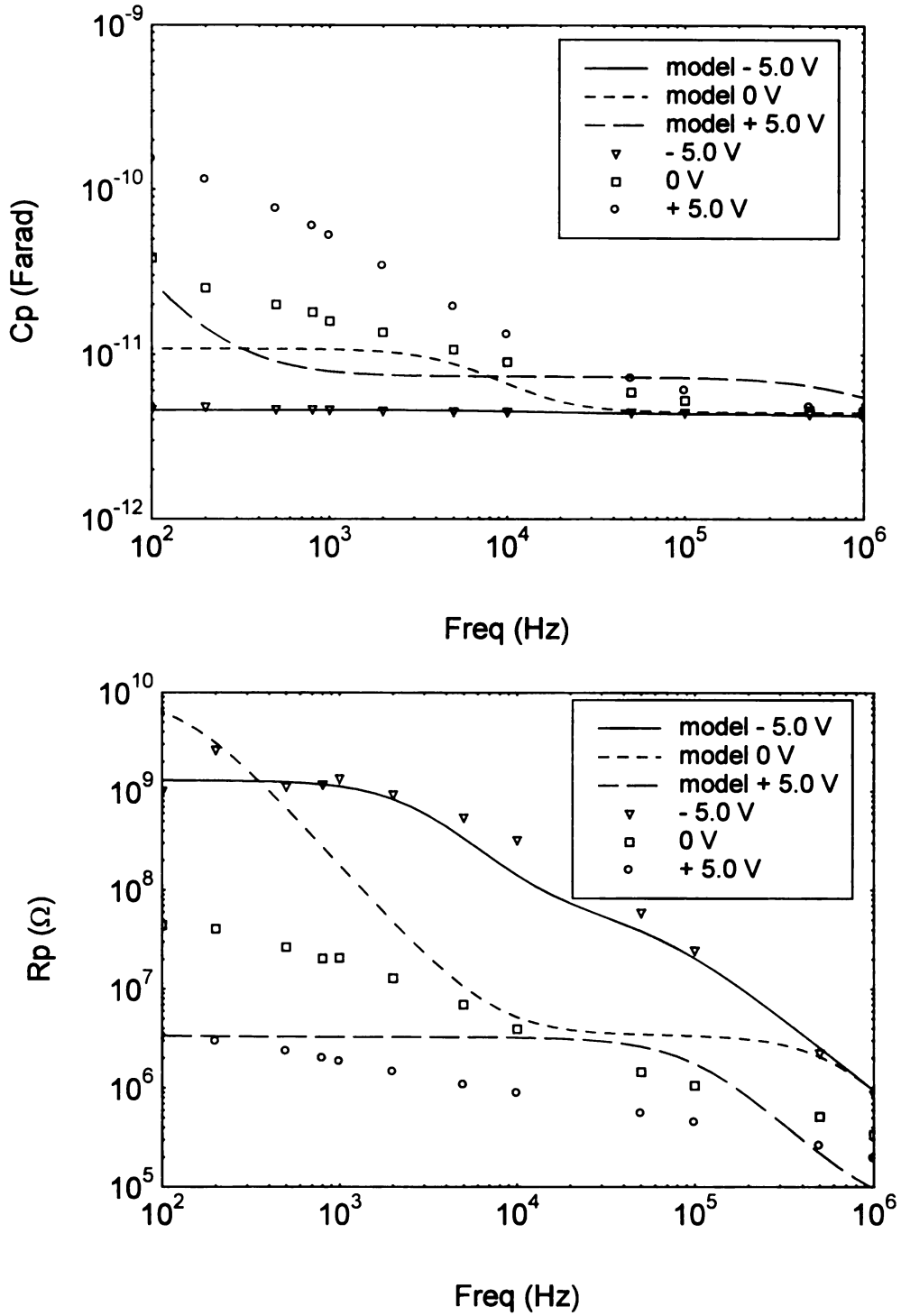

Figure 5.8 Fitting between the C_P, R_P, C_S, and R_S experimental results of BC4 and the model which include Glover's element C_f and R_f. Here B = 2.7×10^{-7} F/(cm^2.sec$^{1/2}$).

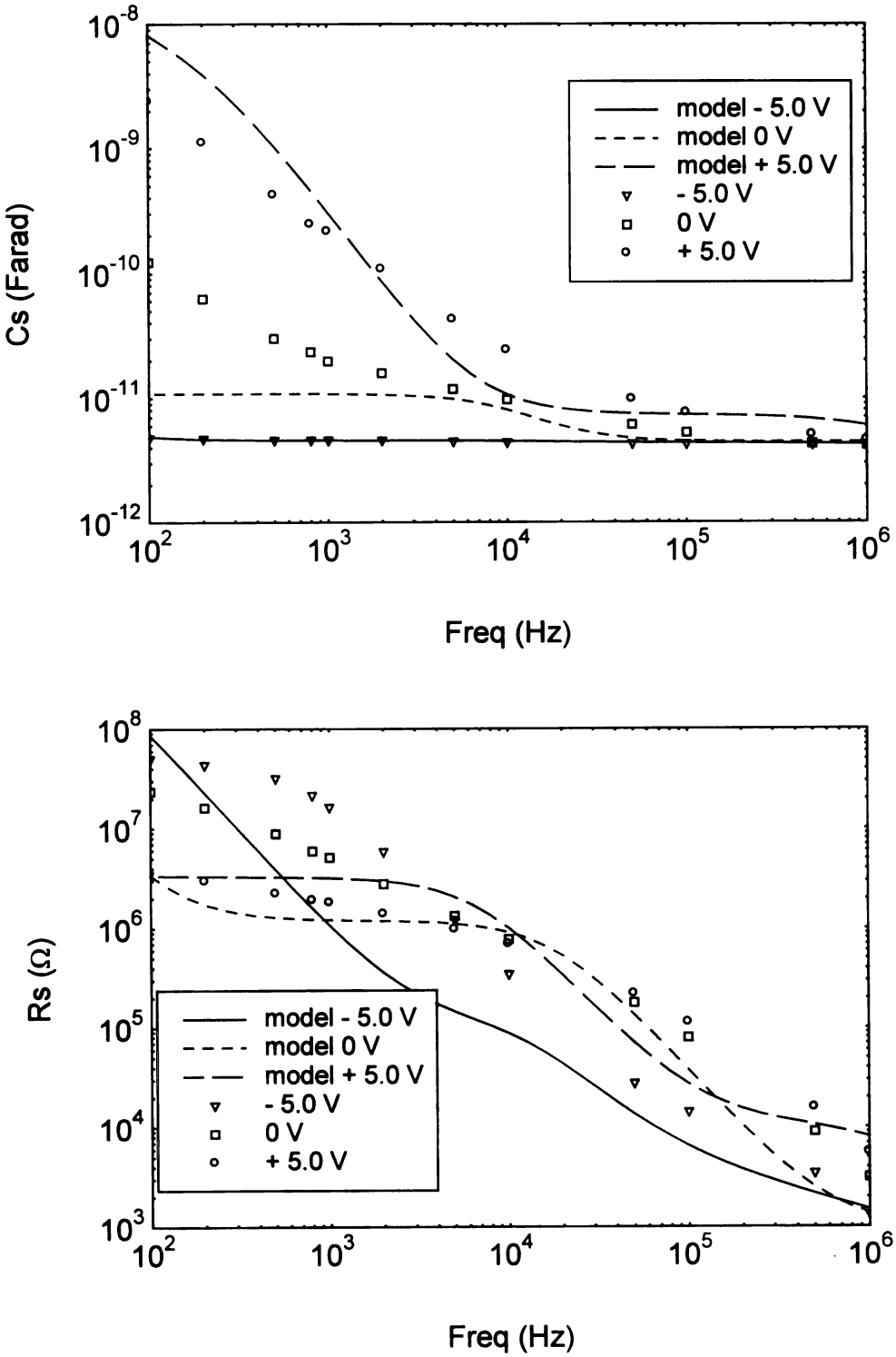

Figure 5.8 Continued.

5.4 Application implications of the small signal results

In the previous sections of this chapter, the focus has been primarily on the implications of the small signal results on diode models. However, diodes are also used for small-signal electronic applications. When reverse biased, they are used as small-signal, voltage-variable capacitors, or varactors. When forward biased, diodes may be used as small-signal, voltage-variable resistors, or varistors.

In terms of using the diamond Schottky barrier diodes as forward-biased varistors, Figure 5.3 which represents the results for a sample on film SK7, one of the faster diodes in the study, shows a significant bias dependence of the small signal resistance R_P well beyond 100 KHz. For example, at 200 KHz, the small signal resistance is approximately 700 KΩ at zero volt bias, 350 KΩ at 2.5 volt bias, and 200 KΩ at 5 volt bias, decreasing with forward bias as expected. By 1 MHz, however, the varistor action is largely lost.

As for the use of diamond diodes in this study as varactors, Figure 5.2 shows that sample BC4 shows appreciable reverse bias variation, decreasing with increasing reverse bias, for frequencies up to about 10 KHz. For sample SK7, the capacitance variation is more complex, as previously discussed, with non-monotonic variations of capacitance with voltage. Speed limitations are discussed in more detail in the next chapter.

CHAPTER 6

Large signal response of diamond Schottky barrier diodes

6.1 Chapter overview

This chapter presents the results of investigations on the large switching signal response of the diodes. The first two sections of this chapter discuss the effects of load resistances and the coaxial connecting cables which give rise to a significant parasitic capacitance in the measurement setup. These parasitic capacitances are incorporated into the SPICE model. The experimental results are then presented and compared to the SPICE simulation results. Next, the sensitivity of the SPICE simulation results to changes in transit time parameter of the diode are considered. The final two section in this chapter discusses possibilities for improving the rectification frequency limit or "speed" of the diamond Schottky diode by mean of area scaling and material doping.

6.2 Measurement circuit considerations

To study diode responses to a large switching signal, basically, we can pass switching signals between forward and reverse bias from a function generator to the

Schottky barrier diode, then, probe the output responses by an oscilloscope. However, there are some circuit considerations needed before the data be presented. Figure 6.1 illustrates the measurement circuit used to obtain the measurement results from the setup in Figure 3.10.

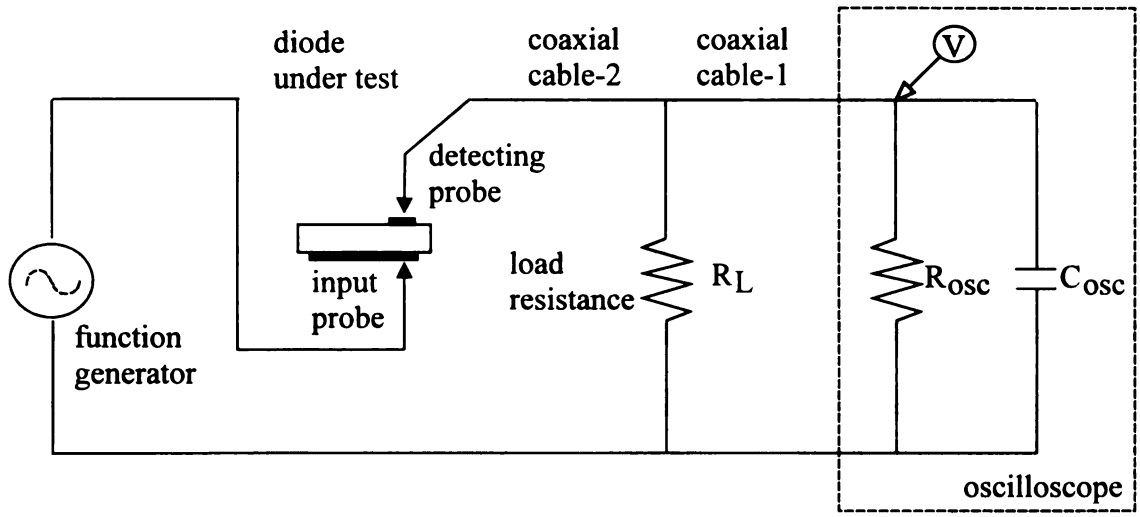

Figure 6.1 Measurement circuit for large switching signal responses experiments.

In Figure 6.1, R_L represents the load resistance used in the setup to adjust the effective input impedance of the oscilloscope. To appreciate the effect of this R_L, let us first consider the HP 54200D oscilloscope without any load resistance R_L. The oscilloscope is connected to the detecting probe via a 50-Ω coaxial cable. The oscilloscope specification indicates its input impedance as a 1 M Ω resistance in parallel with a 14 pF capacitance. However, the effect of the coaxial cable-1, as will be described in the next section, is to cause the effective value of input impedance at 10 KHz to be a 1

MΩ resistance in parallel with a 112 pF capacitance. The RC time constant of these input components is then approximately 112 μs which is even larger than a 100 μs full period of a 10 KHz signal. Figure 6.2 (a) shows the effect of this large time constant for a 10 KHz input, in which the diode plus the RC components basically act as an ac to dc converter, with a ripple voltage. This precludes observation of diode switching action.

By introducing an appropriate load resistance, R_L, into the measurement circuit, this large RC time constant can be reduced to give less effect on the circuit responses. Figures 6.2 (b) to 6.2 (e) show the experimental results when R_L values of 200 KΩ, 51 KΩ, 10KΩ, and 2.01KΩ were used with sample BC4. It can be seen in Figure 6.2(b) to 6.2 (d) that as expected, the lower the value of load resistance R_L, the less effects of the input RC are noticed. However, the response while using a 2.01KΩ load resistance in Figure 6.2 (e) does not show significant differences in shape characteristics from the response while using 10KΩ load resistance in Figure 6.2 (d). At this point, another issue needs to be addressed, which is the lower the value of R_L, the weaker the response signals detected by the oscilloscope. This is simply due to the voltage division resulting from high bulk resistance of the diamond samples. Although similarity in shape of response is observed when using 10KΩ and 2.01KΩ load resistance values, the response is much weaker and exhibits much higher noise when using the 2.01KΩ load resistance. Therefore, a load resistance of 10 KΩ was used in sample BC4 experiment.

By using the same consideration as above, an appropriate value of R_L could be established for other samples. The suitable R_L for other samples used in this research was found to be between 10 KΩ and 50 KΩ.

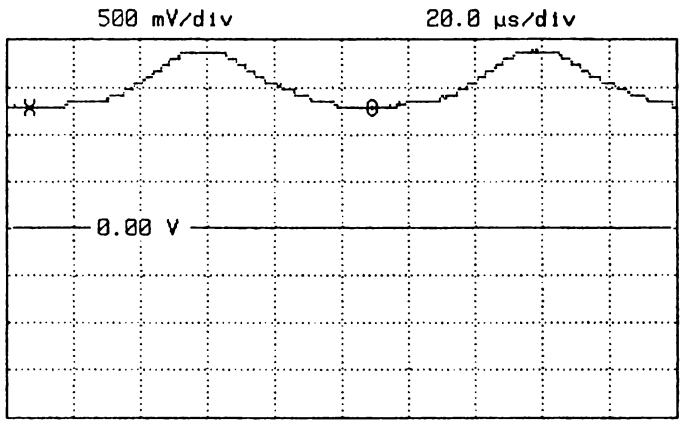

(a)

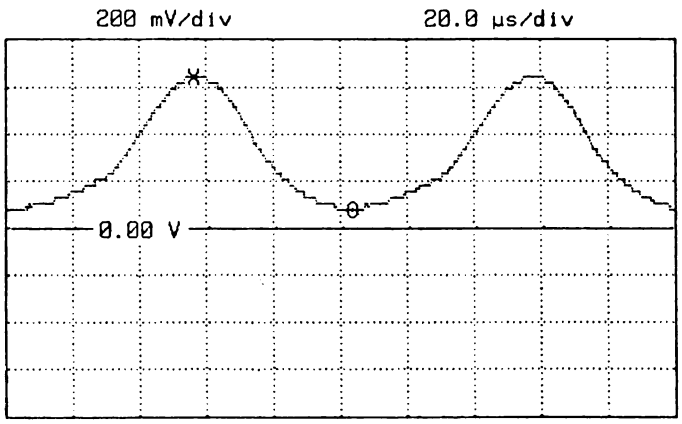

(b)

Figure 6.2 Responses of BC4 to a 20-V_{pp} 10-KHz sine wave with (a) no load resistance, (b) 200 KΩ load resistance, (c) 51 KΩ load resistance, (d) 10 KΩ load resistance, and (e) 2.01 KΩ load resistance.

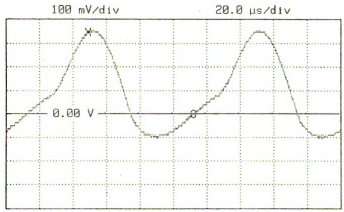

(c)

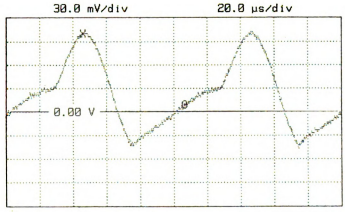

(d)

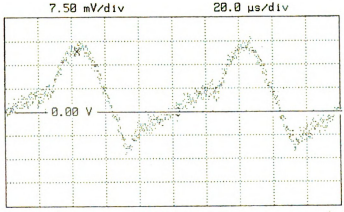

(e)

Figure 6.2 continued

6.3 Effects of connecting cables and load resistance in the measurement circuit

In dc or low frequency testing, normal laboratory practice usually neglects the effects of connecting cables between probes and the measurement equipment. As the frequency of operation is increased, however, connecting cables can have marked effect on the sample under test. In the large signal test part of this research, two coaxial cables were utilized; one to connect from the detecting probe to the load resistance and another from the load resistance to the oscilloscope as shown in Figure 6.1.

To account for the effects of these cables, we begin by considering the simple cable system shown in Figure 6.3. At dc and very low frequencies, the input impedance Z_i would be equal to load resistance Z_r. This is simply the expected behavior of a pair of wires from a circuit point of view [125].

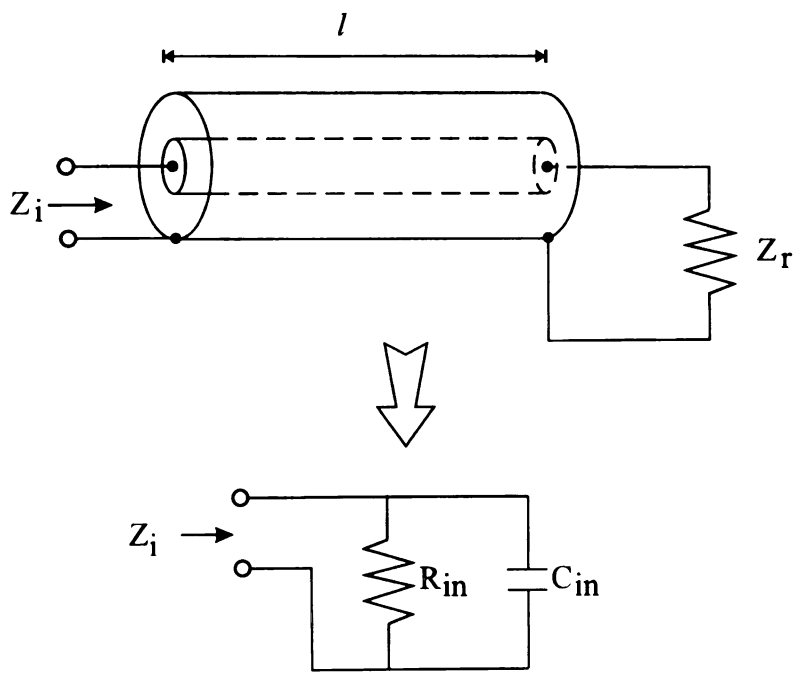

Figure 6.3 Coaxial cable circuit.

However, as frequency is increased, the coaxial cable in Figure 6.3 should be viewed as a transmission line terminated with load Z_r. For the case of a lossless cable under sinusoidal excitation the relationship between Z_r and Z_i for a cable of length l is given by [125] [126]

$$Z_i = Z_O\left(\frac{Z_r + jZ_O \tan(\beta \cdot l)}{Z_O + jZ_r \tan(\beta \cdot l)}\right) \tag{6.1}$$

where Z_O is the characteristic impedance of the cable, and β is the propagation constant. If v_P is defined as the speed at which an electromagnetic wave propagates along the cable, and f is the frequency, the value of β can be found from

$$\beta = \frac{\omega}{v_P} = \frac{2\pi f}{v_P} \tag{6.2}$$

If v_C is the velocity of light, the coaxial cable v_P value can be calculated from its dielectric value of polyethylene medium $\varepsilon = 2.25\ \varepsilon_O$ and $\mu = \mu_O$ as [125] [127]

$$v_P = \frac{1}{\sqrt{2.25 \cdot \varepsilon_O \mu_O}} = 0.68 \cdot v_C \tag{6.3}$$

For a 1-meter 50-Ω coaxial cable connect to a 1MΩ (shunted by 14 pF) oscilloscope, at 10 KHz measurement frequency, $\beta = 1.54 \times 10^{-5}\ m^{-1}$. The effective input resistance R_{in} and capacitance C_{in} can be calculated from

$$Z_1 = 50\Omega\left(\frac{(1\text{M}\Omega\,//\,14\text{PF}) + 50\Omega \cdot j\tan(1.54\cdot 10^{-5})}{50\Omega + (1\text{M}\Omega\,//\,14\text{PF})\cdot j\tan(1.54\cdot 10^{-5})}\right)$$

to be $10^6\Omega$ and 112 pF respectively.

Let us consider our measurement circuit interpretation shown in Figure 6.4. As can be seen from the circuit, the impedance Z_{OSC} of the oscilloscope can be calculated from the parallel circuit of oscilloscope load value R_{OSC} and oscilloscope shunt capacitance C_{OSC}. Equation 6.1 then can be applied to give the input impedance Z_1 as observed "looking in" form the first coaxial cable

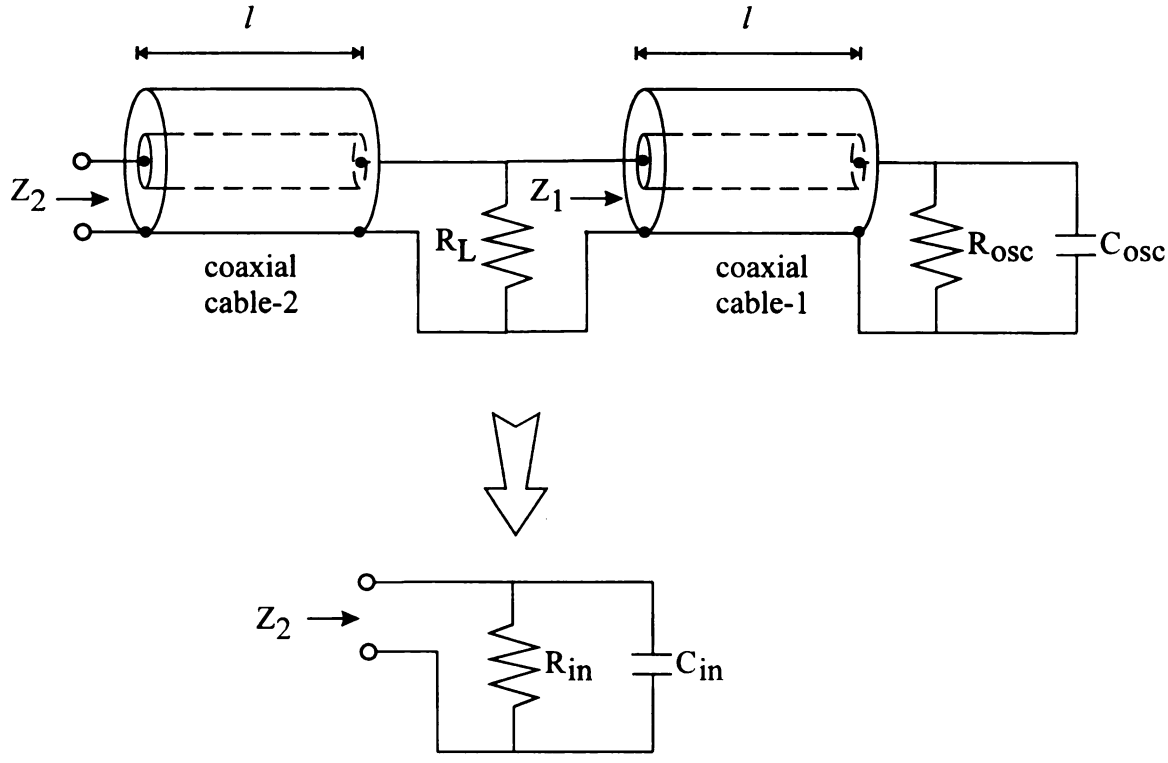

Figure 6.4 Circuit interpretation of the two coaxial cables used in the large signal response measurement.

$$Z_1 = Z_O\left(\frac{Z_{OSC} + jZ_O \tan(\beta \cdot l)}{Z_O + jZ_{OSC} \tan(\beta \cdot l)}\right) \qquad (6.4)$$

Equation 6.1 can also be applied to give the input impedance Z_2 as "looking in" from the second coaxial cable

$$Z_2 = Z_O\left(\frac{Z_L + jZ_O \tan(\beta \cdot l)}{Z_O + jZ_L \tan(\beta \cdot l)}\right) \qquad (6.5)$$

Here, the value of Z_2 is calculated from the parallel combination of the additional load resistance R_L and input impedance Z_1 from the first cable. To utilize the result of Z_2 in our later simulation process, the equivalent circuit resistance R_{in} and capacitance C_{in} can be obtained from real and imaginary part of Z_2 respectively.

For our measurement setup, the HP54200D oscilloscope R_{OSC} and C_{OSC} are, as noted, given as 1MΩ and 14pF respectively. Two 1.0-meter RG-58/U coaxial cables are used. These cables have a nominal characteristic impedance of 53.5 ohms [127]. With a load resistance R_L of 10 KΩ, at a test frequency of 10 KHz, the effective input resistance R_{in} and capacitance C_{in} are calculated to be 9.901 KΩ and 197.2pF respectively. This result shows that the combination of coaxial cables and load resistance will introduce a significant amount of capacitance, which appears in parallel with the input of the oscilloscope and must be included into our simulation model.

6.4 Experimental results and SPICE model comparison

As described in detail in section 3.9, the diode responses to a large switching signal were studied by passing a 20 V_{PP} sine wave from a function generator to the Schottky barrier diode. The output responses were then probed by an oscilloscope with load resistance R_L as in the circuit model of Figure 6.1. All measurements were conducted in the light-tight box. The experimental results at difference input frequency will be presented in this section in comparison to SPICE simulation results.

In SPICE simulation, the response of the diode under an ac signal is modeled not only by the nonlinear current source described earlier in section 4.7, but also by diode capacitances, which are voltage-dependent and represent the charge storage effects of the junction. Table 6.1 shows the addition SPICE diode model parameters for the ac simulation.

SPICE parameter	Compared notation	Parameter description
CJO	C_{jo}	Zero-bias junction capacitance
VJ	V_{bi}	Barrier potential or "built-in" potential
M		Grading coefficient
TT	τ_D	Transit time
FC		Coefficient for forward bias depletion capacitance formula

Table 6.1 Additional SPICE diode model parameters for ac simulation.

SPICE models charge storage in diode with two distinct capacitive mechanisms [26], which are (1) capacitive effect of the depletion region and (2) capacitive effect from mobile carriers (diffusion capacitance). The depletion region capacitance follows the simple approximation that the depletion region serves as the gap between "plates" of a capacitor. The depletion region varies in thickness, and therefore the capacitance varies with applied voltage. The approximation of depletion region capacitance in SPICE implementation is given by

$$CJ = \frac{CJO}{\left(1 - \frac{V}{VJ}\right)^{M}} \tag{6.1}$$

where CJO is the zero-bias junction capacitance value, V is the applied voltage, VJ is the junction barrier potential and M is the grading coefficient. M varies between 1/2 for step junction to 1/3 for linearly graded junction. The above equation is actually the same as equation 2.10 with M equal to 1/2 for Schottky barrier diode.

Inspection of the capacitance equation 2.10 and/or 6.1 reveals that it predicts infinite capacitance for a forward bias, which is not the case for a real junction. For practical reasons, SPICE uses a simple approach: for forward bias beyond some fraction (set by parameter FC which by default = 0.5) of the value of VJ, the capacitance is determined as the linear extrapolation of the capacitance at the departure.

In diodes with both majority and minority carriers, the charge storage due to excess minority carriers injected across the junction under forward bias gives rise to another capacitive effect in SPICE simulation, diffusion capacitance. This charge, and therefore capacitance, is proportional to the total current injected across the junction. The

proportionality constant (SPICE parameter TT) between the current and the charge is a time constant which represents the minimum time required to either store or remove the charge. It is called the transit time of the diode [26]. The total charge Q in the region is therefore

$$Q = \text{device current} \times \text{transit time}$$

SPICE calculates the diffusion capacitance from the derivative of the above equation with respect to bias as the following (see also equation 4.3)

$$\text{diffusion capacitance} = TT \cdot \frac{IS}{N \cdot VT} \cdot EXP\left[\frac{V}{N \cdot VT}\right] \qquad (6.2)$$

Figure 6.5 shows the circuit used to perform the SPICE simulation. It should be noted that one disadvantage of the SPICE diode model is that SPICE neglects the effect of the capacitance due to the bulk part of the thin-film diode and does not include it into its model parameters. Therefore, the element CB representing the bulk capacitance is placed in parallel with the bulk resistance RB. Actually the bulk resistance of the diode may be provided as one of the SPICE diode parameters, namely RS (see section 4.7). However, to simulate both the resistive and capacitive effects of the bulk part, the value of RS in the diode parameters is set to zero and the bulk resistance value is instead placed into RB. Again, CB is calculated from the simple approximation of parallel plate capacitance as in equation 2.14.

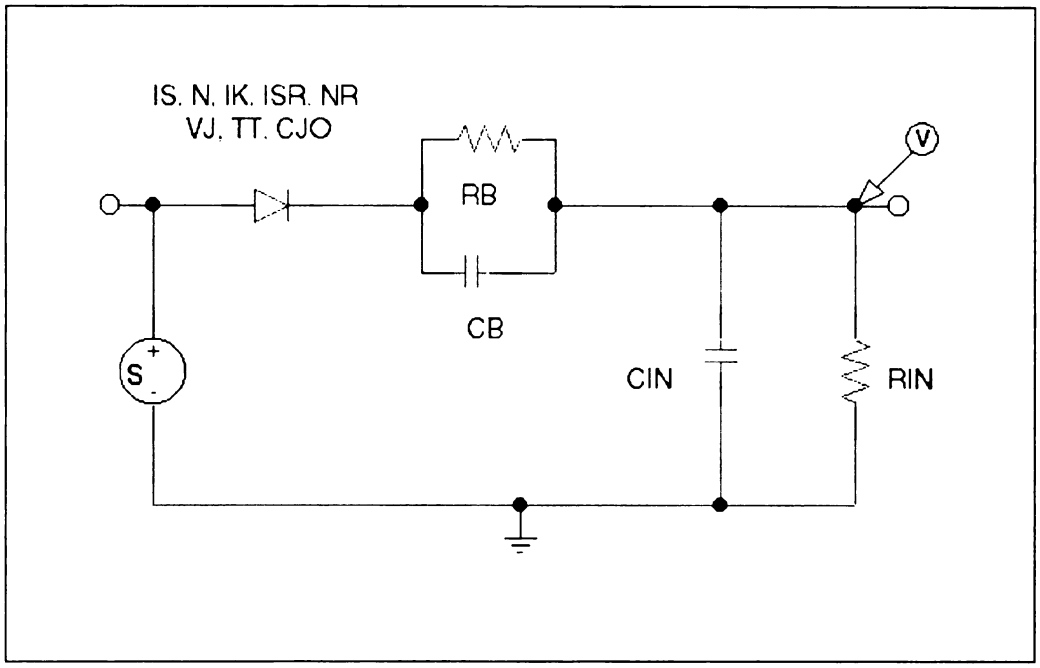

Figure 6.5 Measurement and simulation circuit for diamond diode switching experiments.

In Figure 6.5 the elements RIN and CIN represent the combination of the load resistance, coaxial cables and the oscilloscope input impedance as described in detail earlier in section 6.3. The values of diode parameters – IS, N, RS (now RB), IK, ISR and NR are obtained from dc current-voltage measurement as described in section 4.7. The rest of parameters, which are VJ, TT, CJO and CB, are obtained by adjusting the parameters to fit the SPICE modeled results to the experimental results.

There are some considerations for what range of value of VJ, TT, CJO and CB should be used in the simulation. As discussed in section 4.5, the barrier height value of diode (ϕ_B) obtained from section 4.3 can be used as an upper bound limit and guide line for the built-in potential VJ value. And since Schottky barrier diode operates as a

majority carrier device under low-level injection, small values (between 10^{-18} - 10^{-9} second) were first be used for TT in the SPICE simulation. Also because the value of both CJO and CB are only dependent on the depletion width W as in equation 2.8 and 2.14, one only needs to vary the value of W in the simulation to obtain both CJO and CB. A limitation of the SPICE simulation is that CB is constant for a given simulation ren. In fact, W changes with bias. This is accounted for in SPICE for CJ but not CB. However, as will be shown later in this chapter (section 6.7), CB does not play a dominant role in the switching properties of the diode.

For the switching waveform of sample BC4 in Figure 6.6, the oscilloscope input resistance and capacitance were 1 MΩ and 14 pF respectively. The load resistance was 10 KΩ, so the values of RIN and CIN within the test frequency of 1 KHz to 10 KHz are approximately 9.901 KΩ and 197 pF respectively. The dc current-voltage measurements in chapter 4 on the diode indicated a bulk resistance RB value of 1.2 MΩ. The parameters IS = 1.8 pA, N = 2.40, IK = 1.2 nA, ISR = 4.3 pA and NR = 3.06 were obtained from the fitting between the dc current-voltage experimental result and the dc SPICE simulation as described in section 4.7.

When the values of VJ = 0.8 V, TT ≤ 1 μs, CJO = 10.86 pF and CB = 7.01 pF were used in the SPICE simulation, a good fit to the measured data was obtained within 1 to 20 KHz frequency range as shown in Figure 6.6. Given the film thickness of 0.56 μm, the values of CJO and CB given above correspond to the depletion width of 0.22 μm at zero bias. Note that varying values of TT parameter from 0 to 1 μs did not give significant difference in the SPICE simulation. This will be discussed in the next section.

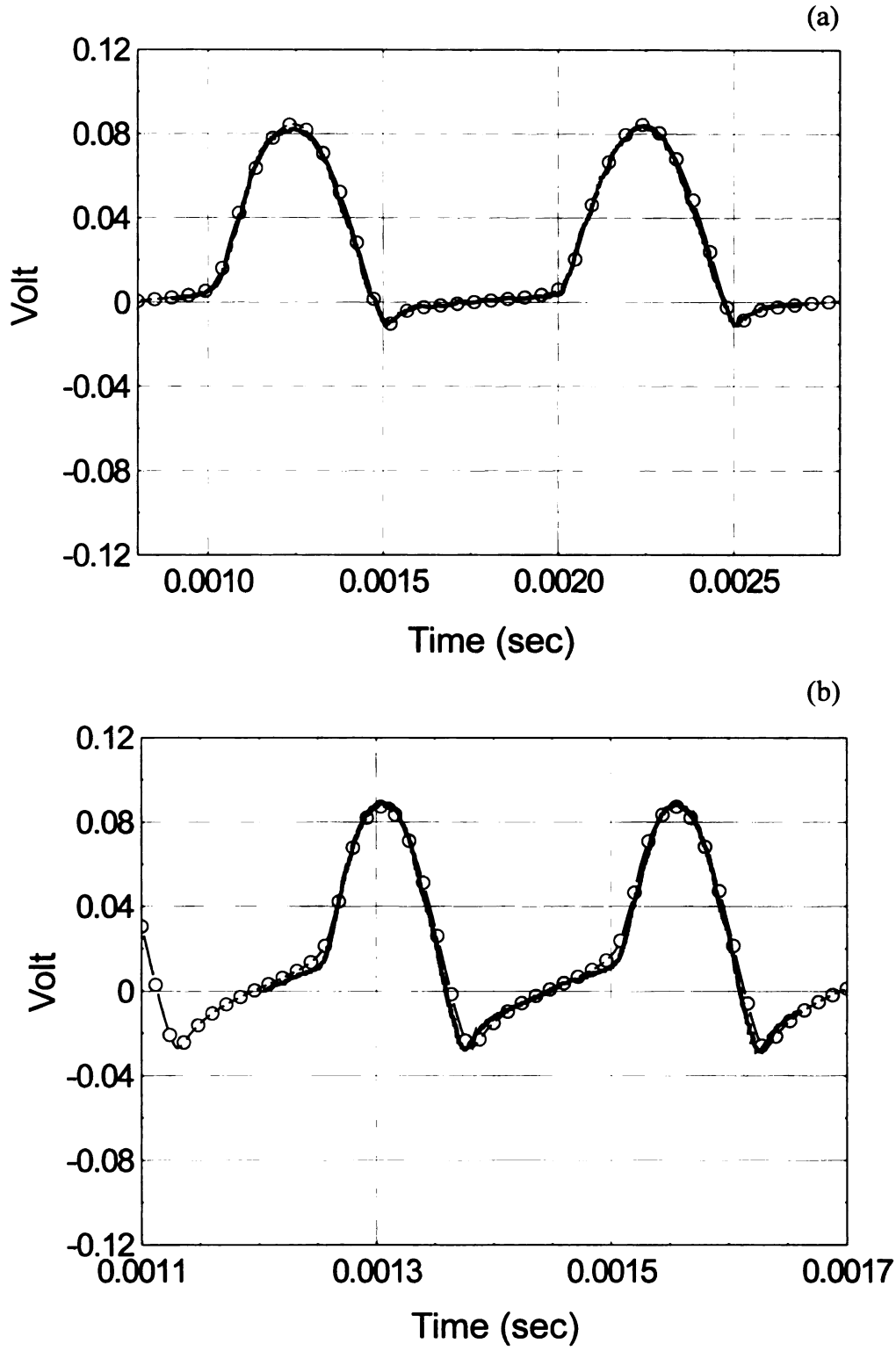

Figure 6.6 Switching responses of sample BC4 at (a) 1 KHz, (b) 4 KHz, (c) 10 KHz, and (d) 20 KHz. Thick solid lines represent experimental results. Thin lines with circle marks represent SPICE simulation results.

(c)

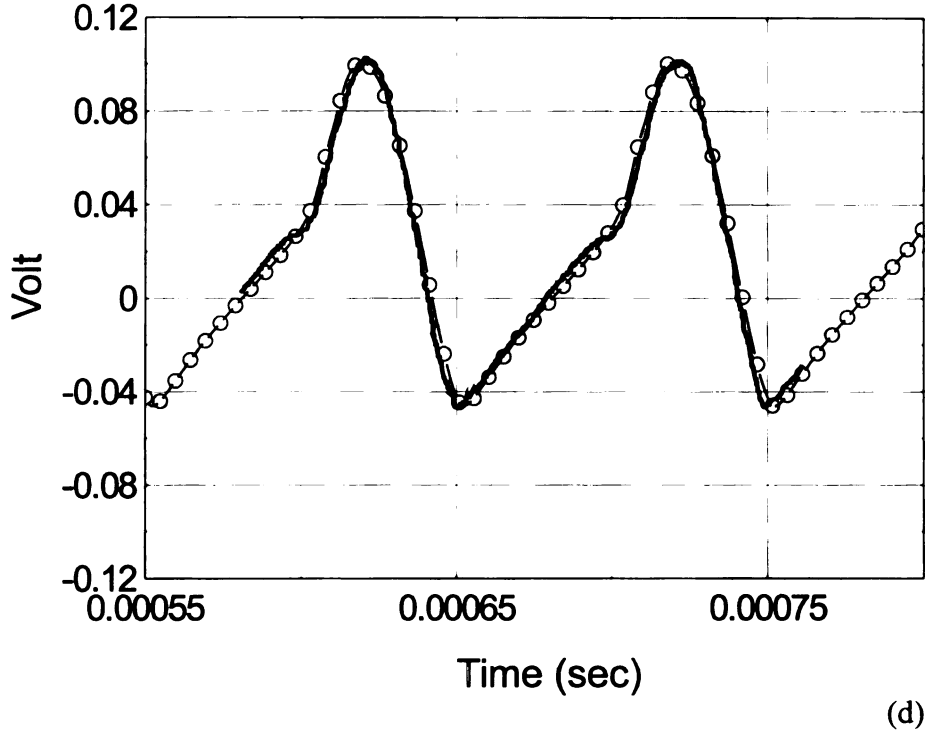

(d)

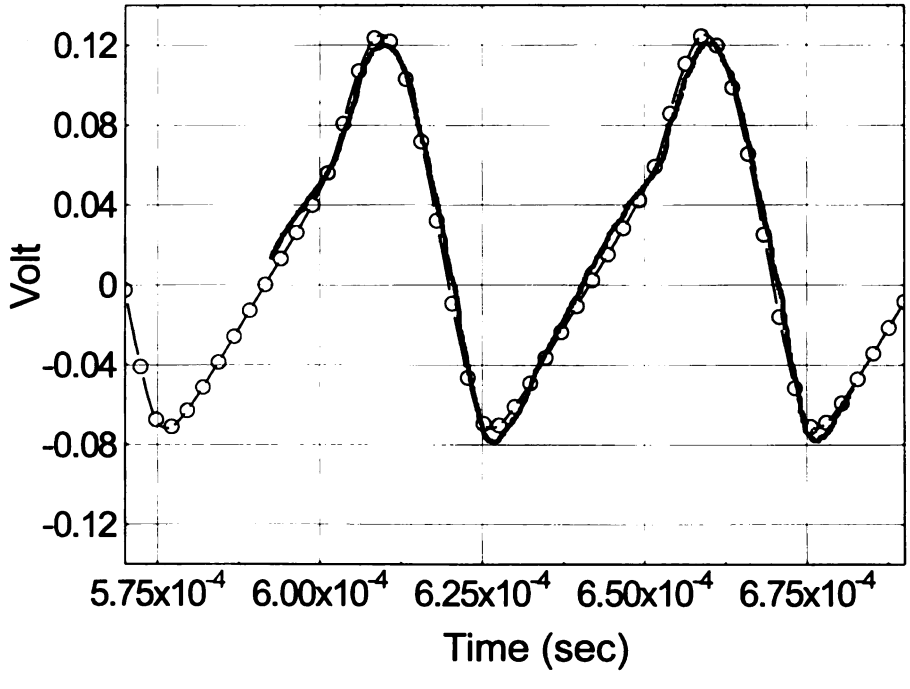

Figure 6.6 Continued

6.5 Sensitivity of SPICE model to changes in transit time parameter TT

As previously mentioned in section 2.5, if an appreciable fraction of the forward bias current in the Schottky barrier diode is due to minority carriers, then upon switching to reverse bias, a reverse current flows while the excess carriers stored in the depletion region are being swept out. This removal process of the excess minority carriers induces a transit time and effects the response of the diode to the excitation.

Minority carrier storage is common in P-N junction diodes and is the cause of the diode's diffusion capacitance, which is added to the ordinary depletion region capacitance when the junction is forward biased. Generally, in Schottky barrier diode, one can assume no minority carrier storage, hence, no diffusion capacitance. In this case, the capacitance of the Schottky barrier should simply due to that of space charge in the depletion region. However, there are reports of minority carrier effects especially at high forward current levels in some Si Schottky barrier. Also the response of few samples under large switching signal in this study, such as BC4 in Figure 6.6, qualitatively resemble that of minority storage effected to the sinusoidal excitation as previously shown in Figure 2.15.

SPICE analysis can provide insight into whether the similarity between responses of diodes in this study such as in Figure 6.6 to that of Figure 2.15 is the evidence of minority carrier storage effect in diamond Schottky barrier diode. In SPICE analysis of the switching responses of sample BC4 at 4 KHz as shown in Figure 6.7, the parameter TT representing transit time in the diode is varied while all other parameters are fixed.

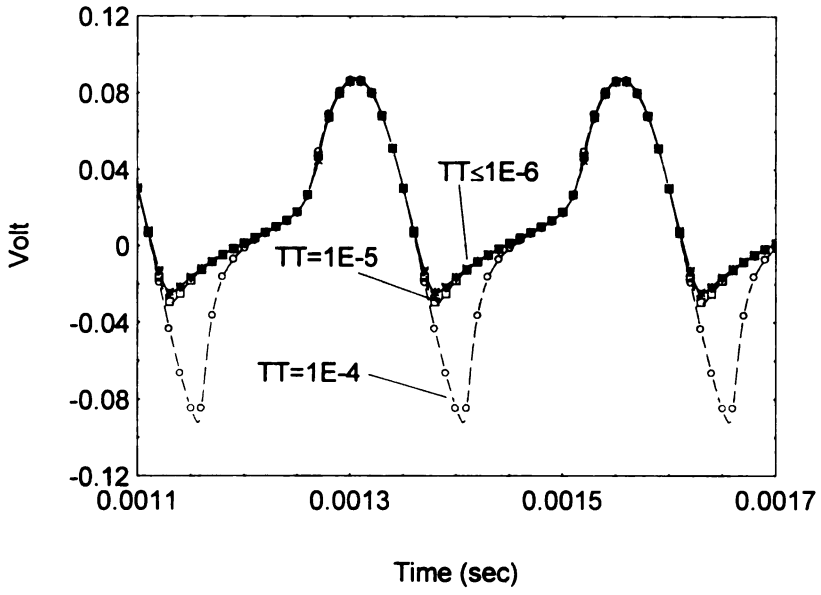

(a)

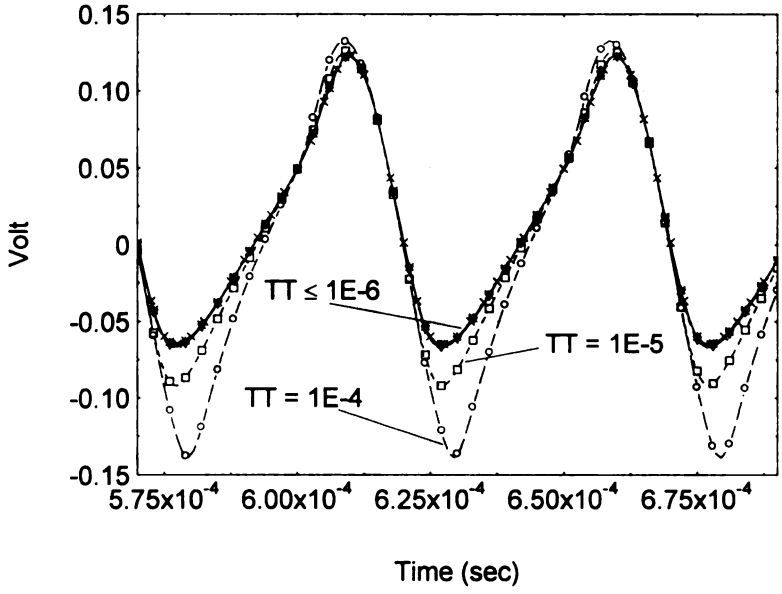

(b)

Figure 6.7 SPICE simulation results of sample BC4 at (a) 4 KHz and (b) 20 KHz. The values of parameter TT are varied between 0 to 10^{-4} second while all other parameters are kept constant as the following: IS = 1.8 pA, N = 2.40, RB = 1.2M Ω, IK = 1.2 nA, ISR = 4.3 pA, NR = 3.06, VJ = 0.8 V, CJO = 10.86 pF and CB = 7.01 pF

From the SPICE analysis in Figure 6.7, it is observed that with the values of TT less than 1 μs, there is no significant different in the results of the simulation. This means that even if the minority carrier storage exists in the diamond Schottky barrier diode, the effects of its diffusion capacitance will not be observed in our KHz experiment unless the storage time of the actual Schottky barrier diode is larger than 1 μs. Compared to Si Schottky barrier diode in which the storage time in range of ns are reported, it is unlikely that diamond Schottky barrier diode will have storage time larger than 1 μs.

Therefore, the similarity between our experimental results and that of Figure 2.15 should not be because of the effects of diffusion capacitance and is not an evidence of minority carrier storage. In fact, the switching response characteristic appearance of BC4 was also found in other samples in this research. To measure the minority carrier storage in Schottky barrier diode, one usually needs to perform the reverse-recovery experiment [29][65][128][131][132][133] on the diode at much higher frequency than KHz range. However, such experiments were not investigated further in this research since at frequencies higher than KHz range, most of our sample no longer yield a good rectifying capability as in Figure 6.6 (c) and (d) for sample BC4.

6.6 Area scaling effect on switching signal response of diamond Schottky diode

From the experimental results in Figure 6.6, sample BC4 shows good rectification at 1 KHz (or less) but does not at appreciably higher frequencies. This section explores the role of diode area on switching performance. The area scaling effect on the switching signal response of the diamond Schottky diode was studied as shown in Figure 6.8 and 6.9. The diodes in Figure 6.8 and 6.9 were fabricated on the same diamond film under identical process but one with the contact area of 4.91×10^{-4} cm^2 (SK7-Y) and the other with contact area of 4.45×10^{-2} cm^2 (SK7-C).

For the switching waveform of diodes in Figure 6.8 and 6.9, the oscilloscope input resistance and capacitance were 1 MΩ and 14 pF respectively. The load resistance of 10 KΩ was used in the measurements. From the result in Figure 6.8, diode SK7-Y with contact area of 4.91×10^{-4} cm^2 shows good rectification up until 4 KHz but does not at higher frequencies of 10 and 20 KHz. Interestingly, the same rectification frequency limit was also obtained from diode SK7-C with larger contact area of 4.45×10^{-2} cm^2 as in Figure 6.9. The response results of Figure 6.9 are very similar to those of Figure 6.8. The different is the amplitude of the responses in Figure 6.9 is in the order of hundred times larger than that of Figure 6.8. From the above results, it is shown experimentally that we do not successfully improve the rectification limit or "speed" of the diode by making the contact area larger or smaller.

To study the area scaling effect on switching signal response of diamond Schottky diode by SPICE, we first fit the SPICE simulation results to the responses of SK7-C with contact area of 4.45×10^{-2} cm^2 at various frequencies as shown in Figure 6.10.

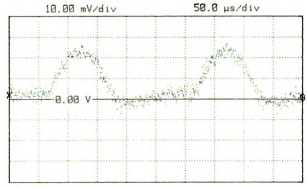

(a)

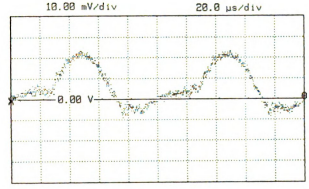

(b)

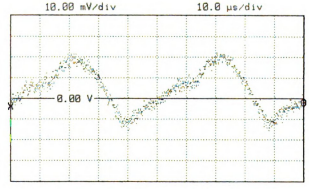

(c)

Figure 6.8 Switching signal responses of diode SK7-Y with contact area of 4.91×10^{-4} cm^2 at (a) 4 KHz, (b) 10 KHz, and (c) 20 KHz.

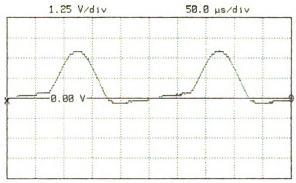

(a)

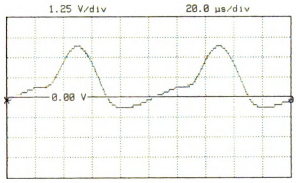

(b)

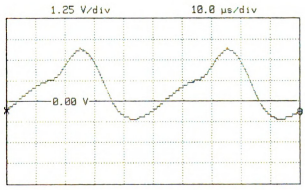

(c)

Figure 6.9 Switching signal responses of diode SK7-C with contact area of 4.45×10^{-2} cm^2 at (a) 4 KHz, (b) 10 KHz, and (c) 20 KHz.

For the switching waveform of sample SK7-C in Figure 6.10, the oscilloscope input resistance and capacitance were 1 MΩ and 14 pF respectively. The 10 KΩ load resistance was used in the measurement. The values of RIN and CIN within the range of test frequency are again calculated to be 9.901 KΩ and 197 pF respectively. The dc current-voltage measurements on the diode (with an area of 4.91×10^{-2} cm^2) indicated a bulk resistance RB value of 17.95 KΩ. The parameters IS = 48 nA, N = 4.47, IK = 400 nA, ISR = 351 pA and NR = 19.98 were also obtained from the dc current-voltage experiment. Although, there was some discrepancy between experimental and SPICE dc results (see Figure 4.21), when the values of VJ = 1.8 V, TT ≤ 1 μs, CB = 270 pF and CJO = 177 pF were used in the SPICE switching signal simulation, a good fit to the measured data was obtained within 1 – 20 KHz frequency range as shown in Figure 6.10.

The values of above parameters are then used as a basis for SPICE simulation on area scaling effect on large switching signal responses of diamond Schottky diode. Assume that we decrease the diode area by factor of 100. For smaller diode areas, the values of N, NR, VJ and TT are assumed unchanged. For smaller area diode, values of IS, IK, ISR, CJO and CB are reduced by factor of. The values of RB are also increased by factor of 100 for small area diode. The simulation results of the diode responses under 4 KHz and 20 KHz are shown in Figure 6.11 and 6.12.

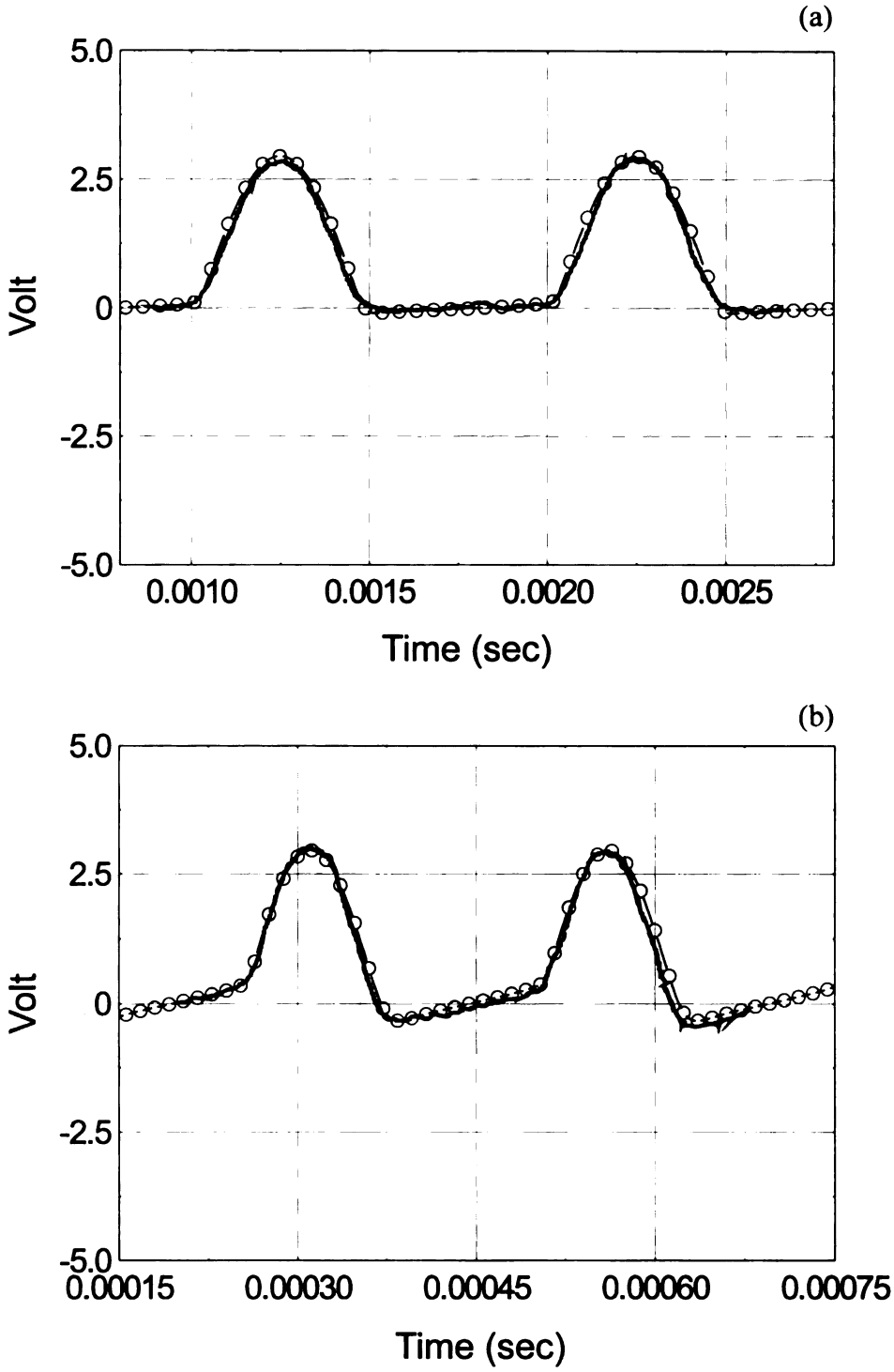

Figure 6.10 Switching responses of sample SK7-C with contact area of 4.45×10^{-2} cm^2 at (a) 1 KHz, (b) 4 KHz, (c) 10 KHz, and (d) 20 KHz. Thick solid lines represent experimental results. Thin lines with circle marks represent SPICE simulation results.

(c)

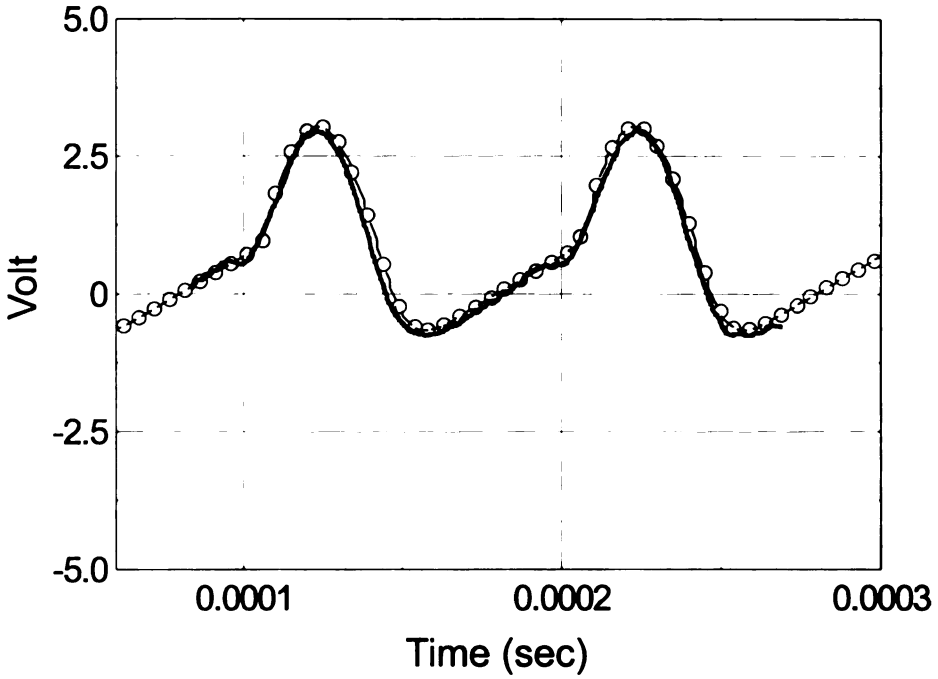

(d)

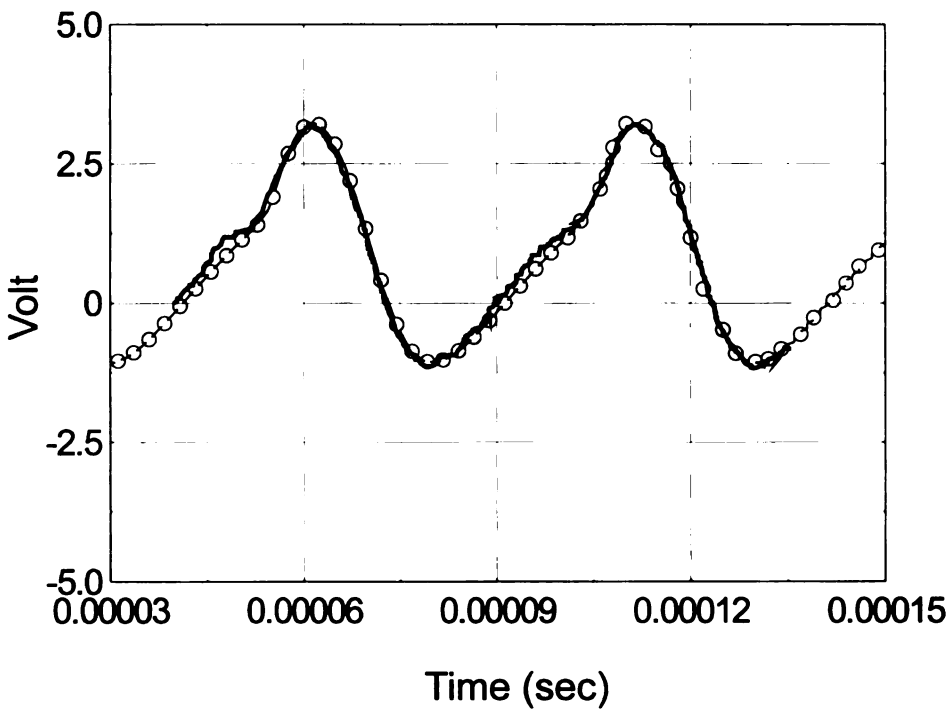

Figure 6.10 continued

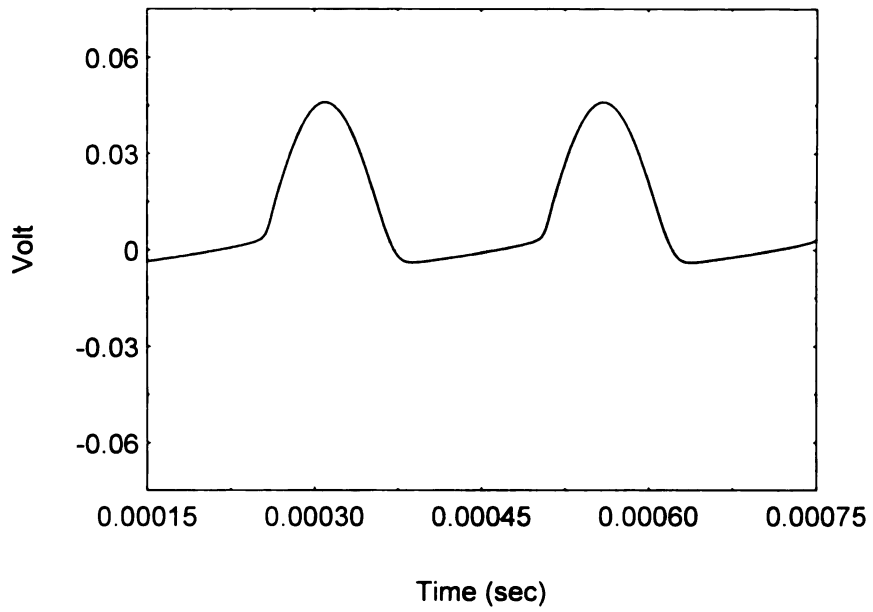

(a)

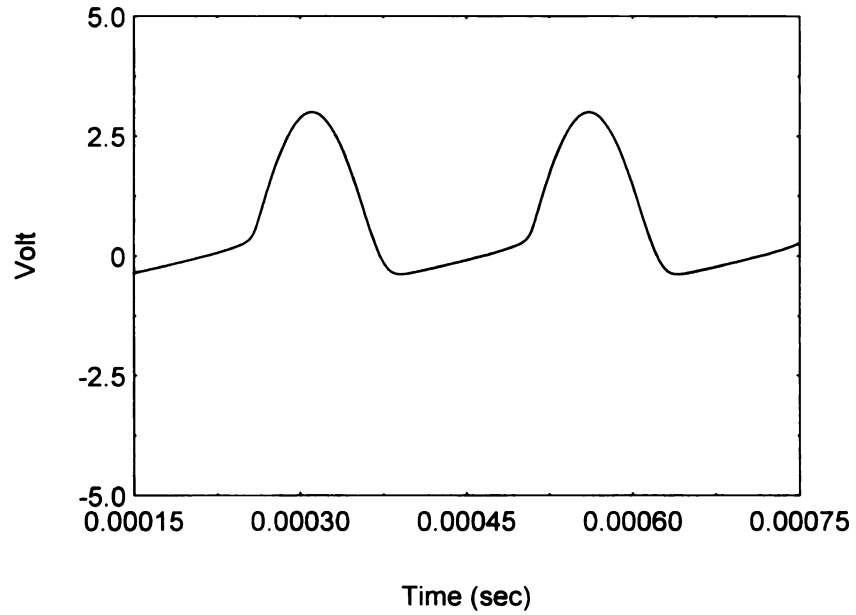

(b)

Figure 6.11 SPICE simulation results at 4 KHz based on the properties of diode SK7-C when diode areas are (a) 4.45×10^{-4} cm^2, and (b) 4.45×10^{-2} cm^2.

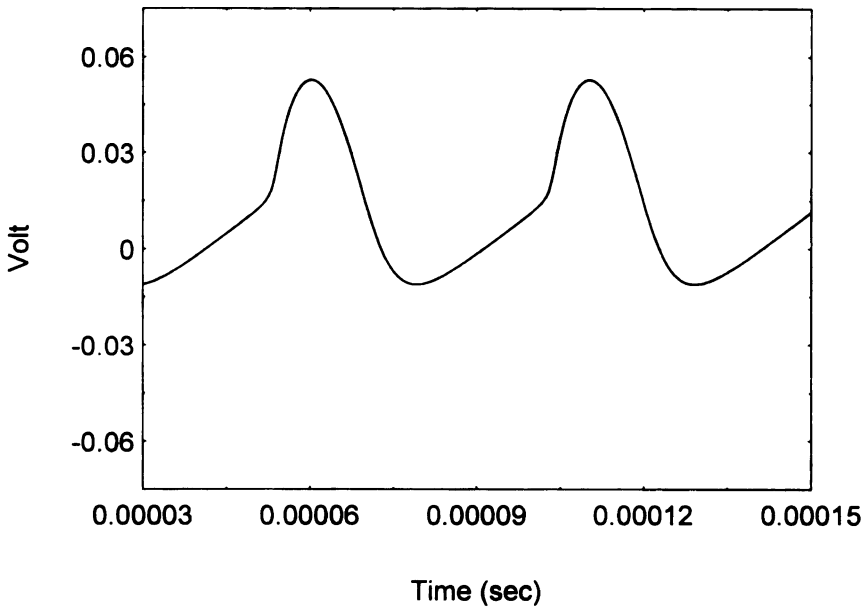

(a)

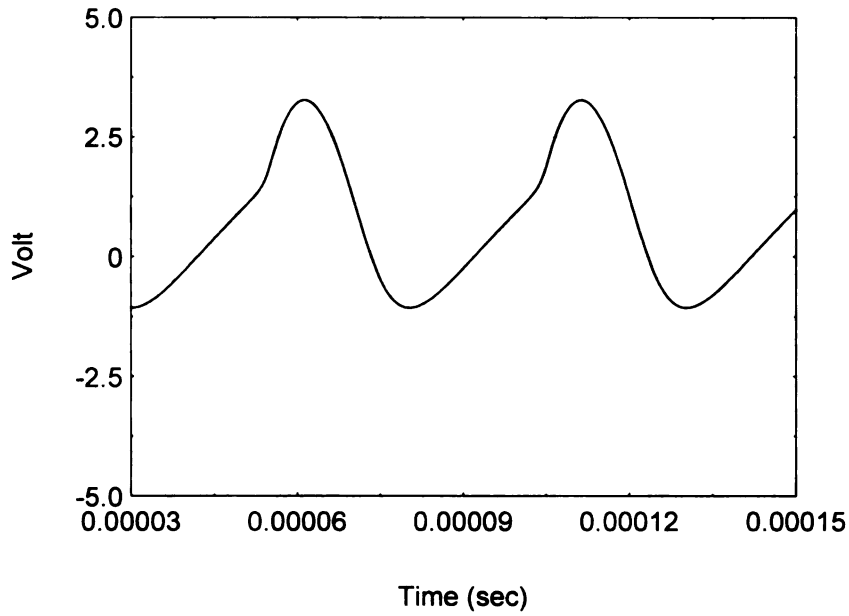

(b)

Figure 6.12 SPICE simulation results at 10 KHz of diode SK7 with diode area of (a) 4.45×10^{-4} cm^2, and (b) 4.45×10^{-2} cm^2.

The results of SPICE analysis in Figure 6.11 and 6.12 verify that changing the diode bulk resistance by scaling the diode area do not significantly improve the speed response of the diode. The results of plot (a) and (b) in both Figures 6.11 and 6.12 are very similar in term of frequencies limitation even thought the area of diode in plot (b) is 100 times larger than that of plot (a).

The experimental and SPICE simulation results on area scaling suggest that speed response of the diode is limited by RC time constant consideration, where R decreases with area and C increases with area. Considering the bulk material, RB = $\rho L/A$ and CB = $\varepsilon A/L$ such that the RC time constant is $\rho\varepsilon$, the dielectric time constant. Here, all of the parameters have usual meanings; ρ is the resistivity, and ε is the dielectric constant of the diamond material. This dielectric time constant can only be reduced by reducing ρ, i.e. by doping the diamond. The next section of this chapter will explore the possibility of improving the rectification frequency limit or "speed" of the diamond Schottky diode by means of doping.

6.7 Anticipated doping effects on the switching performance

The effect of doping on diode frequency response was not studied experimentally. However, as described in this section, simulation studies were used to assess potential improvements in diode switching response that could be achieved by doping. Such doping should ideally be only in the bulk part of the device, since it is desired to keep the space charge layer unchanged. If the entire film were doped, than the space charge layer would become thinner, increasing the junction capacitance and eventually also the leakage current due to tunneling. The best diamond Schottky diodes reported so far were achieved by multi-layer growth of CVD diamond thin film [16][59][124].

Considering the simulation model for the diode, there are two potential benefits for doping the bulk portion of the film. One is that for a given film thickness, R_B would be reduced. Another is that by increasing the film thickness, C_B could be reduced for a given R_B. This section explores the two possibilities. In both cases, it is assumed that the bulk portion of the film has been doped such that the resistivity is decreased by two orders of magnitude. In the first case, the bulk portion of the film is increased in thickness such that R_B is the same as for the undoped case, but C_B is reduced essentially by a factor of 100. In the second case, the film thickness is kept the same such that R_B is reduced by two orders of magnitude, but C_B remains the same.

For this study, we ran SPICE simulation based on properties of sample SK7-C with a contact area of 4.45×10^{-2} cm^2. From section 6.6, the best-fit values for each parameter are then the following; IS = 48 nA, N = 4.47, IK = 400 nA, ISR = 351 pA, NR = 19.98, RB = 17.95 KΩ, VJ = 1.8 V, CB = 270 pF and CJO = 177 pF. Figure 6.13

shows the SPICE simulation response of SK7-C to a 10-Vpp 20-KHz signal while using TT = 1 ps and the load resistance of 10 KΩ.

Now, assume that we dope the bulk portion of the diode such that the resistivity is decreased by two orders of magnitude but we also increased in thickness of the bulk part by two orders. Let us call this sample - hypothetical diode-A. For this diode-A, the value of RB is still maintained at 17.95 KΩ, while CB is reduced essentially by a factor of 100 to 2.70 pF. Also, the values of all other parameters are still the same as in previous paragraph. The response of such diode to a 10-Vpp 20-KHz signal is shown in Figure 6.14(a).

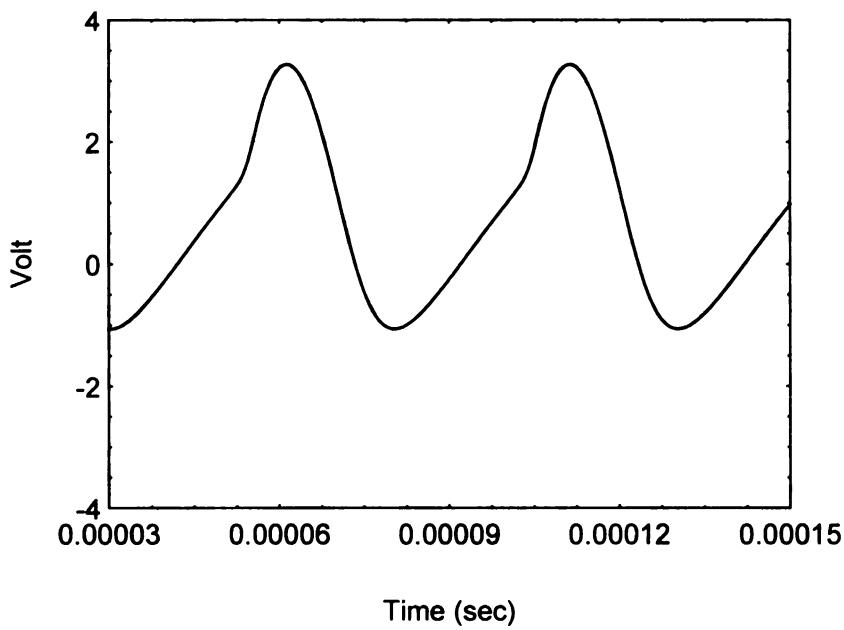

Figure 6.13 A SPICE simulation result of diode SK7-C with a diode area of 4.45×10^{-2} cm^2. The input signal for the simulation is a 10-Vpp 20-KHz sinusoidal waveform. The 1-MΩ /14-pF oscilloscope is in parallel with 10 KΩ load resistance.

Next, suppose we fabricate another diode, hypothetical diode-B, without changing thickness of bulk portion of the diode. In this second case, the value of RB would reduce to 179.5 Ω while the value of CB would maintain at 270 pF. The 179.5 Ω bulk resistance in our diode would correspond to a resistivity in order of 10^4 Ω-cm, which is very achievable in doped CVD diamond. The lowest resistivity for doped diamond reported so far is between 10^{-2} –10^{-3} Ω-cm [12] [49] [95]. The response of the second diode to the same 10-Vpp 20-KHz signal is shown in Figure 6.14(b).

It is shown by the simulation in Figure 6.14(a) that reducing CB while maintaining RB (diode-A) does not significantly change the speed response of the diode. In fact, the response in Figure 6.14(a) is similar to the response of the undoped diamond film SK7-C in Figure 6.13. On the other hand, the response of diode-B in Figure 6.14(b) shows both amplitude and speed improvement over that of undoped diode SK7-C. Therefore, the potential advantages of doping are primarily in reducing RB not CB.

As noted earlier, diode SK7-C showed good rectification up until 4 KHz but does not at higher frequencies. Figures 6.15 and 6.16 show how the doped diode-B response to higher frequency signals, compared to SK7-C. In order to see the performance advantage more clearly, the load resistances in Figure 6.15 and 6.16 were reduced to 50 Ω. This mainly to reduce the time constant associated with the measuring setup (R_{in}-C_{in}, see section 6.2).

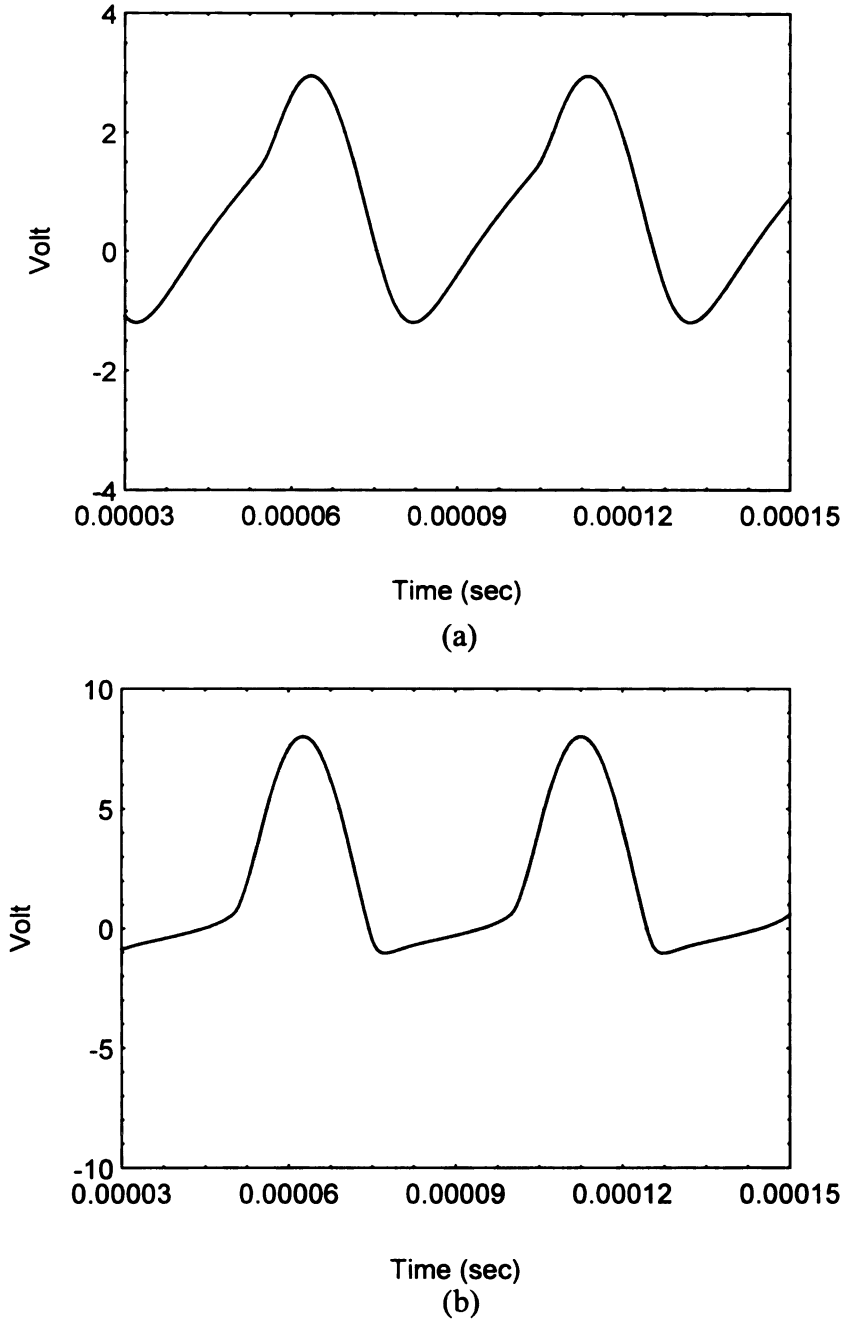

Figure 6.14 SPICE simulation results of two hypothetical diodes based on properties of SK7-C but with the difference in (a) CB = 1/100 of that of SK7-C, and (b) RB = 1/100 of that of SK7-C .The input signal for the simulation is a 10-Vpp 20-KHz sine wave. The load resistance RL is 10 KΩ.

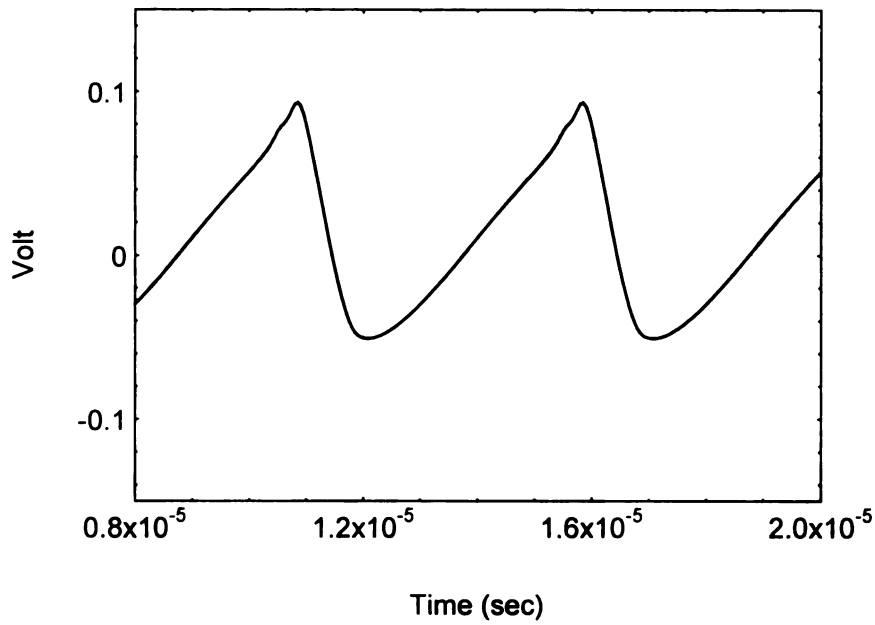

(a)

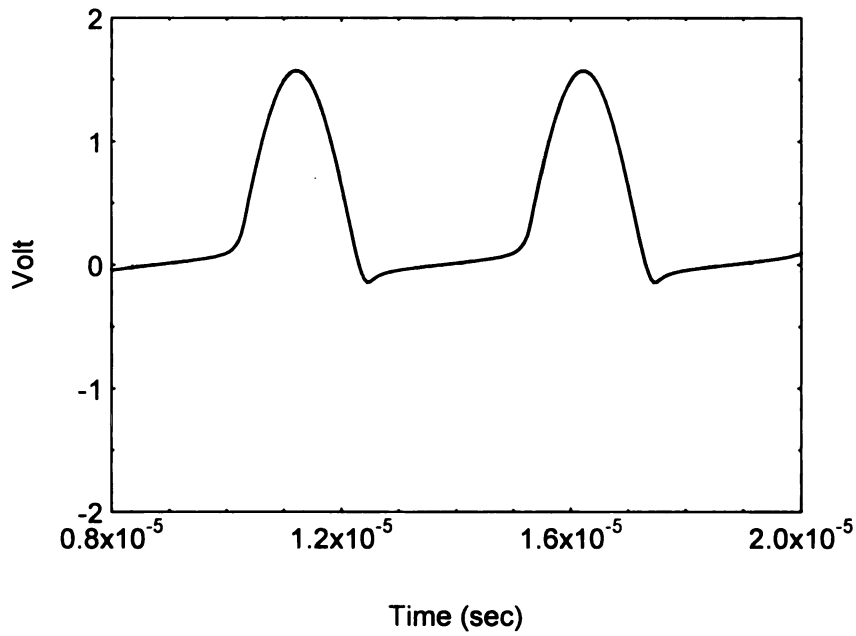

(b)

Figure 6.15 SPICE simulation results of (a) SK7-C, and (b) a hypothetical doped diode with RB = 1/100 of that of SK7-C.The input signal for the simulation is a 10-Vpp 200-KHz sine wave. The load resistance RL is 50 Ω.

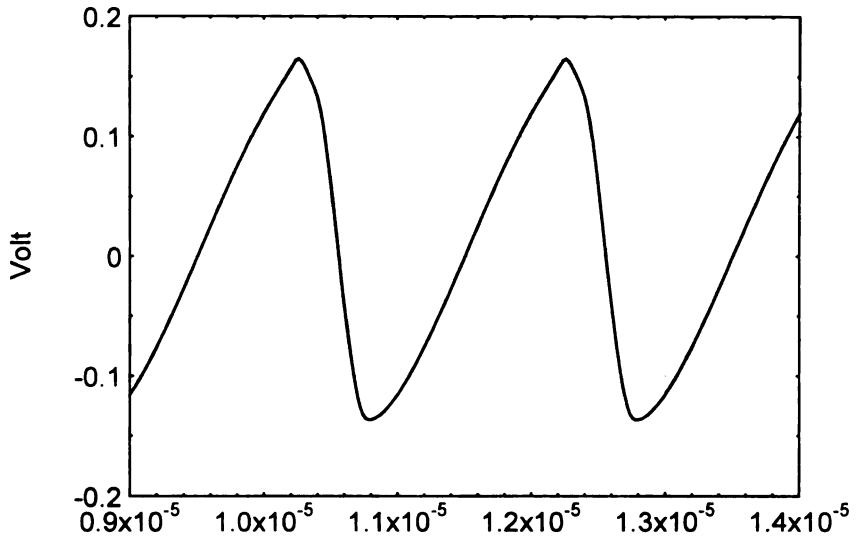

(a)

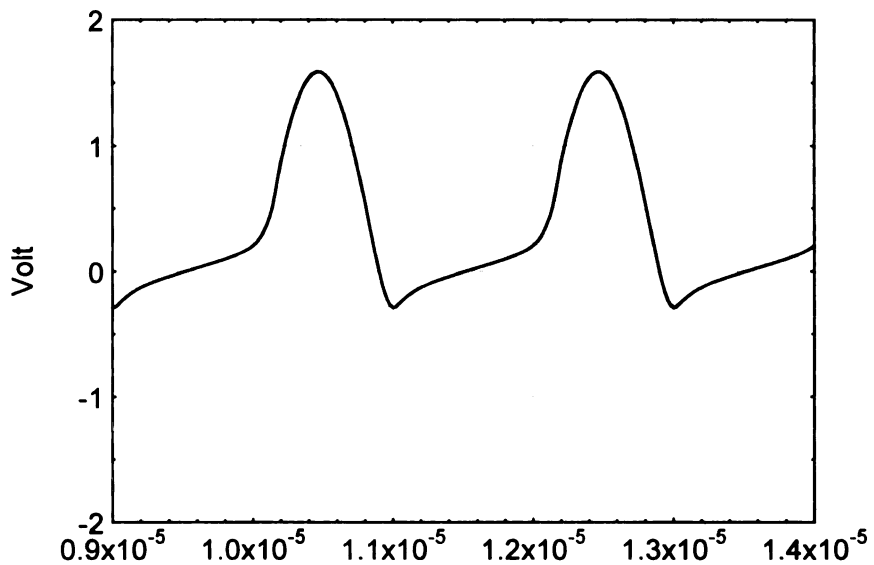

(b)

Figure 6.16 SPICE simulation results of (a) SK7-C, and (b) a hypothetical doped diode with RB = 1/100 of that of SK7-C.The input signal for the simulation is a 10-Vpp 500-KHz sine wave. The load resistance RL is 50 Ω.

Figures 6.15 and 6.16 show the responses of diode SK7-C and diode-B to the 10-Vpp 200-KHz and the 10-Vpp 500-KHz sine wave, respectively. With load resistance of 50 Ω in both cases, the value of R_{in} and C_{in} were found to be 49.99 Ω and 92 pF, respectively. Also, the diode parameters in the simulations were set at IS = 48 nA, N = 4.47, IK = 400 nA, ISR = 351 pA, NR = 19.98, VJ = 1.8 V, TT = 1 ps, CB = 270 pF and CJO = 177 pF. However, the value of RB was 17.95 KΩ for diode SK7-C and 179.5 for diode-B.

In Figure 6.15(a), diode SK7-C does not show good rectification performance to the 200 KHz signal. Compare to SK7-C, diode–B in Figure 6.15(b) shows significant improvement in the signal rectification. Similar result is found as shown in Figure 6.16 for 500 MHz input signal. At several MHz, however, even the doped diode–B does not rectify well. Further simulation showed that this is the case even if the doping is reduced further. The reason for this is that the switching speed is now substantially effected by R_{in} and C_{in} of the measurement circuit, also, the relatively large junction capacitance associated with these diodes becomes an issue. For higher speeds a low resistance, low capacitance measurement circuit combined with small area diode would be desired.

In summary, the speed limitation of diamond Schottky barrier diodes in this study is the result of high bulk resistance of the undoped diamond film. As shown by the simulation in this study, doping the diamond film and constructing diodes with a lower RB would significantly improve the switching performance or "speed" of the diode.

CHAPTER 7

Summary and future work

This chapter summarizes the results of the research work which is described in the earlier chapters, and discusses related research issues which need to be further investigated

In this research, ohmic and rectifying contacts, and consequently Schottky barrier diodes, were successfully formed on undoped polycrystalline CVD diamond films deposited by microwave plasma-assisted deposition. It was found that increasing the CH_4 concentration in the diamond film growth process does not reduce the resistance of the diode beyond a CH_4 concentration of 2.5 - 4 %. The results of dc current-voltage measurements are well modeled by SPICE analysis. The diode parameters extracted from the dc analysis were used in the frequency-related part of the research.

The small signal responses in term of capacitance and resistance of diamond Schottky barrier diodes were investigated in the frequency range from 100 Hz to 1 MHz at various voltages under both forward and reverse biases. The capacitance and resistance results were modeled over the above frequency range by three types of equivalent circuits model. The frequency-independent elements from simple geometric considerations were developed as the first model. The contact resistance, although small enough to produce a negligible voltage drop under dc or large switching signal measurements and claimed to

have marked effect under small signal measurement by few authors, was included into the second model. The third model accommodated the effect of deep trap states as a series combination of frequency-dependent capacitance and resistance into the simple model.

It was demonstrated by model simulations that the frequency dependent properties of diamond Schottky barrier diode under small signal measurement, beyond those expected as a result of the samples geometric consideration, can be associated with contact effects and/or deep trap states inside the diamond. Although the responses could possibly be the combination of both effects, at this time, the results indicated that the response is an effect of trap states in diamond.

Recent work by Liu [114][129] indicates an effect of surface states in boron-doped CVD diamond Schottky diodes on the C-V results. They suggest that Glover [19] overlooked the effect of these surface states which gives a very strong influence at low ac frequency. Although diamond samples in this study are not doped, it is a good idea to give some attention to the effect of surface states and possibly incorporate into the diode model.

The results from the large switching response measurements in this study are believed to be the first large signal data reported on polycrystalline CVD diamond Schottky barrier diode. The responses of diamond Schottky barrier diodes to the test frequency range up to 20 KHz are reported and well fitted to the SPICE model analysis. The experimental and SPICE analysis suggest that speed response of the diamond Schottky barrier diode is primarily limited by the large bulk resistance of the diode. The reduction of bilk resistance of the diode by changing the contact area in order to improve

speed response of the diode proved to be unsuccessful. The results shown by the simulation in this study indicate that doping the diamond film and constructing diodes with a lower R_B would significantly improve the speed responses of the diode.

The next logical step would be to experimentally test diamond diodes fabricated on doped diamond films. However, an undoped diamond layer is crucial to high-quality diamond Schottky barrier diode [130] apparently because a doped diamond layer has sufficient defects to reduce the space charge layer to the point where tunneling contributions are non-negligible. The solution may be to grow a base layer of low resistivity doped diamond, followed by undoped diamond, possibly in a quarter of a micron thickness range. Such work would ideally be coupled with SIMS (secondary ion mass spectroscopy) analysis to document the dopant profile in the diamond films.

REFERENCES

[1] H. Pierson, "Handbook of carbon, graphite, diamond and fullerenes : properties, processing and application", , 1st Ed., pp.; 1993.

[2] M. W. Geis, Diamond transistor performance and fabrication, Proc. IEEE, Vol.79 No.5, pp.669-676; 1991.

[3] C. R. Zeisse et.al., An ion-implanted diamond metal-insulator-semiconductor field-effect transistor, IEEE Elec. Dev. Lett, Vol.12 No.11, pp.602-604; 1991.

[4] J.P. Bade, et.al., Fabrication of diamond thin-film thermistors for high-temperature applications, Diamond Rel. Mat., 2(1993), pp.816-819; 1993.

[5] M. W. Geis et.al., Diamond cold cathod, IEEE Elec. Dev. Lett, Vol.12 No.8, pp.456; 1991.

[6] D. R. Kania, M. I. Landstrass, M. A. Plano, L. S. Pan, and S. Han, Diamond radiation detectors, Diamond Rel. Mat., 2(1993), pp.1012-1019; 1993.

[7] V. F. Dvoryakin et.al., CVD Diamond films for X-ray detectors, Applications of diamond films and related materials 3rd international conference, A. Feldman, Y. Tzeng, W. A. Yarbrough, M. Yoshikawa, and M. Murakawa (editors), pp.128-132; 1995.

[8] M. Marchywka et.al., Ultraviolet photoresponse characteristics of diamond diodes, Appl. Optics., Vol.30 No.34, pp.5011-5013; 1991.

[9] R. J. Trew, J. Yan, P. M. Mock, The potential of diamond and SiC electronic devices for microwave and millimeter-wave power applications, Proc. IEEE, Vol.79 No.5, pp.598-620; 1991.

[10] L. S. Pan et.al., Electrical properties of high quality diamond films, Diamond Rel. Mat., 2(1993), pp.820-824; 1993.

[11] J. W. Vandersande, and L. D. Zoltan, Using high-temperature electrical resistivity measurements to determine thr quality of diamond films, Diamond Rel. Mat., 4(1995), pp.641-644; 1995.

[12] T. Iwasaki et.al., Formation of ohmic contacts on semiconducting diamond grown by chemical vapor deposition, Diamond Rel. Mat., 3(1993), pp.30-34; 1993.

[13] D. G. Jeng, and H. S. Tuan, Thin-film Al/diamond Schottky diode over 400-V breakdown voltage, J. Appl. Phys., 68(11), pp.5902-5904; 1990.

[15] W. P. Kang, J. L. Davidson, Y. Gurbuz, and D. V. Kerns, Temperature dependance and effect of series resistance on the electrical characteristics of a polycrystalline diamond metal-insulator-semiconductor diode, J. Appl. Phys., 78(2), pp.1101-1107; 1995.

[16] W. Ebert, A. Vescan, T. H. Borst, and E. Kohn, Epitaxial diamond schottky barrier diode with on/off current ratios in excess of 10^7 at high temperature, International Electronic Devices Meeting, IEDM 94, pp.419-422; 1994.

[17] V. Venkatesan, K. Das, and J. A. von Windheim, Effect of back contact impedance on frequency dependence of capacitance-voltage measurements on metal/diamond diodes, Appl. Phys. Lett., 63(8), pp.1065-1067; 1993.

[18] G. Sh. Gildenblat, S. A. Grot, C. R. Wronski, A. R. Badzian, T. Badzian, and R. Messier, Electrical characteristics of Schottky diodes fabricated using plasma assisted chemical vapor deposited diamond films, Appl. Phys. Lett., 53(7), pp.586-588; 1988.

[19] G. H. Glover, The C-V characteristics of Schottky barriers on laboratory grown semiconducting diamonds, Solid State Electronics, Vol.16, pp.973-983; 1972.

[20] G. Sh. Gildenblat, S. A. Grot, and C. R. Wronski, Schottky diodes with thin film diamond base, International Electronic Devices Meeting, IEDM 88, pp.626-629; 1988.

[21] J. A. von Windheim, V. Venkatesan, D. M. Malta, and K. Das, Comparison of the electric properties of single-crystalline diamond by Hall effect and capacitance-voltage measurements, Diamond Rel. Mat., 2(1993), pp.841-846; 1993.

[22] B. G. Streetman, "Solid State Electronic Devices", , 3rd Ed., pp.; 1990.

[23] S. M. Sze, "Physics of semiconductor devices", , 1st Ed., pp.; 1969.

[24] D. H. Navon, "Semiconductor microdevices and materials", , 2nd Ed., pp.; 1986.

[25] H. K. Henisch, "Semiconductor contacts : an approach to ideas and models", , 1st Ed., pp.2; 1984.

[26] G. Massobrio, PN-junction diode and Schottky diode, "Semiconductor device modeling with SPICE", P. Antognetti, and G. Massobrio (editors), pp.1-36; 1988.

[27] E. H. Rhoderick, "Metal-Semiconductor Contacts", , 1st Ed., pp.; 1980.

[28] H. Kiyota et al., Electrical properties of Schottky barrier formed on as-grown and oxidized surface of homoepitaxially grown diamond (001) film, Appl. Phys. Lett., 67(24), pp.3596-3598; 1995.

[29] M. Avali, Minortity carrier injection in Schottky barrier diodes, Ph.D. Dissertation, Michigan State University, pp.; 1986.

[30] H. K. Henisch etal., Schottky barrier ideality, real and imagined, Solid State Electronics, Vol.27, pp.1033-1034; 1984.

[31] H. Norde, A modified forward I-V plot for Schottky diodes with high series resistance, J. Appl. Phys., 50(7), pp.5052-5053; 1979.

[32] K. Sato, and Y. Yasumura, Study of forward I-V plot for Schottky diodes with high series resistance, J. Appl. Phys., 58(9), pp.3655-3657; 1985.

[33] M. Alavi, D. K. Reinhard, and C. W. Yu, Minortity-carrier injection in Pt-Si Schottky-barrier diodes at high current densities, IEEE Trans. Elec. Dev, Vol.34 No.5, pp.1134-1140; 1987.

[34] L. Xu, D. K. Reinhard, and M. G. Thompson, RF sputtered gold-amorphous silicon Schottky-barrier diodes, IEEE Trans. Elec. Dev, Vol.Ed-29 No.6, pp.1004-1008; 1982.

[35] J. Beichler, W. Fuhs, H. Mell, and H. M. Welsch, Capacitance studies on amorphous silicon Schottky barrier diodes, J. Non-crystalline Solids, Vol.35-36, pp.587-592; 1980.

[36] P. Viktorovitch and D. Jousse, Determination of the electronic density of states in hydrogenatedamorphous silicon (a-SiH) from Schottky diode capacitance-voltage and conductance-voltage measurements, J. Non-crystalline Solids, Vol.35-36, pp.569-574; 1980.

[37] A. J. Snell, K. D. Mackenzie, P. G. Le Comber, and W. E. Spear, The metal-amorphous silicon barrier, interpretation of capacitance and conductance measurements, J. Non-crystalline Solids, Vol.35-36, pp.593-598; 1980.

[38] G. W. Neudeck, The PN junction diode, "Modular series on solid state devices", Vol.2, pp.89-101; 1983.

[39] A. R. West, D. C. Sinclair, and N. Hirose, Characterization of electrical materials, especially ferroelectrics, by impedance spectroscopy, J. Electroceramics, Vol.1 No.1, pp.65-71; 1997.

[40] G. Sh. Gildenblat, S. A. Grot, and A. Badzian, The electrical properties and device applications of homoepitaxial and polycrystalline diamond films, Proc. IEEE, Vol.79 No.5, pp.647-668; 1991.

[41] K. Shenai, R. S. Scott, and B. J. Baliga, Optimum semiconductors for high power electronics, IEEE Trans. Elec. Dev, Vol.36 No.9, pp.1811; 1989.

[42] N. Fujimori, Electrical Applications of CVD diamond films, "New diamond science and technology", MRS international conference proceed, pp.901-908; 1991.

[43] B. Huang, and D. K. Reinhard, Electric field-dependent conductivity of polycrystalline diamond thin film, Appl. Phys. Lett., 59(12), pp.1494-1496; 1991.

[44] K. Plamann and D. Fournier, Thermal conductivity of CVD diamond : methods and results, Phys. Stat. Sol. A, Vol. 154, pp.351-369; 1996.

[45] K. L. Moazed, J. R. Zeidler, and M. J. Taylor, A thermal activated solid state reaction process for fabricating ohmic contacts to semiconducting diamond, J. Appl. Phys., 68(5), pp.2246-2254; 1990.

[46] B. Huang, Electrical properties and physical characteristics of polycrystalline diamond films deposited in a microwave plasma disk reactor, Ph.D. Dissertation, Michigan State University, pp.; 1992.

[47] M. I. Landstrass, and K. V. Ravi, Hydrogen passivation of electrically active defects in diamond, Appl. Phys. Lett., 55(14), pp.1391-1393; 1989.

[48] S. A. Grot et.al., The effect of surface treatment on the electrical properties of metal contacts to Boron-doped homoepitaxial diamond film, IEEE Elec. Dev. Lett, Vol.11 No.2, pp.100-102; 1990.

[49] K. L. Moazed, R. Nguyen, and J. R. Zeidler, Ohmic contacts to semiconducting diamond, IEEE Elec. Dev. Lett, Vol.9 No.7, pp.350-351; 1988.

[50] S. A. Grot, S. Lee, G. Sh. Gildenblat, C. W. Hatfield, and C. R. Wronski, Rectification and internal photoemission in metal/CVD diamond and metal/CVD diamond/silicon structures, J. Mater. Res., Vol.5 No.11, pp.2497-2501; 1990.

[51] M. W. Geis et.al., Electrical, crystallographic, and optical properties of ArF laser modified diamond surfaces, Appl. Phys. Lett., 55(22), pp.2295-2297; 1989.

[52] G. Sh. Gildenblat, S. A. Grot, C. W. Hatfield, A. R. Badzian, and T. Badzian, High-temperature Schottky diodes with thin-film diamond base, IEEE Elec. Dev. Lett, Vol.11 No.9, pp.371-372; 1990.

[53] K. Miyata, and D. L. Dreifus, Metal-intrinsic semiconductor-semiconductor structures using polycrystalline diamond films, Appl. Phys. Lett, 60(4), pp.480-482; 1992.

[54] T. Tachibana, and J. T. Glass, Effects of argon presputtering on the formation of aluminum contacts on polycrystalline diamond, J. Appl. Phys., 72(12), pp.5912-5918; 1992.

[55] R. D. McKeag, S. M. Chan, C. Johnson, P. R. Chalker, and R. B. Jackman, High temperature stability of chemically vapour deposited diamond diodes, Mat. Sci. Eng. B, B 29, pp.223-227; 1995.

[56] M. C. Hicks, C. R. Wronski, S. A. Grot, and G. Sh. Gildenblat, The barrier height of Schottky diodes with a chemical-vapor-deposited diamond base, J. Appl. Phys., 65(5), pp.2139-2141; 1989.

[57] F.J. Himpsel, P. Heimann, and D. E. Eastman, Schottky barriers on diamond (1 1 1), Solid State Communications, Vol.36 No.7, pp.631-633; 1980.

[58] K. Das, V. Venkatesan, K. Miyata, D. L. Dreifus, and J. T.Glass, A review of the electrical characteristics of metal contacts on diamond, "Application of diamond films and related materials", Y. Tzeng, M. Yoshikawa, M. Murakawa, and A. Feldman (editors), pp.301-308; 1991.

[59] W. Ebert, A. Vescan, T. H. Borst, and E. Kohn, High current p/p+ diamond Schottky diode, IEEE Elec. Dev. Lett, Vol.15 No.8, pp.289-291; 1994.

[60] M. W. Geis, D. D. Rathman, D.J. Ehrlich, R. A. Murphy, and W. T. Lindley, High-temperature point-contact transistors and Schottky diodes formed on synthetic boron-doped diamond, IEEE Elec. Dev. Lett, Vol.8 No.8, pp.341-343; 1987.

[61] A. Vescan, I. Daumiller, P. Gluch, W. Ebert, and E. Kohn, Very high temperature operation of diamond Schottky diode, IEEE Elec. Dev. Lett, Vol.18 No.11, pp.556-558; 1997.

[62] S. Nath, J. I. B. Wilson, Impedance measurements on CVD diamond, Diamond Rel. Mat., 5(1996), pp.65-75; 1996.

[63] T. Sugino, Y. Muto, K. Karasutani, J. Shirafuji, and K. Kobashi, Trap state elucidated by a.c. conductance measurement in polycrystalline chemically vapour-deposited diamond films, Diamond Rel. Mat., 2(1993), pp.803-807; 1993.

[64] G. Zhao, T. Stacy, E. J. Charlson, E. M. Charlson, C. J. Meese, G. Popovivi and M. Prelas, Silver on diamond Schottky diodes formed on boron doped hot-filament chemical vapor deposited polycrystalline diamond films, Appl. Phys. Lett., 61(9), pp.1119-1121; 1992.

[65] S. M. Krakauer, Harmonic generation, rectification and lifetime evaluation with the step recovery diode, Proc. IRE, Vol.50, pp.1665-1676; 1962.

[66] B.E. Williams and J. T. Glass, Characterization of diamond thin flm: Diamod phase identification, surface morphology, and defect structures, J. Mater. Res., Vol.4 No.1, pp.373; 1989.

[67] G. S. Yang, M.Aslam, K. P. Kuo, D. K. Reinhard and J. Asmussen, Effect of ultrahigh nucleation density on diamond growth at different growth rates and temperaturs, J. Vac. Sci. Tech. B, Vol.13 No.3, pp.1030-1036; 1995.

[68] H. Windischman, and G. F. Epps, Intrinsic stress in diamond films prepared by microwave plasma CVD, J. Appl. Phys, 69(4), pp.2231-2237; 1991.

[69] Y. Muranaka et.al., Low temperature (approximately 400 degrees C) growth of polycrystalline diamond films in the microwave plasma of CO/H/sub 2/ and CO/H/sub 2//Ar systems, J. Vac. Sci. Tech. B, Vol.9 No.1, pp.76; 1991.

[70] S. Yugo, T. Kanai, T. Kimura, and T. Muto, Generation of diamond nuclei by electric field in plasma chemical vapor deposition, Appl. Phys. Lett., 58(10), pp.1036-1038; 1991.

[71] A. Masood, Technology and electronic properties of diamond film microsensor for thermal signals, Ph.D. Dissertation, Michigan State University, pp.; 1993.

[72] S. Khatami, Controlled synthesis of diamond films using a microwave discharge (non-equilibrium plasma), Ph.D. Dissertation, Michigan State University, pp.; 1997.

[73] S. Iijima, Y. Aikawa, and K. Baba, Growth of diamond particles in chemical vapor deposition, J. Mater. Res., Vol.6 No.7, pp.1491-1497; 1991.

[74] M. P. Everson, and M. A. tamor, Studies of nucleation and growth morphology of boron-doped diamond microcrystals by scanning tunneling microscope, J. Vac. Sci. Tech. B, Vol.9, pp.1570; 1991.

[75] P. A. Dennig, and D. A. Stevenson, Influence of substrate topology on the nucleation of diamond thin films, "Applications of diamond films and related materials", Y. Tzeng, M. Yoshikawa, M. Murakawa, and A. Feldman (editors), pp.383-388; 1991.

[76] M. Ulczynski, Low-temperature deposition of transparent diamond films with a microwave cavity plasma reactor, Ph.D. Thesis, Michigan State University, pp.; 1998.

[77] J. Zhang, B. Huang, D. K. Reinhard, and J. Asmussen, An investigation of electromagnetic field patterns during microwave plasma diamond thin film deposition, J. Vac. Sci. Tech. A, Vol.8 No.3 Pt.1, pp.2124-2128; 1990.

[78] K. Kuo, and J. Asmussen, An experimental study of high pressure synthesis of diamond films using a microwave cavity plasma reactor, Diamond Rel. Mat., 6(1997), pp.1097-1105; 1997.

[79] J. Asmussen, T. A. Grotjohn, P. Mak, and M. A. Perrin, The design and application of electron cyclotron resonance dischages, IEEE Trans. Plasma Sci., Vol.25 No.6, pp.1196-1221; 1997.

[80] A. Guthrie, "Vacuum technology", , 1st Ed., pp.1-48; 1963.

[81] C. M. van Atta, "Vacuum science", , 1st Ed., pp.1-51; 1965.

[82] J. Mossbrucker, and T. A. Grotjohn, Determination of local crystal orientation of diamond using polarized Raman spectra, Diamond Rel. Mat., 5(1996), pp.1333-1343; 1996.

[83] B. Huang, D. K. Reinhard, and J. Asmussen, Electrical properties of undoped large-grain and small-grain diamond films, Diamond Rel. Mat, 2(1993), pp.812-815; 1993.

[84] P. Gluche, S. D. Wolter, T. H. Borst, W. Ebert, A. Vescan, and E. Kohn, Highly rectifying Au-contacts on diamond-on-silicon substrate, IEEE Elec. Dev. Lett, Vol.17 No.6, pp.270-272; 1996.

[85] T. Sugino, and J. Shirafuji, Electrical characteracteristics of chemical vapor deposited diamond films, Phys. Stat. Sol. A, Vol. 154, pp.371-383; 1996.

[86] T. Sugino, Y. Muto, and J. Shirafuji, Electrical conduction mechanisms in polycrystalline chemically vapour deposited diamond films, Diamond Rel. Mat., 2(1993), pp.797-802; 1993.

[87] P. Gluch, A. Aleksov, A. Vescan, W. Ebert, and E. Kohn, Diamond surface-channel FET structure with 200 V breakdown voltage, IEEE Elec. Dev. Lett, Vol.18 No.11, pp.547-549; 1997.

[88] M. W. Geis, and N. N. Efremow, High-conductance, low-leakage diamond Schottky diodes, Appl. Phys. Lett., 63(7), pp.952-954; 1993.

[89] S. Albin, and L. Watkins, Electrical properties of hydrogenated diamond, Appl. Phys. Lett, 56(15), pp.1454-1456; 1990.

[90] Y. Muto, T. Sugino, K. Kobashi, and J. Shirafuji, Frequency-dependent conductivity in polycrystalline chemical vapor deposited diamond films, Jpn. J. Appl. Phys., Vol.31 Pt.2 No.1A/B, pp.L4-L6; 1992.

[91] M. I. Landstrass, and K. V. Ravi, Resistivity of chemical vapor deposited diamond films, Appl. Phys. Lett., 55(10), pp.975-977; 1989.

[92] Y. Mori et.al., Electrical properties of boron-implanted homoepitaxial diamond films, Jpn. J. Appl. Phys., Vol.32 Pt.2 No.4B, pp.L601-L603; 1993.

[93] C. J. Rauch, _, Proceeding of international conference on the physics of semiconductors, Inst of Phys & Phys Soc., pp.276-280; 1962.

[94] B. V. Spitsyn, L. L. Bouilov, and B. V. Derjaguin, Vapor growth of diamond on diamond and other surfaces, J. Crystal Growth, Vol.52, pp.219; 1981.

[95] N. Fujimori, T. Imai, and A. Doi, Characterization of conductive diamond film, Vacuum, Vol.36, pp.99; 1986.

[96] R. E. Harper et.al., Electrical and electronic properties of diamond films, "Application of diamond films and related materials", Y. Tzeng, M. Yoshikawa, M. Murakawa, and A. Feldman (editors), pp.335-340; 1991.

[97] Y. Muto, T. Sugino, J. Shirafuji, and K. Kobashi, Electrical conduction in undoped diamond films prepared by chemical vapor deposition, Appl. Phys. Lett., 59(7), pp.843-845; 1991.

[98] J. Wei, H. Kawarada, J. Suzuki, and A. Hiraki, Growth of diamond films at low pressure using magneto-microwave plasma CVD, J. Crystal Growth, Vol. 99, pp.1201-1205; 1990.

[99] A. T. Collins, M. Kamo, and Y. Sato, A spectroscopic study of optical centers in diamond grown by microwave-assisted chemical vapor deposition, J. Mater. Res., Vol.5 No.11, pp.2507-2514; 1990.

[100] H. Lux, Influence of the gas composition on the electrical resistivity of the diamond thin film synthesized by the tantalum hot-filament method, Diamond Rel. Mat., 3(1994), pp.277-280; 1994.

[101] M. W. Geis, J. A. Gregory, and B. B. Plate, Capacitance-voltage measurements on metal-SiO2-diamond structures fabricated with (100) and (111) oriented substrates, IEEE Trans. Elec. Dev, Vol.38 No.3, pp.619-626; 1991.

[102] G. Kawaguchi, J. Nakanishi, A. Otsuki, T. Oku, and M. Murakami, Dependence of contact resistance on metal electronegativity for B-doped diamond films, J. Appl. Phys., Vol.75 No.10, pp.5165-5170; 1994.

[103] K. Miyata et.al., Characteristics of metal point contacts on diamond thin films, "New diamond science and technology", MRS international conference proceed, pp.981-986; 1991.

[104] S. M. Baker, G. R. Rossman, and J. D. Baldeschwieler, Observation of surface charge screening and Fermi level pinning on a synthetic, boron-doped diamond, J. Appl. Phys., 74(6), pp.4015-4019; 1993.

[105] Y. Mori, H. Kawarada, and A. Hiraki, Properties of metal/diamond interfaces and effects of oxygen adsorbed onto diamond surface, Appl. Phys. Lett., 58(9), pp.940-941; 1991.

[106] P. K. Bauman, and R. J. Nemanich, Electron affinity and Schottky barrier height of metal-diamond (100), (111), and (110) interfaces, J. Appl. Phys., 83(4), pp.2072-2082; 1998.

[107] C. E. Nobel, M. Stutzmann, F. Lacher, P. Koidl, and R. Zachai, Carrier trapping and release in CVD-diamond films, Diamond Rel. Mat., 7(1998), pp.556-559; 1998.

[108] S. Ashok, and K. Srikanth, Space-charge-limited current in thin-film diamond, Appl. Phys. Lett., 50(12), pp.763-765; 1987.

[109] J. W. Glesener, K. A. Snail, and A. A. Morrish, Admittance spectroscopy of boron doped diamond, Appl. Phys. Lett., 62(2), pp.181-183; 1993.

[110] P. Gonon, S. Prawer, Y. Boiko, and D. jamieson, Electrical conduction in polycrystalline diamond and the effects of UV irradiation, Diamond Rel. Mat., 6(1997), pp.860-864; 1997.

[111] S. Albin, and L. Watkins, Electrical propeties of thin film and bulk diamond treated in hydrogen plasma, "Diamond, silocon carbide, and related wide bandgap semiconductors" MRS Proceeding, Vol.162, pp.303-308; 1990.

[112] P. W. Tuinenga, "SPICE - A guide to circuit simulation and analysis using Pspice", , 3rd Ed., pp.; 1995.

[113] MicroSim Corporation, "MicroSim Pspice A/D reference manual", , Version 6.3, pp.4_20; 1996.

[114] K. Liu et.al., Measurement of doping concentration in boron-doped diamond film from capacitance spectroscopy, J. Appl. Phys., 82(1), pp.286-290; 1997.

[115] K. Liu et.al., Measurement of electron affinity in boron-doped diamond from capacitance spectroscopy, Appl. Phys.Lett., 70(21), pp.2891-2893; 1997.

[116] B. A. Fox, M. L. Hartsell, D. M. Malta, H.A. Wynands, G. J. Tessmer, and D. L. Dreifus, Electrical properties of diamond for device applications, "Diamond for electronic applications", MRS symposium proceed - volume 416, pp.319-329; 1996.

[117] H. J. Looi, L. Y. S. Pang, A. B. Molly, F. Jones, J.S. Foord, and R. B. Jackman, An insight into the mechanism of surface conductivity in thin film diamond, Diamond Rel. Mat., 7(1998), pp.550-555; 1998.

[118] J. Osvald, and E. Burian, C-V dependence of inhomogeneous Schottky diodes, Solid State Electronics, Vol.42 No.2, pp.191-195; 1995.

[119] X. Wu, and E. S. Yang, Interface capacitance in metal-semiconductor junctions, J. App. Phys., 65(9), pp.3560-3567; 1989.

[120] J. Werner, A. Levi, R. T. Tung, M. Anzlowar, and M. Pinto, __, Phys. Rev. Lett, 60(1), pp.53-56; 1988.

[121] J. J. Liou, and D. C. Malocha, Modeling the non-quasi-static metal-semiconductor space-charge-region capacitance, J. Appl. Phys., 65(4), pp.1783-1787; 1989.

[122] M. M. Bataineh, D. K. Reinhard, An impedance spectroscopy investigation of polycrystalline diamond from dc to 1 GHz, Diamond Rel. Mat., 6(1997), pp.1689-1696; 1997.

[123] E. Schibli, and A. G. Milnes, Effects of deep impurities on n+p junction reverse-biased small-signal capacitance, Solid State Electronics, Vol.11, pp.323-334; 1968.

[124] J. Mort, M. A. Machonkin, and K. Okumura, Density of states distribution in diamond thin films, Appl. Phys. Lett., 59(4), pp.455-457; 1991.

[125] B. D. Wedlock, and J. K. Roberge, "Electronic components and measurements", , 1st Ed., pp.287-294; 1969.

[126] W. H. Hayt, Jr., "Engineering Electromagnetics", , 4th Ed., pp.433; 1981.

[127] H. E. Thomas, "Handbook of microwave techniques and equipment", , 1st Ed., pp.29; 1972.

[128] M. Silver et.al., Study of the electronic structure of amorphous silicon using reverse-recovery techniques, Appl. Phys. Lett., 41(10), pp.935-937; 1982.

[129] K. Liu, and J. Chu, Measurement of electrical activation energy in boron-doped diamond using flatband capacitance method, J. Appl. Phys., 83(8), pp.4202-4205; 1998.

[130] K. Miyata, K. Kobayashi, and D.L. Dreifus, ___, Diamond Rel. Mat., 2(1993), pp.812-815; 1993.

[131] M. Derdouri, P. Leturcq, and A. Muñoz-Yagüe, A comparative study of methods of measuring carrier lifetime in p-I-n devices, IEEE Trans. Elec. Dev., Vol.Ed.27 No.11, pp.2097-2101; 1980.

[132] R. H. Dean, C. J. Nuese, A refined step-recovery technique for measuring minority carrier lifetimes and related parameters in asymmetric p-n junction diodes, IEEE Trans. Elec. Dev., Vol.Ed.18 No.3, pp.151-158; 1971.

[133] B. Tien, C. Hu, Determination of carrier lifetime from rectifier ramp recovery waveform, IEEE Elec. Dev. Lett, Vol.9 No.10, pp.553-555; 1988.